

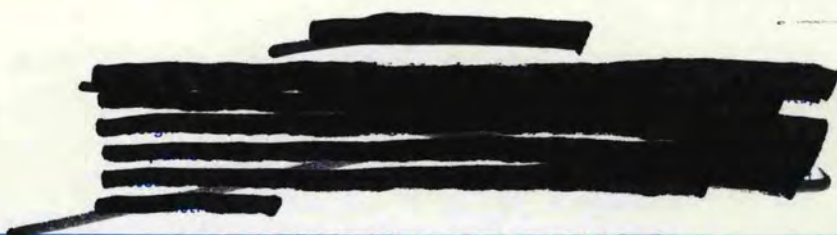


3 4456 0555878 6

Cg 37

**Analyses of the Preliminary In-Vessel
and Enclosure Shield System Designs
for the Clinch River Breeder Reactor
(July, 1973-July, 1975)**

W. W. Engle, Jr.
L. R. Williams
J. H. Swanks
F. R. Mynatt
Lorraine S. Abbott



OAK RIDGE NATIONAL LABORATORY

CENTRAL RESEARCH LIBRARY

DOCUMENT COLLECTION

LIBRARY LOAN COPY

DO NOT TRANSFER TO ANOTHER PERSON

If you wish someone else to see this
document, send in name with document
and the library will arrange a loan.

UCN-7969
(3 3-67)

OAK RIDGE NATIONAL LABORATORY

OPERATED BY UNION CARBIDE CORPORATION FOR THE ENERGY RESEARCH AND DEVELOPMENT ADMINISTRATION

Printed in the United States of America. Available from
the Energy Research and Development Administration,
Technical Information Center
P.O. Box 62, Oak Ridge, Tennessee 37830
Price: Printed Copy \$5.00 ; Microfiche \$2.25

This report was prepared as an account of work sponsored by the United States Government. Neither the United States nor the Energy Research and Development Administration, nor any of their employees, nor any of their contractors, subcontractors, or their employees, makes any warranty, express or implied, or assumes any legal liability or responsibility for the accuracy, completeness or usefulness of any information, apparatus, product or process disclosed, or represents that its use would not infringe privately owned rights.

ORNL/TM-5338
UC-79d - Liquid Metal
Fast Breeder Reactor
Physics

Contract No. W-7405-eng-26

Neutron Physics Division

ANALYSES OF THE PRELIMINARY IN-VESSEL AND ENCLOSURE SHIELD
SYSTEM DESIGNS FOR THE CLINCH RIVER BREEDER REACTOR
(July, 1973 - July, 1975)

Analyses performed by: W. W. Engle, Jr.
L. R. Williams
J. H. Shanks*

Work directed by: F. R. Mynatt
Report written by: Lorraine S. Abbott
Manuscript prepared by: LaWanda Klobe
Virginia Glidewell
Gail Raiford

MARCH 1976

*Operations Division

OAK RIDGE NATIONAL LABORATORY
Oak Ridge, Tennessee 37830
operated by
UNION CARBIDE CORPORATION
for the
ENERGY RESEARCH AND DEVELOPMENT ADMINISTRATION

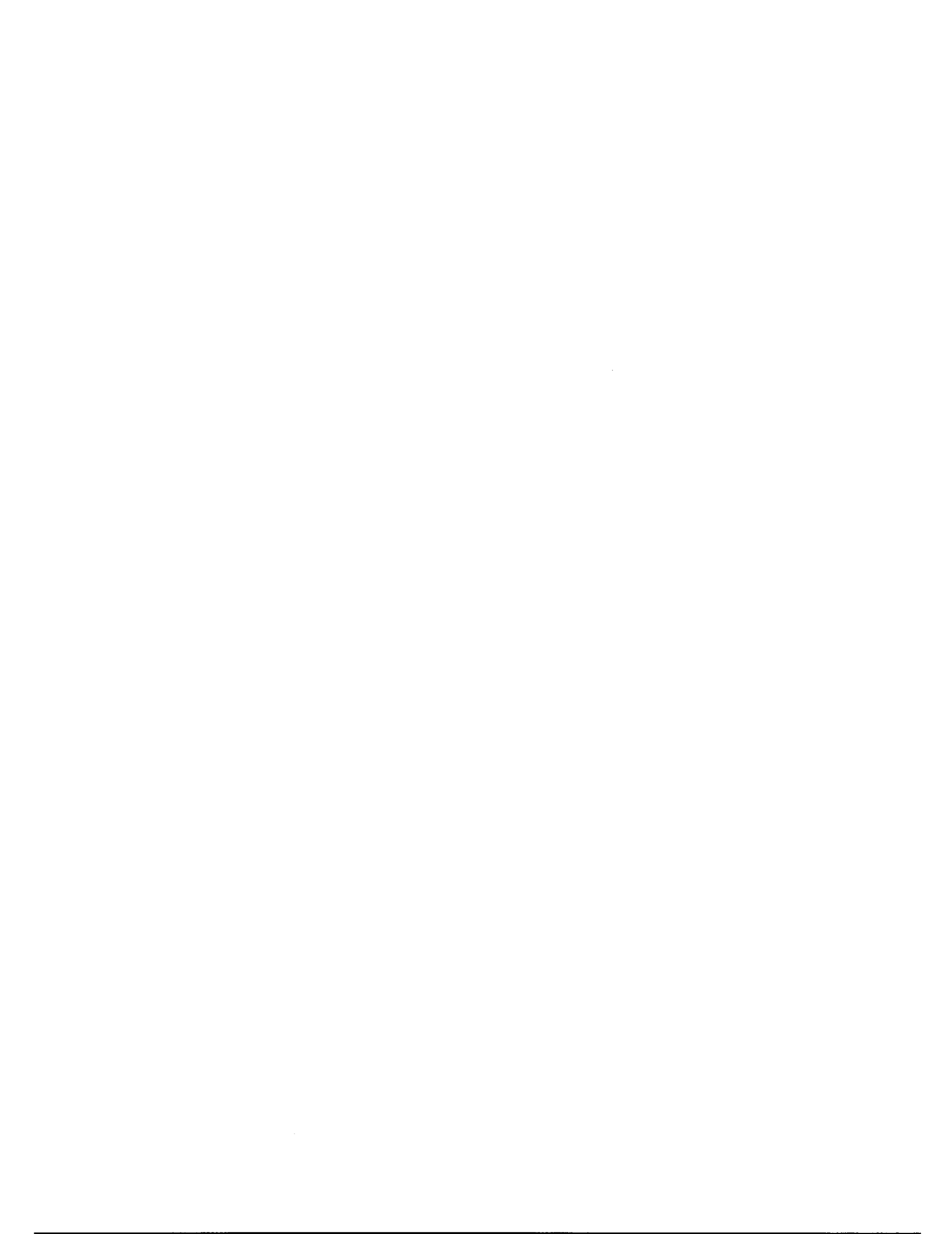


3 4456 0555878 6



TABLE OF CONTENTS

	<u>Page No.</u>
ABSTRACT -----	v
1. INTRODUCTION -----	1
2. INITIAL CALCULATIONS OF NEUTRON FLUXES IN CRBR LOWER AXIAL REGION -----	6
3. FULL-ASSEMBLY CALCULATIONS FOR EARLY CRBR MODEL -----	13
3.1. Power Density of "Beginning-of-Life" Core -----	14
3.2. Neutron Fluxes and Dose Rates Throughout Assembly -----	20
3.3. Activation Gamma-Ray Dose Rates at Ex-Vessel Detectors -----	24
4. FULL-ASSEMBLY CALCULATIONS FOR REVISED CRBR MODEL -----	25
4.1. Power Density of Equilibrium Core -----	31
4.2. Neutron Fluxes and Dose Rates in Lower Axial Region -----	31
4.3. Two-Boundary Source for Above-Core Calculations -----	43
4.4. Neutron and Secondary Gamma-Ray Fluxes and Dose Rates Below Reactor Head and Vessel Support System -----	46
4.5. Penetration of Radiation Through Reactor Head and Vessel Support System -----	46
5. SUMMARY AND CONCLUSIONS -----	77
REFERENCES -----	80



ABSTRACT

The first three series of calculations in ORNL's radiation shielding analysis program for the Clinch River Breeder Reactor (CRBR) are described here. The initial calculations concentrated on the neutron fluxes in the lower axial region of the reactor vessel, the results of these and subsequent calculations leading to a substantial reduction in the thickness of the lower axial shield. The second series consisted of "full-assembly" calculations for a CRBR system that closely resembled the Fast Flux Test Facility, utilizing the same vessel support system, in-vessel stored-fuel modules, and reactor cavity shields. The third series began with a CRBR design having a much-simplified vessel support system and no stored-fuel modules or reactor cavity shields, but when initial calculations yielded dose rates above the reactor head that were excessively high, a B₄C shield was reintroduced in the reactor cavity. At the same time the vessel support system was redesigned so that a portion of the support ring set on top of the concrete support ledge. A subsequent calculation for the new design with the B₄C shield showed that the dose rates were not adequately reduced, and more shielding was added in both the upper and lower sections of the support ring. With the added shielding, the dose rates were greatly reduced but were still above the criteria. A re-evaluation of the head compartment access requirements by WARD led to a relaxation of radiation criteria. The next analysis sequence will evaluate the dose levels and uncertainties based on the new criteria.



1. INTRODUCTION

This report describes the first three series of calculations performed by Oak Ridge National Laboratory in its radiation shielding analysis program for the Clinch River Breeder Reactor Plant (CRBRP). As was the case for the Fast Flux Test Facility (FFTF),¹ each major study in the shielding analysis program for the CRBR consists of an iterative series of radiation transport calculations that determine the radiation levels within and above the reactor vessel and the surrounding cavity for given design modifications of the system. The designs are developed by Westinghouse Electric Corporation's Advanced Reactors Division (WARD), which has the lead design responsibility for the reactor, and specific calculations are performed at the request of WARD.

A near-current design of the CRBR reactor vessel and head region is represented in Figs. 1 and 2 (ref. 2). With respect to shielding, an important feature is the largest of three eccentric rotating plugs that introduces a possible radiation streaming gap at the top of the reactor cavity. Other gaps exist in the region where the vessel support structure mates with a concrete support ledge (not shown in Figs. 1 and 2), and it is in this region that many of the shielding analysis studies are being concentrated.

The evolution of the vessel support concept through several designs is illustrated in Fig. 3 (ref. 3). It began with a design that was essentially copied from the FFTF (sketch A in Fig. 3). Later the vessel support straps inherent in the FFTF concept were eliminated from the CRBR design and the distance between the vessel and the concrete support ledge was reduced (sketch B). In a subsequent design a portion of the support structure was elevated above the support ledge (sketch C), and finally the inner bolt circle visible in Figs. 1 and 2 was eliminated (sketch D). ORNL has considered these various evolutionary stages, plus the effect of adding shielding in the cavity outside the reactor guard vessel.

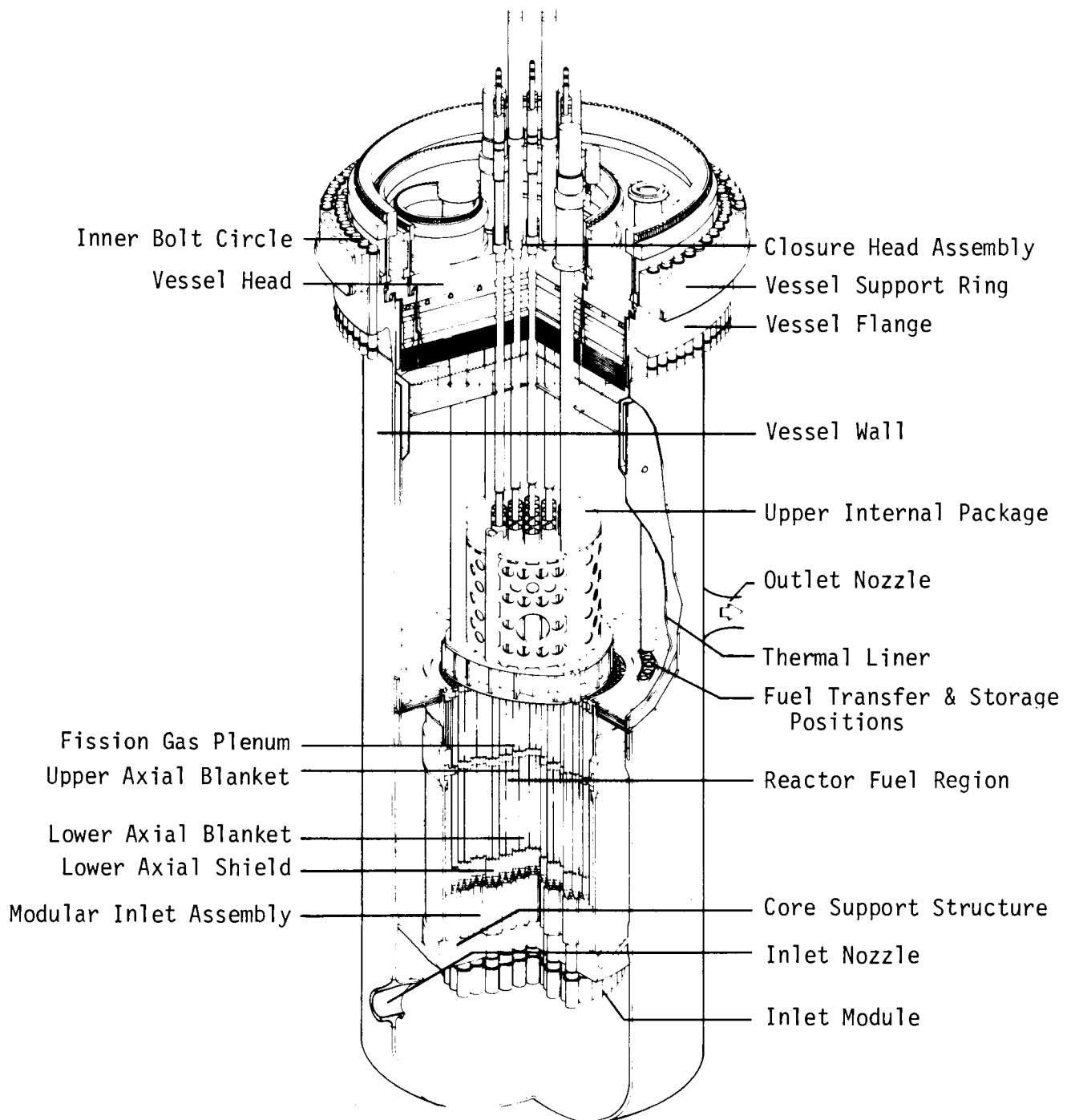


Fig. 1. Cutaway View of Clinch River Breeder Reactor Vessel.

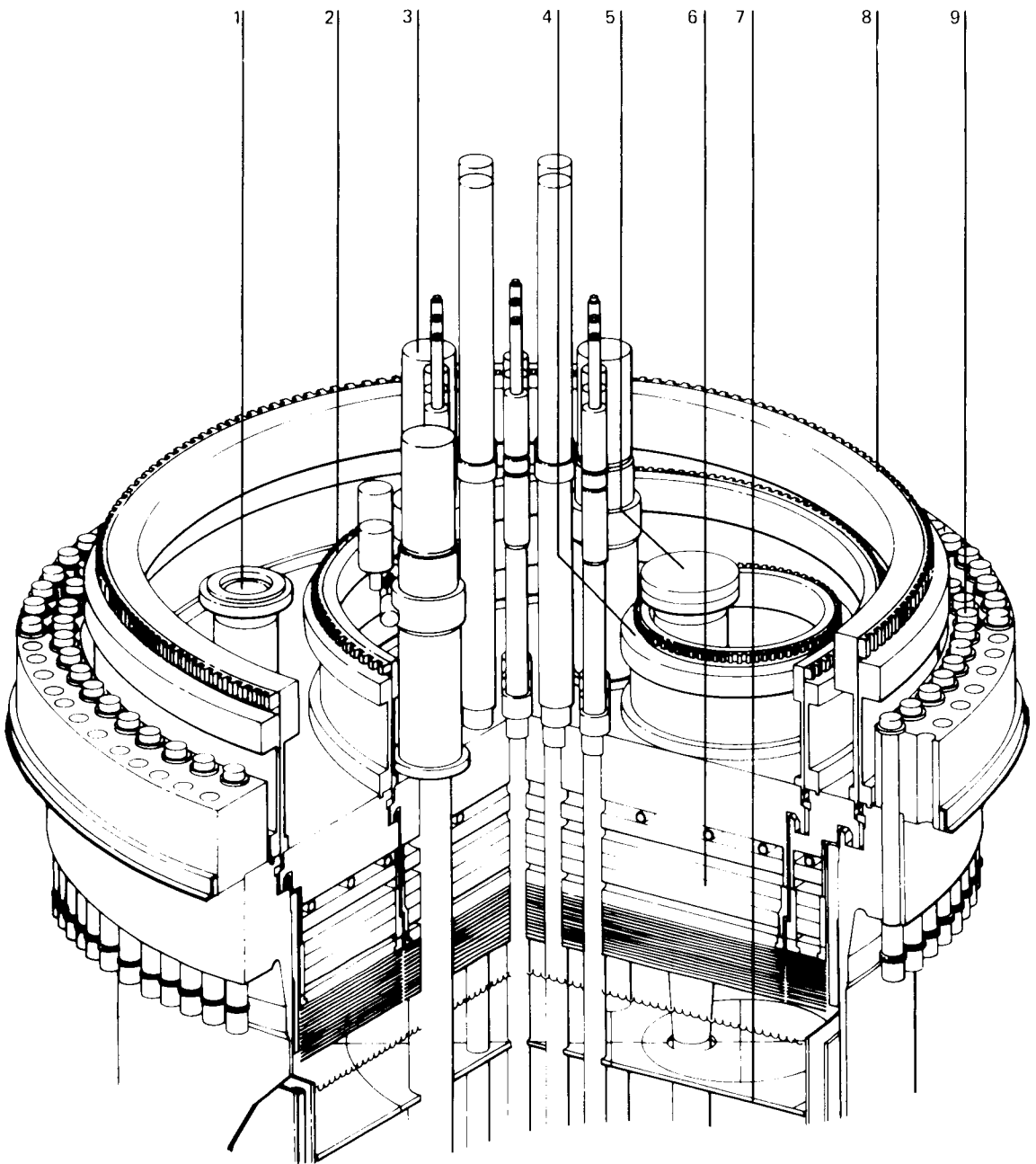
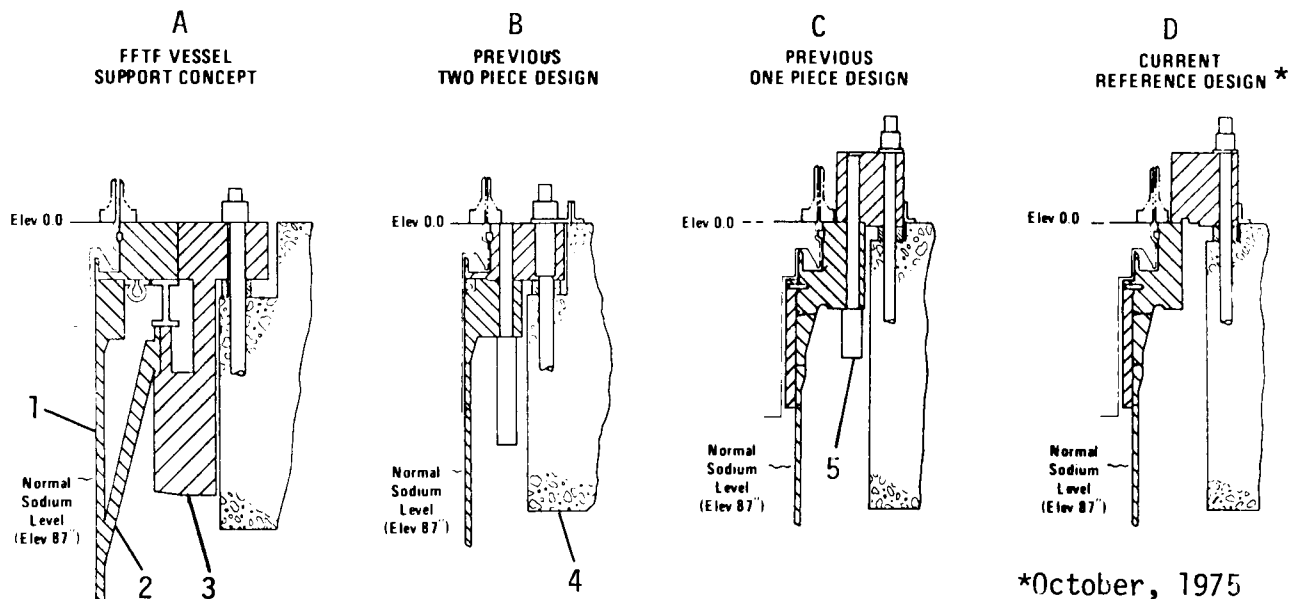


Fig. 2. Clinch River Breeder Reactor Vessel Head Assembly.
1, Ex-Vessel Transfer Machine Port; 2, Intermediate Rotating Plug; 3,
Control Rod Drive Mechanism; 4, Small Rotating Plug; 5, In-Vessel Transfer
Machine Port; 6, Shielding; 7, Suppressor Plate; 8, Large Rotating Plug;
9, Stationary Ring.



*October, 1975

Fig. 3. Evolution of Clinch River Breeder Reactor Vessel Support Design. 1, Reactor Vessel; 2, Support Strap; 3, Support Ring; 4, Concrete Support Ledge; 5, Inner Bolt Circle.

ORNL has also considered several design concepts of the lower axial region of the reactor, where the primary radiation concern first was damage to the core support structure and second to the modular inlet assembly (see Fig. 1). These structures are protected by steel shielding incorporated in the lower section of each fuel assembly as shown in Fig. 4 (ref. 2), and one of the earliest design problems was establishing the thickness of shielding required to ensure an adequate lifetime for the support plate. In fact, the first shielding study performed by ORNL for the CRBR was a study of the neutron fluxes incident on the support plate, as was the first shielding study performed by ORNL for the FFTF. For the CRBR, however, calculational methods were at hand for the study, whereas for the FFTF the investigation was necessarily primarily experimental.

This report presents the various calculations in chronological order, beginning with the initial calculation of the lower axial region performed in mid-1973. Descriptions of two series of "full-assembly" calculations follow, where "full-assembly" means that the calculations covered the full

- 1 Outlet Nozzle
- 2 Wire Wrap Spacer
- 3 217 Fuel Rods/Assembly
- 4 Load Pad
- 5 Inlet Nozzle
- 6 Discrimination Post

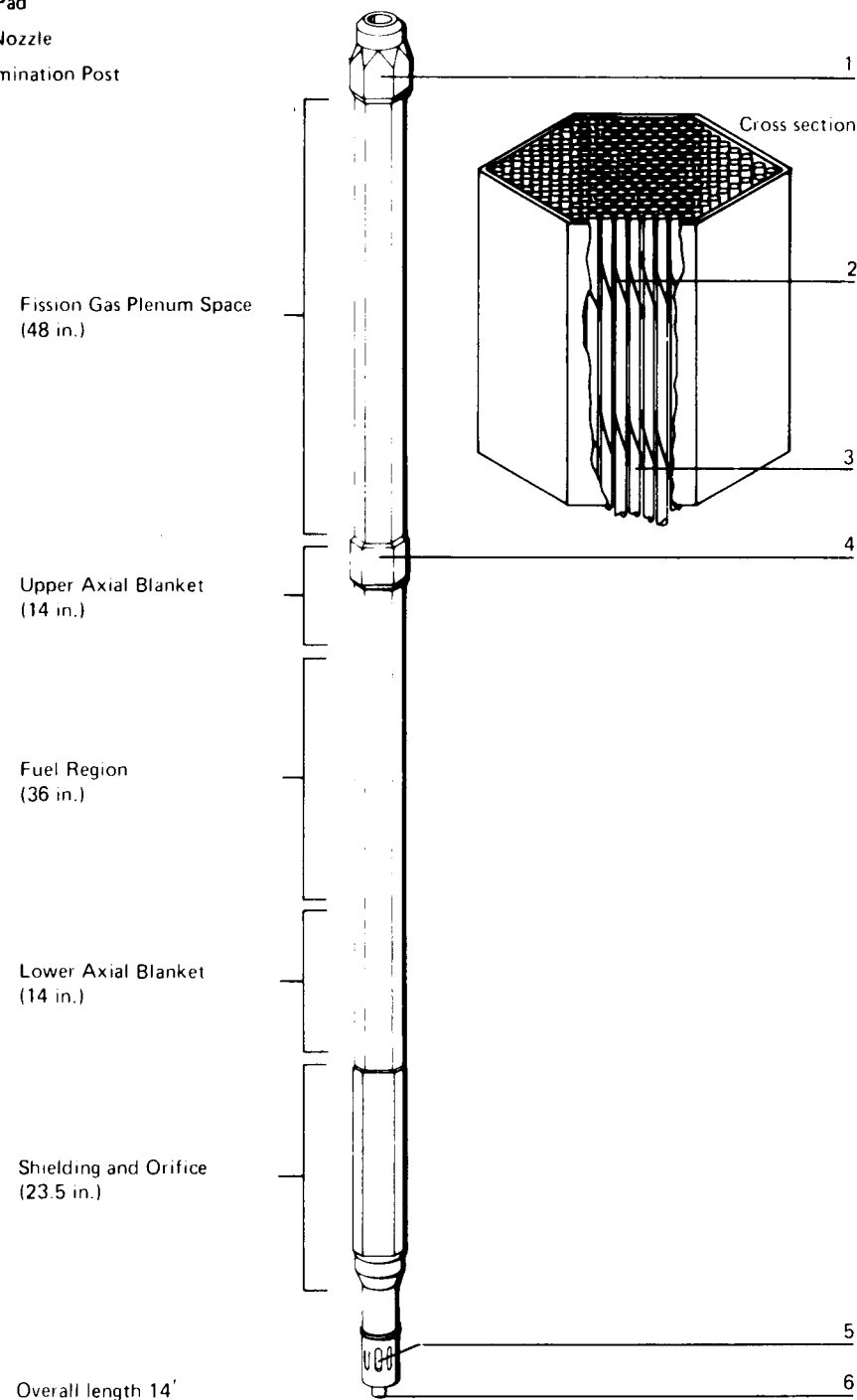


Fig. 4. Clinch River Breeder Reactor Fuel Assembly.

region from the reactor core to and through the reactor head. Radially they extended through the reactor cavity. In conjunction with both these series, which were performed during the period between the Fall of 1973 and mid-1975, further studies were made of the lower axial region, with the thickness of the lower axial shield reduced each time.

In all cases, the calculations were performed with the discrete ordinates transport method, primarily with Version III of the two-dimensional code DOT.⁴ A few runs were also made with the one-dimensional code ANISN.⁵ For the first two series, the cross-section multigroup library used was the 50-group neutron library developed for the FFTF,¹ which was not coupled to a gamma-ray cross-section set. By the time the last series was performed, however, a new coupled cross-section library containing 51 neutron groups and 25 gamma-ray groups had been developed specifically for the CRBR, and thus the last series includes secondary gamma-ray data whereas the first two do not. Initially the 51-25 cross-section library was based on ENDF/B-III data, but before these calculations were completed it was updated with ENDF/B-IV data for all important elements.

2. INITIAL CALCULATIONS OF NEUTRON FLUXES IN CRBR LOWER AXIAL REGION

When the first calculations of the neutron fluxes incident on the reactor support plate were performed,⁶ the CRBR design called for a 5.08-cm-thick (2-in.) type 304 stainless steel grid plate protected by a 74.9-cm-thick (29.5-in.) type 316 stainless steel shield. Immediately below the core was a 35.56-cm-thick (14-in.) blanket of depleted uranium oxide separated from the upper end of the shield by a 10.414-cm-thick (4.1-in.) fuel rod attachment. The shield itself was to be fabricated as closely fitting pieces that were hexagonal in cross section and were penetrated by orifices to allow the flow of sodium coolant over the full length of the shield. The location of the coolant holes in each piece is shown in Fig. 5.

ORNL-DWG 73-11405

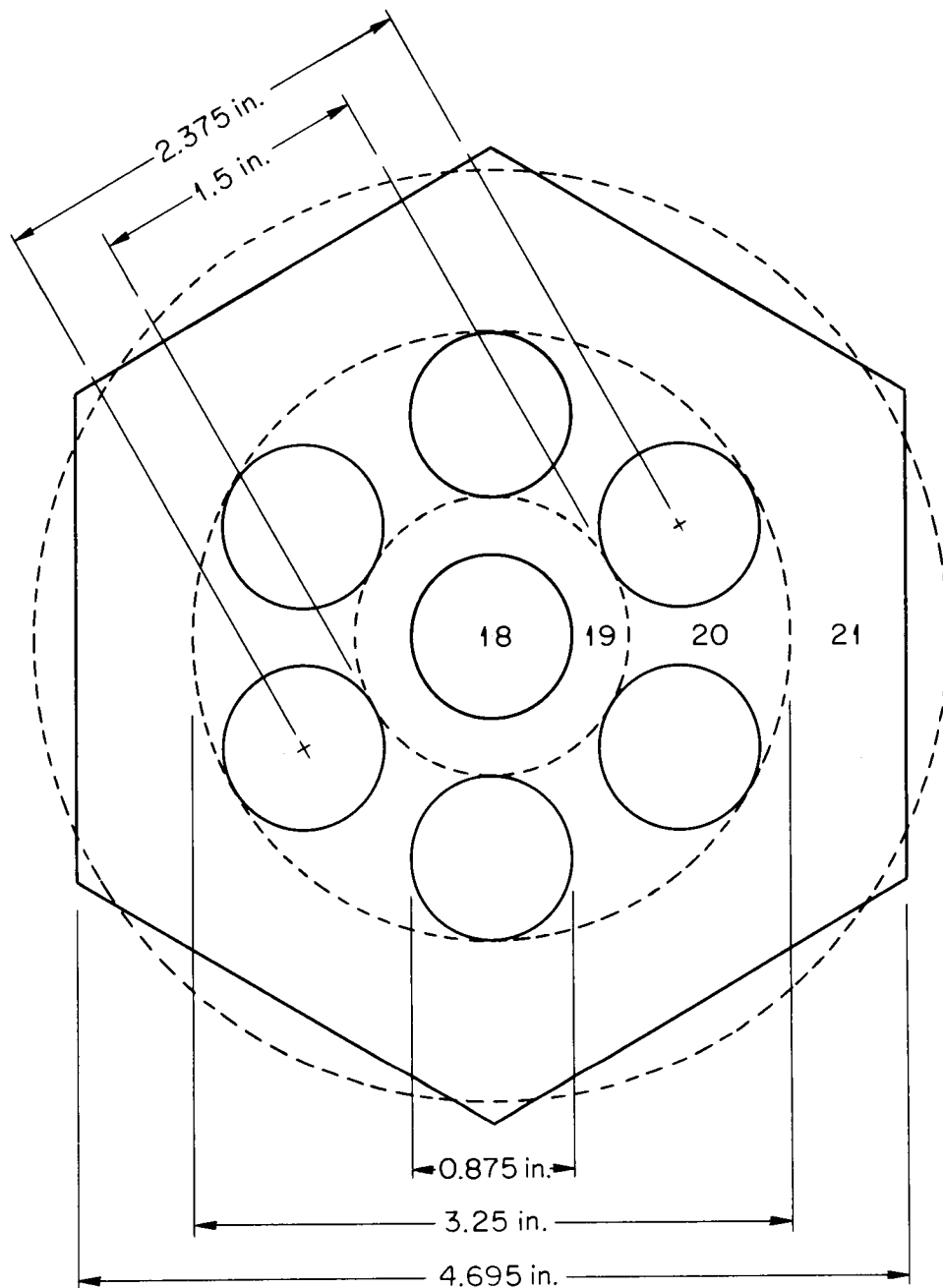


Fig. 5. Cross Section of Hexagonal Axial Shield Section Showing Location of Coolant Holes. Dashed lines indicate regions used in calculation (see text). (Metric dimensions on this drawing, top to bottom, are 6.0325 cm, 3.81 cm, 2.2225 cm, 8.255 cm, and 11.925 cm.)

The geometry for the calculations included the lower half of the core (half-height = 45.72 cm = 18 in.) and extended radially into the sodium region beyond the core-reflector radial restraint. Below the core it extended well below the grid plate. The various regions in the geometry are identified in Table 1 and in Figs. 6, 7, and 8, all of which will be discussed later.

The fission source distribution within the lower half of the core was obtained from DOT diffusion theory calculations using the 50-group FFTF neutron cross-section library.¹ In one calculation the central control-rod channel was assumed to be filled with sodium, and in a second calculation it was assumed to be filled with fuel. The corresponding k_{eff} values were 0.979 and 0.983 respectively. Because of these low values, a separate S₄P₁ calculation was performed for the case of sodium in the central channel. This calculation yielded a k_{eff} value of 0.984, and it was assumed that the diffusion theory calculations were adequate for use. However, for the shield calculations with the sodium-filled channel, the fission source distribution obtained from the S₄P₁ run was used rather than that from diffusion theory since it was assumed to have a more accurate angular flux distribution. In both cases the upper half of the core was accounted for by using a reflected boundary condition at the core midplane.

The calculations for the shield were performed for two cases: one in which the entire lower axial shield was represented by a homogenized region of 74.6% type 316 stainless steel and 25.45% sodium, and another in which the center section of the shield more nearly resembled the real case. This section was described as a central cylinder of sodium (representing the center hole) and three surrounding cylindrical annuli as shown by the dashed lines in Fig. 5. The first annulus was steel, the second a homogenized region of sodium and steel (to include the other six coolant holes), and the third a final region of steel. The remainder of the shield was the same as in the homogenized case.

Table 1. Description of Zones in Initial Calculations for CRBR Lower Axial Region

Zone No.	Identification	Material
1a	Control rod channel No. 1 (central channel) (radius = 6.391 cm = 2.516 in.)	Fuel
1b*	Control rod channel No. 1 (central channel)	Sodium
2	Inner core (half height = 45.72 cm = 18 in.)	Fuel
3	Control rod channel No. 2	~95% sodium, ~5% stainless steel
4	Inner core	Fuel
5	Control rod channel No. 3	~95% sodium, ~5% stainless steel
6	Inner core	Fuel
7	Control rod channel No. 4	~95% sodium, ~5% stainless steel
8	Outer core	Fuel
9	Radial blanket	Depleted uranium oxide
10	Radial reflector	~90% stainless steel, ~10% sodium
11	Radial restraint	Inconel
12-13	Radial sodium zones not included in figures	
14	Lower inner axial blanket (thickness = 35.56 cm = 14 in.)	Depleted uranium oxide
15	Lower outer axial blanket	Depleted uranium oxide
16	Radial blanket extension	Depleted uranium oxide
17	Fuel rod attachment (thickness = 10.414 cm = 4.1 in.)	80% sodium, 20% type 316 stainless steel
18	Center of mockup of shield section (radius = 1.111 cm = 0.4375 in.)	Sodium
19	First annulus of shield section mockup (thickness = 0.75 - 0.4375 in.) (= 0.7938 cm)	Type 316 stainless steel
20	Second annulus of shield section mockup (thickness = 1.625 in. - 0.75 in.) (= 2.22 cm)	55.26% sodium, 44.74% type 316 stainless steel
21	Third annulus of shield section mockup (thickness = 2.516 in. - 1.625 in.) (= 2.26 cm)	Type 316 stainless steel
22	Shield (thickness = 74.93 cm = 29.5 in.)	25.4% sodium, 74.6% type 316 stainless steel
23	Transition zone (thickness = 7.366 cm = 2.9 in.)	65% sodium, 35% type 316 stainless steel
24	Grid plate (thickness = 5.08 cm = 2 in.)	36% sodium, 64% type 304 stainless steel
25	Transition zone (thickness = 35.56 cm = 14 in.)	65% sodium, 35% type 316 stainless steel

*Zone 1b extends down through blanket.

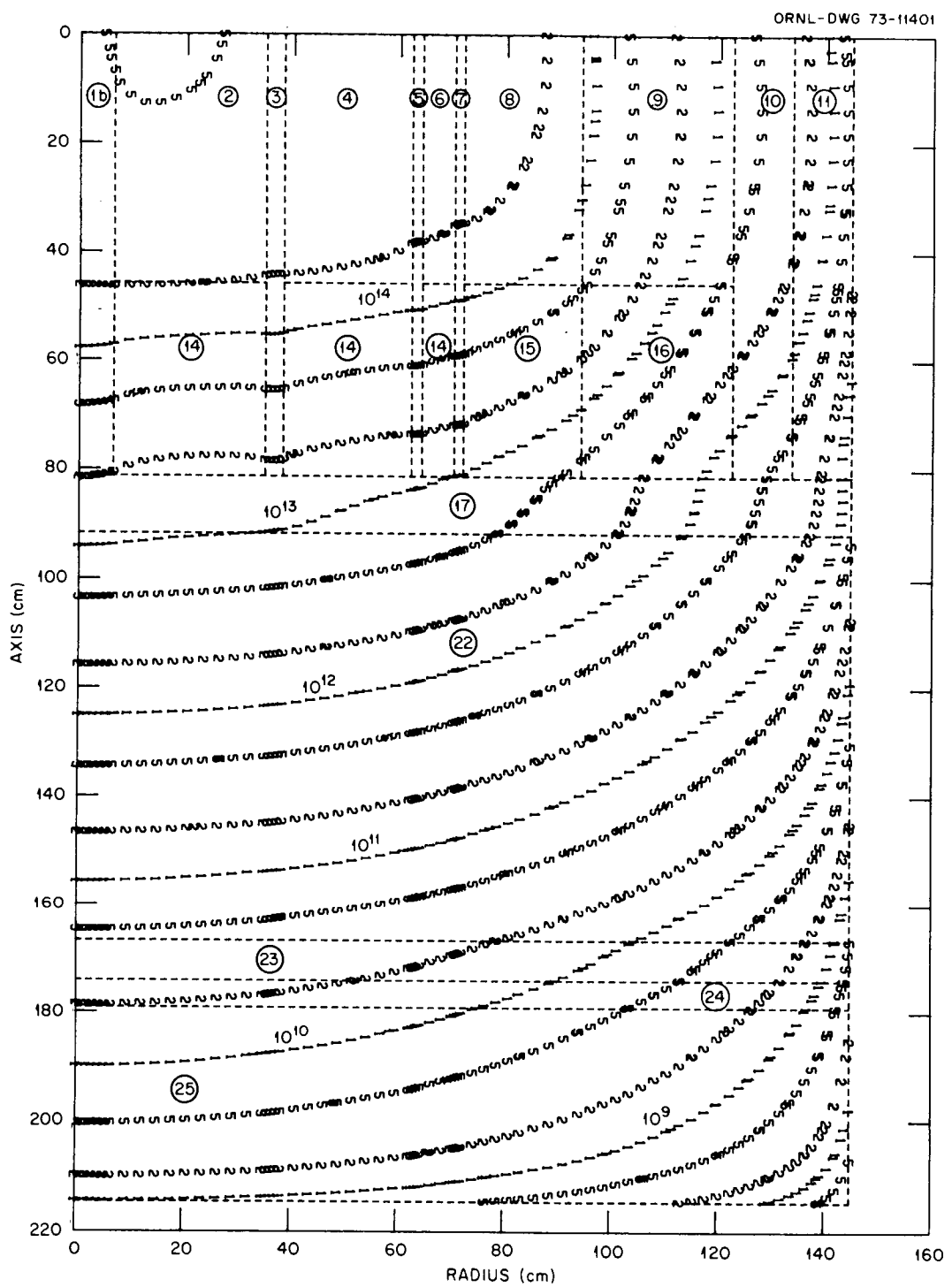


Fig. 6. Neutron Dose-Rate Contours (mrem/hr) in CRBR Lower Axial Shield and Grid-Plate Region: Sodium in Central Control-Rod Channel; Homogenized Shield (Case 1).

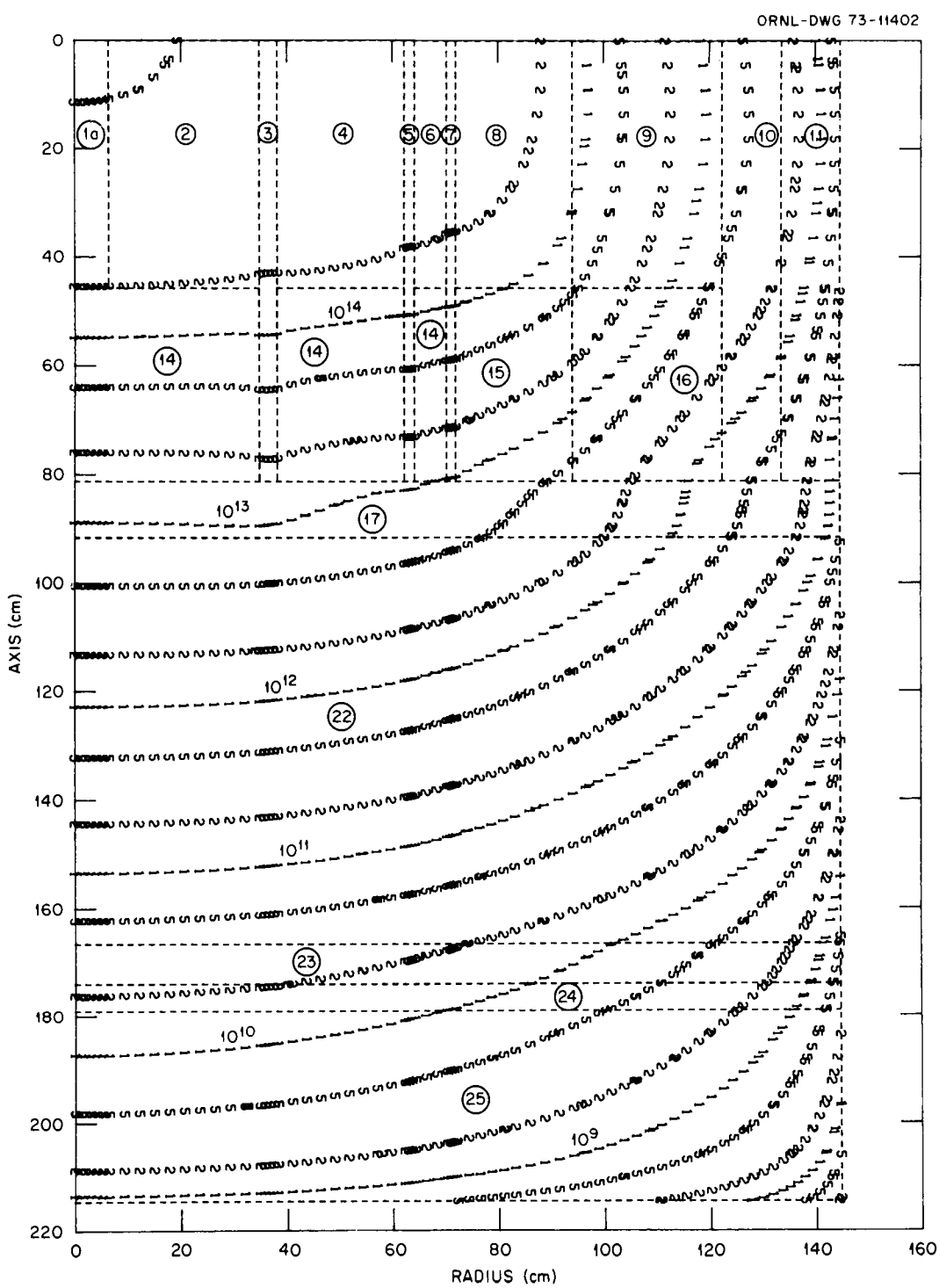


Fig. 7. Neutron Dose-Rate Contours (mrem/hr) in CRBR Lower Axial Shield and Grid-Plate Region: Fuel in Central Control-Rod Channel; Homogenized Shield (Case 2).

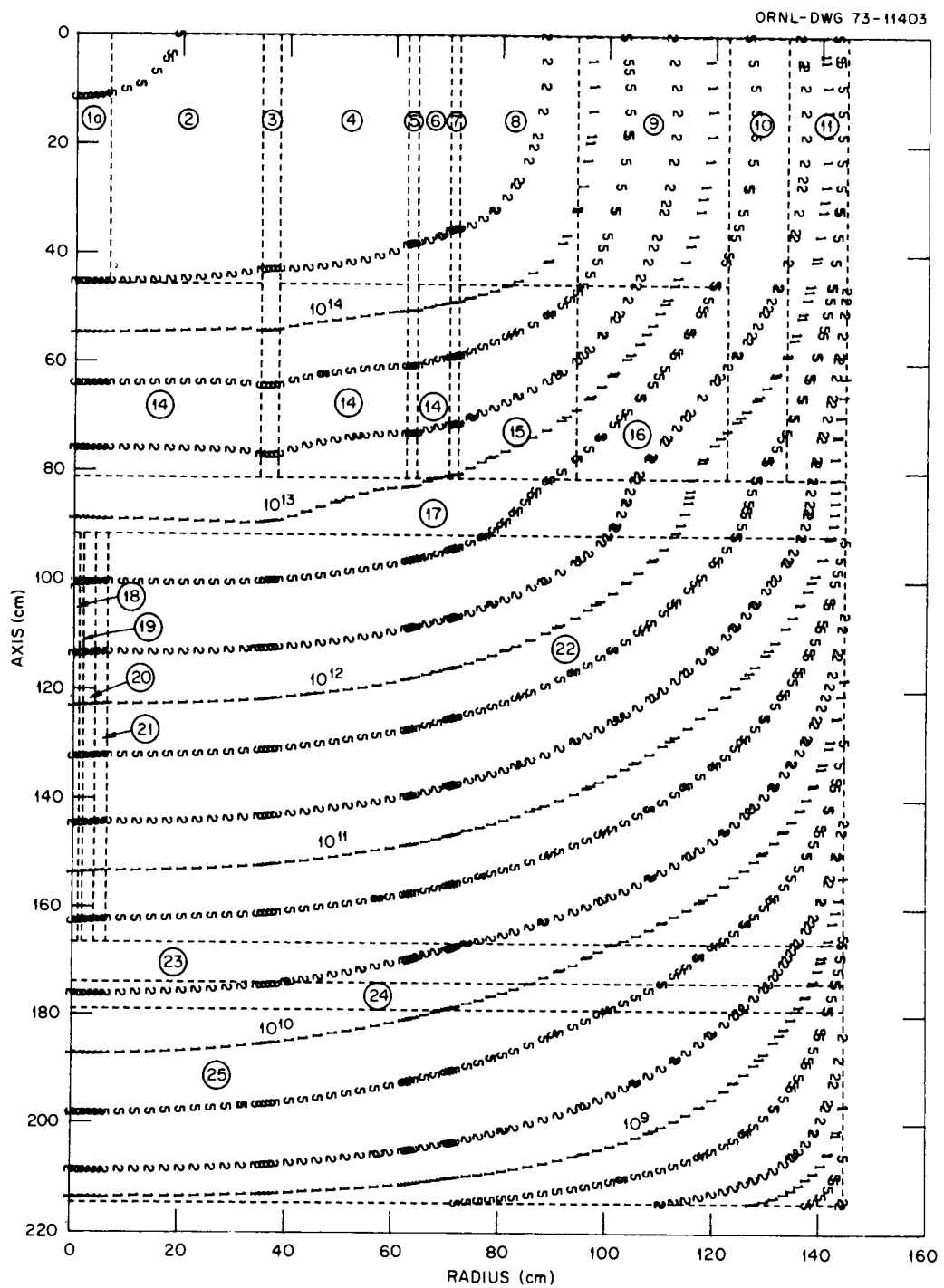


Fig. 8. Neutron Dose-Rate Contours (mrem/hr) in CRBR Lower Axial Shield and Grid-Plate Region: Fuel in Central Control-Rod Channel; Center Section of Shield Represented by Concentric Annuli (Case 3).

The calculations were performed with the 50-group cross sections, using 147 angles and P_3 scattering. To aid in visualizing radiation contours, dose-rate results from the homogenized-shield runs were obtained in the form shown in Figs. 6 and 7 for the cases of the central control-rod channel being filled with sodium and fuel, respectively. (When sodium was in the central channel, the region extended down through the blanket.) The results from the run in which the center section of the shield was mocked up are shown in Fig. 8, the fission source distribution being that calculated for the case of fuel in the central control-rod channel.

The total neutron fluxes calculated for specific locations within the assembly are given in Table 2. With the fluxes shown for the grid plate, together with a maximum total fluence of 9.5×10^{21} nvt to be allowed at the plate (an FFTF criterion), the life times of the grid plate would be 166 yr, 194 yr, and 193 yr for Cases 1, 2, and 3 respectively.

Flux tapes were provided to WARD in order that they might perform damage evaluations based on energy-dependent damage data. These studies showed even longer lifetimes and the thickness of the lower axial shield was gradually reduced prior to the calculations described in Sections 3 and 4.

3. FULL-ASSEMBLY CALCULATIONS FOR EARLY CRBR MODEL

The first "full-assembly" calculations for the CRBR were based on the model shown in Fig. 9. These calculations, begun in the Fall of 1973, were performed while studies for the FFTF were still under way and the similarity of the model to the FFTF is obvious. In addition to the FFTF-type vessel support straps and support ring pointed out in Section 1 above, this model assumed that fuel would be stored within the CRBR vessel in approximately the same location as in the FFTF vessel. It also assumed that the concrete reactor cavity shield and the B_4C collar on the top of the guard vessel would be necessary.

Table 2. DOT-Calculated Neutron Fluxes Along Axis of CRBR Lower Axial Region

Location	Total Neutron Flux ^a (neutrons·cm ⁻² ·sec ⁻¹)		
	Sodium in Control-Rod Channel; Homogenized Shield (Case 1)	Fuel in Control-Rod Channel Homogenized Shield (Case 2)	Orificed Shield (Case 3)
Core midplane	9.62(15) ^b	9.61(15)	9.61(15)
Top of blanket	4.65(15)	4.30(15)	4.30(15)
Bottom of blanket	8.30(14)	6.01(14)	6.01(14)
Top of shield	5.30(14)	4.33(14)	4.28(14)
Top of grid plate	1.81(12)	1.55(12)	1.56(12)

^aBased on total source of 4.19×10^{19} neutrons/sec.

^bRead: 9.62×10^{15} .

3.1. Power Density of "Beginning-of-Life" Core

These calculations began with a DOT-III r-z calculation of the power density in the CRBR "beginning-of-life" core using an S₄ quadrature, P₁ scattering, and the FFTF 50-group neutron cross-section library.¹ In the axial direction the geometry extended from 160 cm below the core horizontal midplane to 225 cm above the midplane; radially it extended through the core barrel. The various regions included in the calculation are shown in Fig. 10 and Table 3, with the corresponding atomic densities of the materials given in Tables 4-7. Volume percentages of the stainless steel and sodium in the various regions are given in Table 8, except for those regions which are covered in the previous tables. This calculation yielded a k_{eff} value of 0.95.

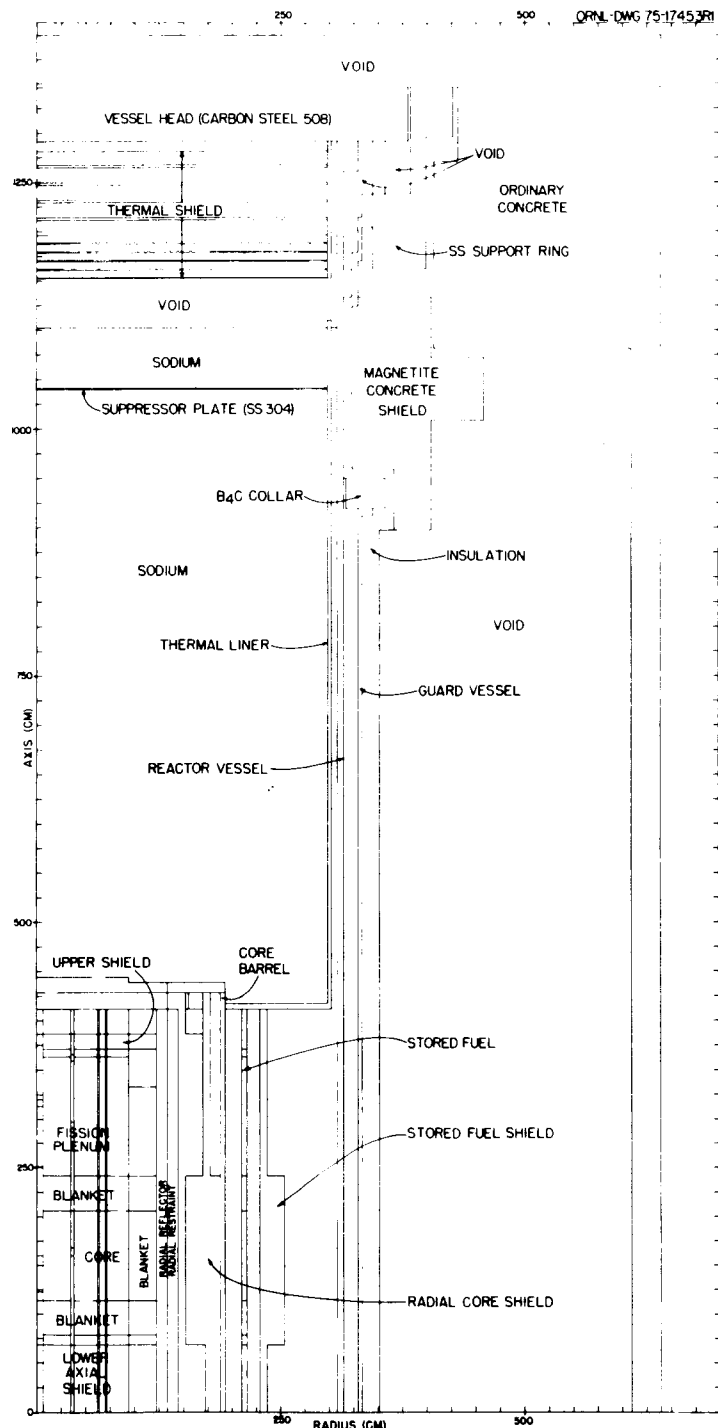


Fig. 9. Calculational Model for Early Conceptual Design of CRBR.
Note similarity of design to Fast Flux Test Facility; that is, it includes an in-vessel stored-fuel region, a B4C collar on the guard vessel, a magnetite concrete reactor cavity shield, and a reactor support ring with support straps.

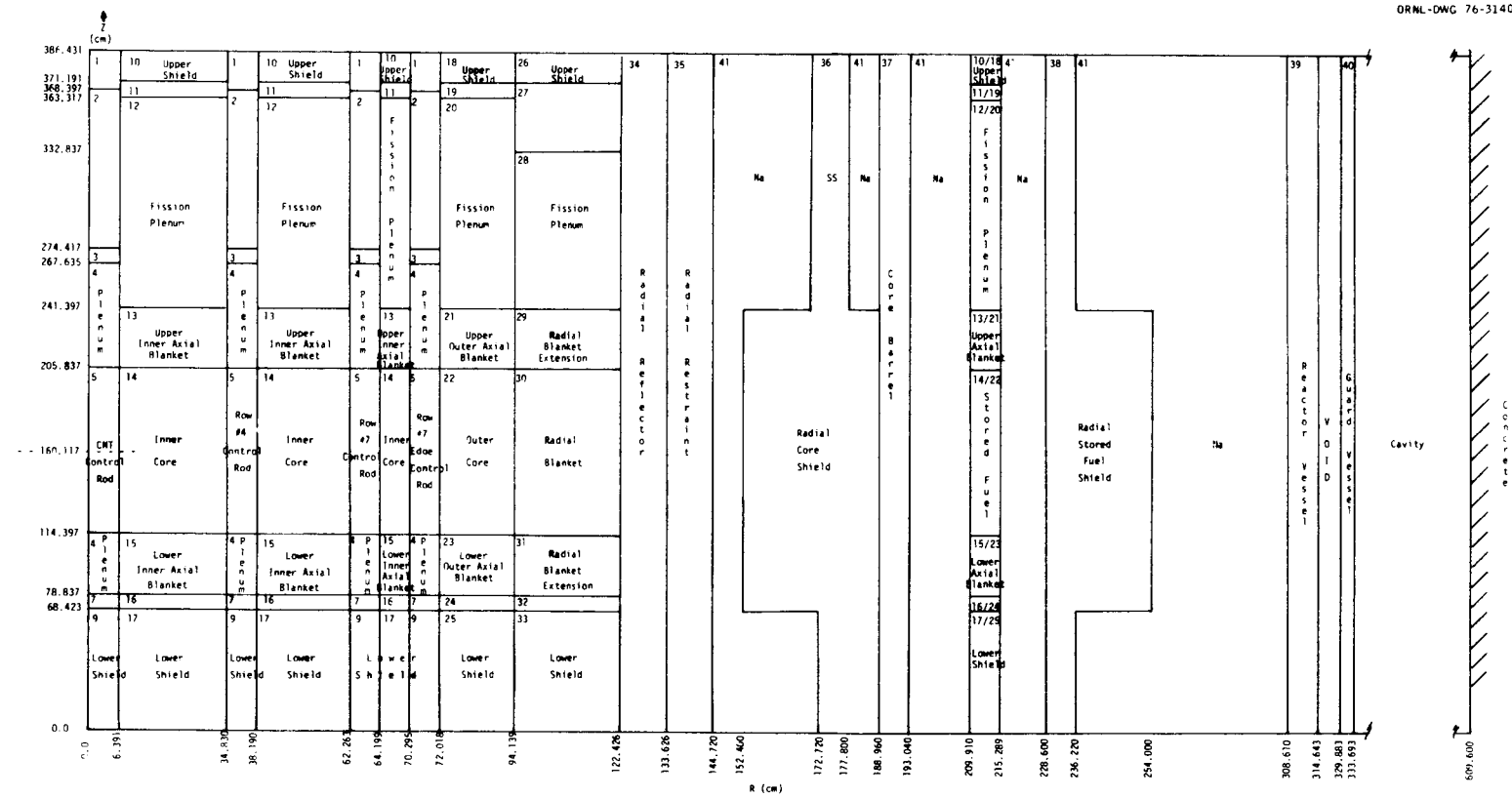


Fig. 10. Model Used for Calculations of Power Density of Beginning-of-Life Core.
 (Not to scale)

Table 3. Description of Regions Used in CRBR Calculations
for Beginning-of-Life Core^a

<u>Region No.</u>	<u>Component Description</u>
	Control rods
1	Collar
2	Travel region
3	Upper transition
4	Helium plenum
5	Natural boron (center rod)
6	40% enriched boron (other rods)
7	Lower transition
8	Sodium-filled channel
9	Lower shield
	Inner core fuel assembly
10	Upper shield
11	Upper transition
12	Fission plenum
13	Upper inner axial blanket
14	Inner core
15	Lower inner axial blanket
16	Lower transition
17	Lower shield
	Outer fuel assembly
18	Upper shield
19	Upper transition
20	Fission plenum
21	Upper outer axial blanket
22	Outer core
23	Lower outer axial blanket
24	Lower transition
25	Lower shield
	Radial blanket assembly
26	Upper shield
27	Upper transition
28	Fission plenum
29	Upper radial blanket extension
30	Radial blanket
31	Lower radial blanket extension
32	Lower transition
33	Lower shield
34	Radial reflector
35	Radial restraint spring
36	Radial core barrel shield
37	Core barrel
38	Radial stored-fuel shield
39	Reactor vessel
40	Guard vessel
41	Sodium

^aSee also Figs. 9 and 10 and Tables 4-6.

Table 4. Atomic Densities of Plutonium and Uranium Isotopes in CRBR Beginning-of-Life Core and Blanket^a

Region	Atomic Densities					
	^{239}Pu	^{240}Pu	^{241}Pu	^{242}Pu	^{238}U	^{235}U
Inner Core (Region 14)	8.229(-4) ^b	2.9674(-4)	1.7555(-4)	5.407(-5)	5.8705(-3)	1.172(-5)
Outer Core (Region 22)	1.1927(-3)	4.3021(-4)	2.5427(-4)	7.834(-5)	5.2863(-3)	1.059(-5)
Radial Blanket (Region 30)					1.323(-2)	2.65(-5)
Upper Axial Blanket (Region 29)					7.633(-3)	1.53(-5)
Lower Axial Blanket (Region 31)					7.633(-3)	1.53(-5)

^aSee also Fig. 10 and Tables 5 and 6.

^bRead: 8.229×10^{-4} .

Table 5. Atomic Densities of Other Constituents in CRBR Beginning-of-Life Core and Blanket^a

Region	Atomic Densities				
	Na	O	Fe	Cr	Ni
Inner Core (Region 14)	8.865(-3) ^b	1.433(-2)	1.416(-2)	3.642(-3)	2.277(-3)
Outer Core (Region 22)	8.916(-3)	1.438(-2)	1.416(-2)	3.642(-3)	2.277(-3)
Radial Blanket (Region 30)	5.451(-3)	2.625(-2)	9.689(-3)	2.492(-3)	1.558(-3)
Upper Axial Blanket (Region 29)	7.928(-3)	1.514(-2)	1.636(-2)	4.207(-3)	2.63(-3)
Lower Axial Blanket (Region 31)	8.450(-3)	1.514(-2)	1.636(-2)	4.207(-3)	2.63(-3)

^aSee also Fig. 6 and Tables 2 and 4.

^bRead: 8.865×10^{-3} .

Table 6. Compositions of Control Rods in
CRBR Beginning-of-Life Core^a

Nuclide	Atomic Densities		
	Natural Boron Rod (Central Rod)	40% Enriched Boron Rod (Offset Rod)	Na-Filled Channel
Na	7.334(-3) ^b	7.334(-3)	2.053(-2)
C	9.072(-3)	9.206(-3)	
¹⁰ B	7.177(-3)	1.473(-2)	
¹¹ B	2.911(-2)	2.209(-2)	
Fe	1.709(-2)	1.709(-2)	5.814(-3)
Cr	4.40(-3)	4.40(-3)	1.497(-3)
Ni	2.75(-3)	2.75(-3)	9.335(-4)

^aSee also Fig. 6 and Tables 2 and 3.

^bRead: 7.334 x 10⁻³.

Table 7. Composition of Various Components in and
Near CRBR Beginning-of-Life Core

Component	Atomic Densities						
	Na	C	Fe	Cr	Ni	Mn	Si
Pool Sodium	2.186(-2) ^a						
Stainless Steel 304			5.96(-2)	1.74(-2)	7.70(-3)	1.30(-3)	
Carbon Steel 508		8.2(-4)	8.176(-2)	3.2(-4)		5.3(-4)	4.3(-4)
Radial Reflector	2.6567(-3)		5.385(-2)	1.553(-2)	7.421(-3)		
Radial Restraint			1.246(-2)	1.529(-2)	5.925(-2)		

^aRead: 2.186 x 10⁻².

Table 8. Volume Percentages of Sodium and Type 304 Stainless Steel Assumed for Various Regions in CRBR Calculations for Beginning-of-Life Core^a

Region No.	Volume Percent		Region No.	Volume Percent	
	Steel	Na		Steel	Na
1	44	56	17	80	20
2	16	84	18	60	40
3	67	33	19	30	70
4	37	27	20	34	28
7	58	42	24	37	63
9	92	8	25	80	20
10	60	40	26	60	40
11	30	70	27	10	90
12	34	28	28	34	28
16	37	63	32	37	63
			33	80	20

^aSee Table 3 for region descriptions.

3.2. Neutron Fluxes and Dose Rates Throughout Assembly

The results from the core power density calculation were used as the source for calculations of the neutron fluxes and dose rates throughout the full geometry depicted in Fig. 9, that is, radially through 1 ft of the concrete cavity wall and axially up through the vessel head. In order to cover such a large region, it was necessary to use coarse spatial and angular grids and thus the calculations must be considered to be crude; however, they did yield order-of-magnitude results which served as a basis for later design changes.

These full-assembly calculations used an S_6 quadrature, P_1 scattering, and the 50-group cross-section library. The compositions of the ordinary and magnetite concretes used are given in Table 9, and the resulting neutron isoflux and isodose plots are shown in Figs. 11 and 12 respectively. The peak neutron dose rate on the reactor head, occurring directly above

Table 9. Compositions of Concretes Used in CRBR Calculations

Constituent	Atomic Densities	
	Ordinary Concrete	Magnetite Concrete
Na	0.1050(-2) ^a	
O	0.4385(-1)	0.4379(-1)
Si	0.1580(-1)	0.1640(-2)
Mg	0.1400(-3)	0.2700(-3)
Fe	0.3100(-3)	0.2008(-1)
H	0.7860(-2)	0.7170(-2)
Al	0.2390(-2)	0.1380(-2)
Ca	0.2920(-2)	0.2470(-2)
K	0.6900(-3)	
C		0.6000(-4)

^aRead: 0.1050×10^{-2} .

the support strap, was 2.56×10^{-4} mrem/hr, which was well below the criterion of a maximum of 2 mrem/hr.

In these calculations the power of the stored fuel was not considered; therefore the plots shown in Figs. 11 and 12 do not exhibit streaming effects in the reactor cavity due to stored-fuel neutrons escaping from the side of the reactor vessel. In fact, the fluxes and dose rates in the cavity are lower than they would be if the stored fuel were not present, since additional attenuation of the core neutrons within the reactor vessel is effected both in the stored fuel and in the stored-fuel shield. It was recognized that in future calculations the production of neutrons in the stored fuel during reactor operations would have to be considered. In the meantime, however, the influence of the stored fuel on the ex-vessel monitoring system for the shutdown reactor became of concern. As a result, a separate study was conducted⁷ to determine the effect of neutrons produced by spontaneous fission of plutonium and by the oxygen (α, n) reaction on the ex-vessel ^{235}U fission detectors serving as neutron-flux

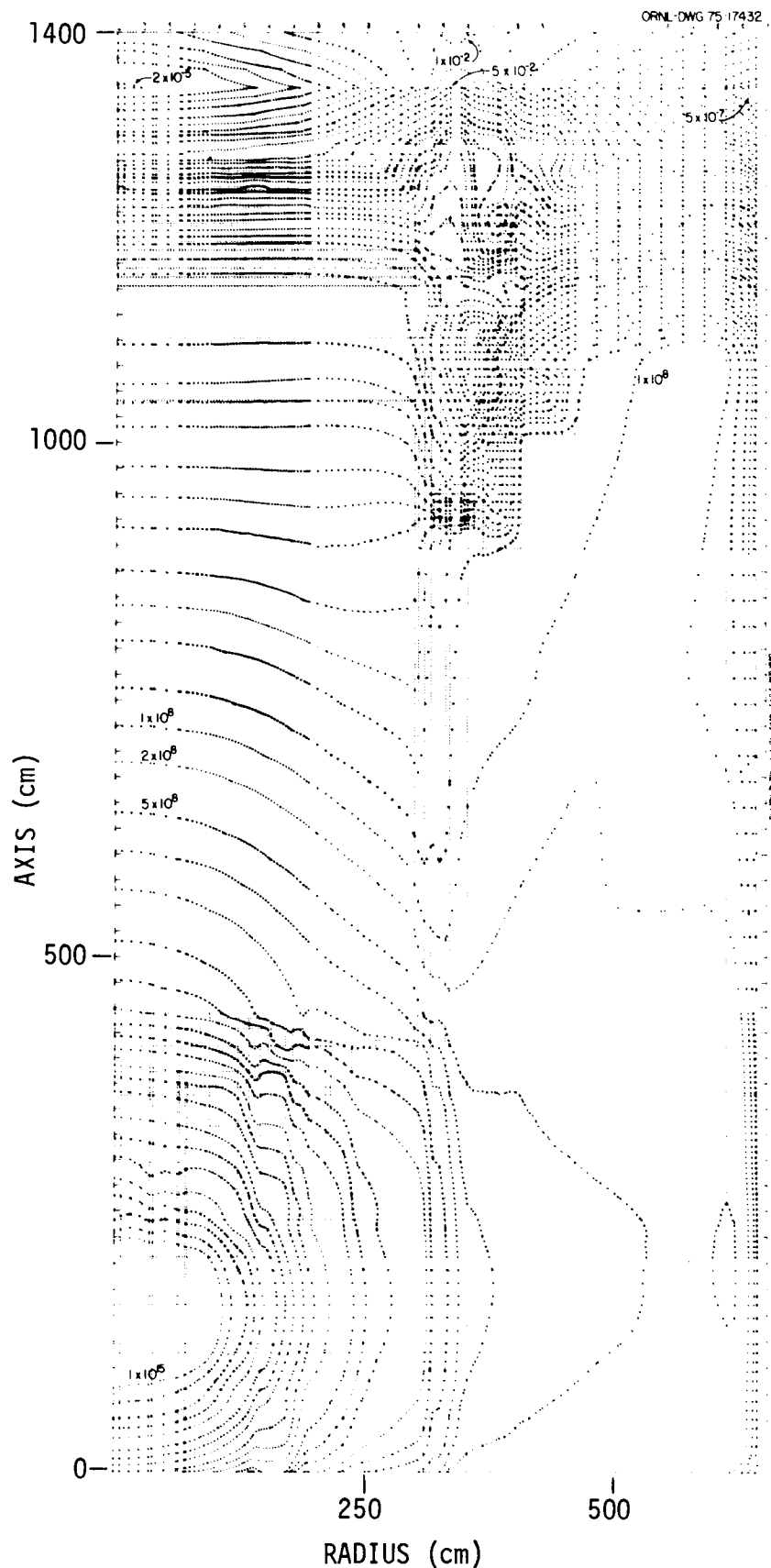


Fig. 11. Total Neutron Fluxes Calculated for Early CRBR Model with Attenuation in Stored Fuel and Stored Fuel Shield Included. See Fig. 9 for geometry. Units are $\text{neutrons} \cdot \text{cm}^{-2} \cdot \text{sec}^{-1}$.

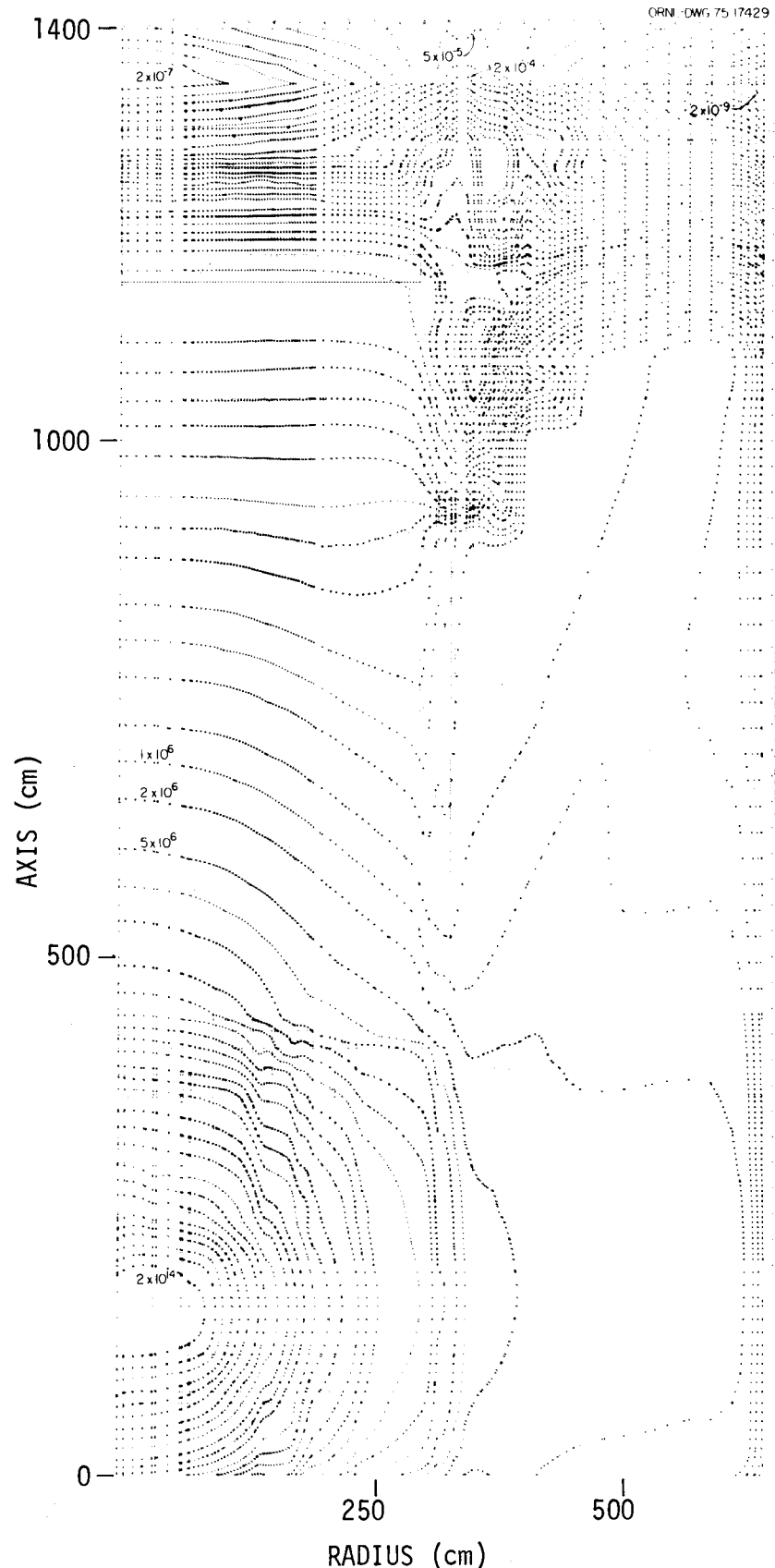


Fig. 12. Neutron Dose Rates Calculated for Early CRBR Model with Attenuation in Stored Fuel and Stored-Fuel Shield Included. See Fig. 9 for geometry. Units are mrem/hr; peak dose rate on head is 2.56×10^{-4} mrem/hr at $R = 347$ cm (see X).

monitors during reactor shutdown. These detectors are located in the core horizontal midplane just outside the guard vessel. This study indicated that an unacceptably high ratio of stored-fuel neutrons to core neutrons existed at these positions and resulted in a decision not to routinely store fuel in the reactor vessel.

Following this decision, the full-assembly calculations were repeated for the model but with both the stored fuel and the stored-fuel shield removed. The results are plotted in Figs. 13 and 14. While the fluxes and dose rates in the reactor cavity were higher due to the removal of the stored fuel and its shield, the peak dose rate on the reactor head was substantially unchanged. This would seem to indicate that the peak dose rate was due to neutrons penetrating upward through the reactor vessel, but as pointed out above, the calculation was too crude for detailed analysis to be meaningful.

3.3. Activation Gamma-Ray Dose Rates at Ex-Vessel Detectors

The next group of calculations in this early CRBR series was performed to determine the effect of after-shutdown gamma rays on the ex-vessel detectors comprising the reactor's neutron-monitoring system. The ex-vessel detectors are contained in three modules positioned symmetrically outside the guard vessel in the reactor's horizontal mid-plane. At the time these calculations were performed, each module consisted of five ^{235}U fission chambers embedded in graphite. The concern was that after-shutdown gamma rays might overpower the fission chambers, and a maximum dose rate of 1.3×10^6 r/hr at the detectors had been established.

In the first two calculations, the gamma-ray fluxes produced by the activation of cobalt and tantalum were determined, both these materials being present in the system as impurities in the stainless steel components. The procedure was first to assume that each element was distributed throughout the full system at the same density at which it occurred in stainless steel, and then to calculate the activation of

each element by the neutron fluxes from the run described above. Then those gamma-ray sources along a radius in the core midplane that corresponded to locations of the stainless steel at the midplane were used as distributed sources in one-dimensional ANISN calculations of the activation gamma-ray dose rates at the ex-vessel detector positions. The results are plotted in Fig. 15, along with similar calculations of the activation gamma-ray dose rates due to the sodium coolant. In these calculations the graphite, which simulated the detector box, was assumed to have a mass density of 1.85 g/cc and an atomic density of 0.9275×10^{-1} atoms**barn** $^{-1} \cdot \text{cm}^{-1}$.

In another calculation the sodium activation gamma-ray dose rates throughout the system were determined from an additional DOT run in which it was assumed that an activation source of 22 mCi/cm³ was distributed uniformly throughout the sodium. The results are shown in Fig. 16, in which the ex-vessel detector location is marked by the "X."

Since ^{24}Na decays with a 15-hr half-life, it was not anticipated that sodium activation gamma rays would present a problem of any duration. The plots in Figs. 15 and 16 indicate that they will not create a problem at all, the maximum dose rate in the ex-vessel region due to this source being 2×10^3 r/hr. The tantalum and cobalt gamma-ray dose rates are also well below the criterion, not exceeding 7×10^1 and 2×10^2 r/hr, respectively. The maximum total dose rate from the three sources would be 2.3×10^3 r/hr -- well below the criterion for the fission detector.

4. FULL-ASSEMBLY CALCULATIONS FOR REVISED CRBR MODEL

With the elimination of the stored-fuel source from the reactor vessel, it no longer appeared mandatory that the CRBR design include the magnetite concrete shield or the B₄C collar in the reactor cavity and they were therefore eliminated. Concomitantly a vessel support system evolved which was simpler in design and resulted in the concrete support ledge being moved closer to the reactor vessel (compare sketches A and B in Fig. 3). With such major changes, a new series of calculations was

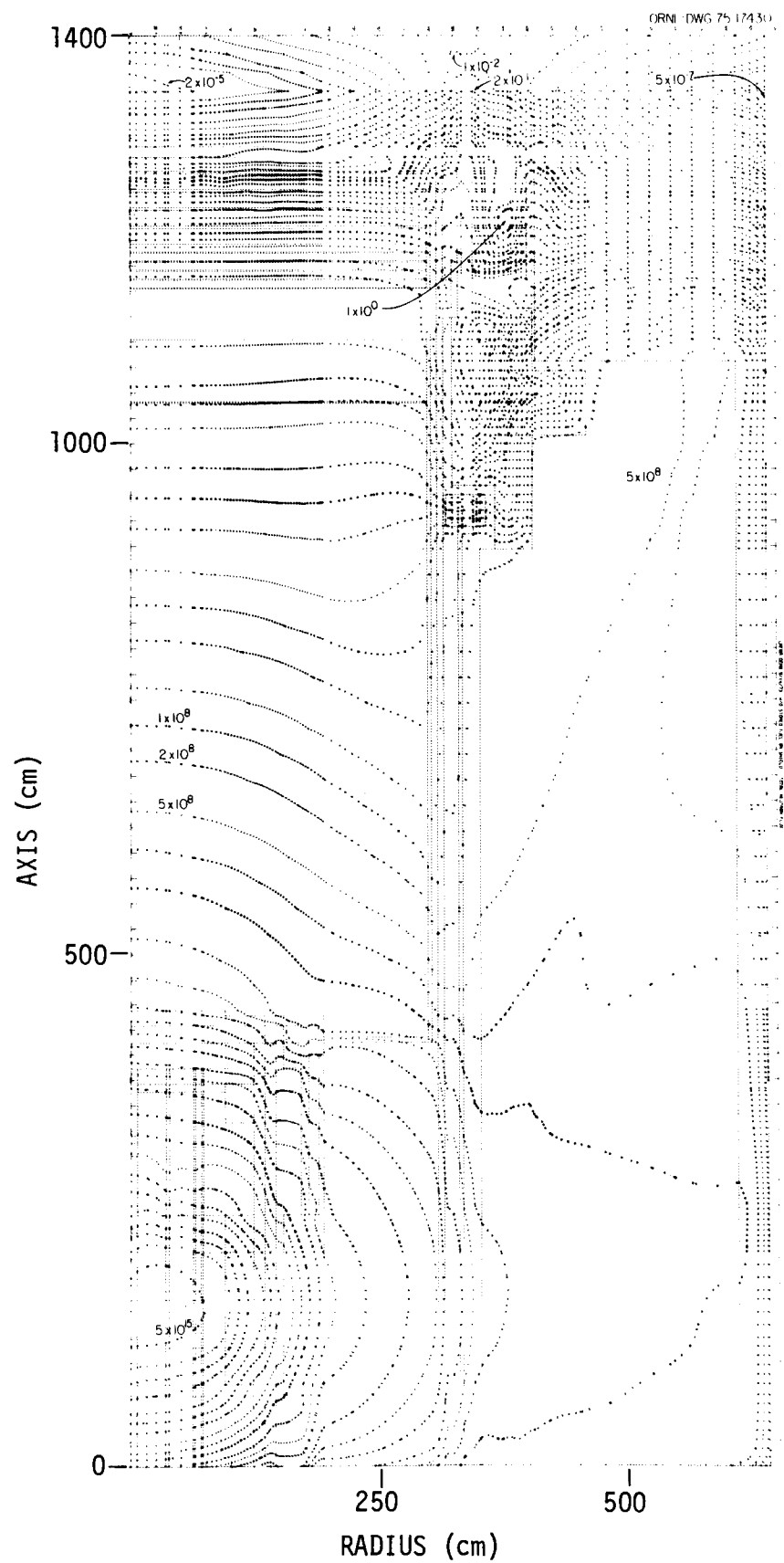


Fig. 13. Neutron Fluxes Calculated for Early CRBR Model Without Stored Fuel and Stored-Fuel Shield. Units are $\text{neutrons} \cdot \text{cm}^{-2} \cdot \text{cm}^{-1}$.

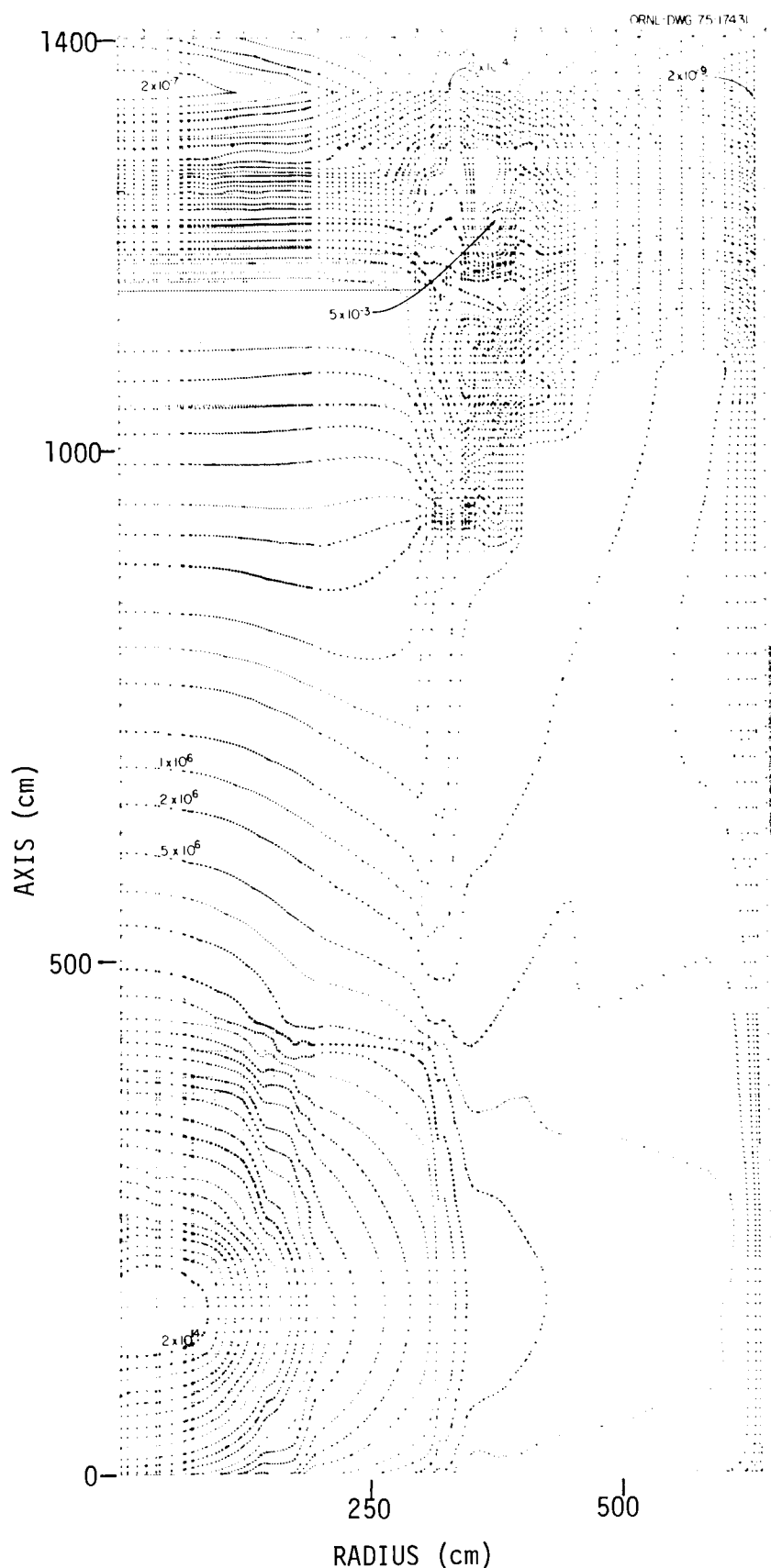


Fig. 14. Neutron Dose Rates Calculated for Early CRBR Model Without Stored Fuel and Stored-Fuel Shield. Units are mrem/hr; peak dose rate on head is $\sim 2 \times 10^{-4}$ at $R = 340$ cm (see X).

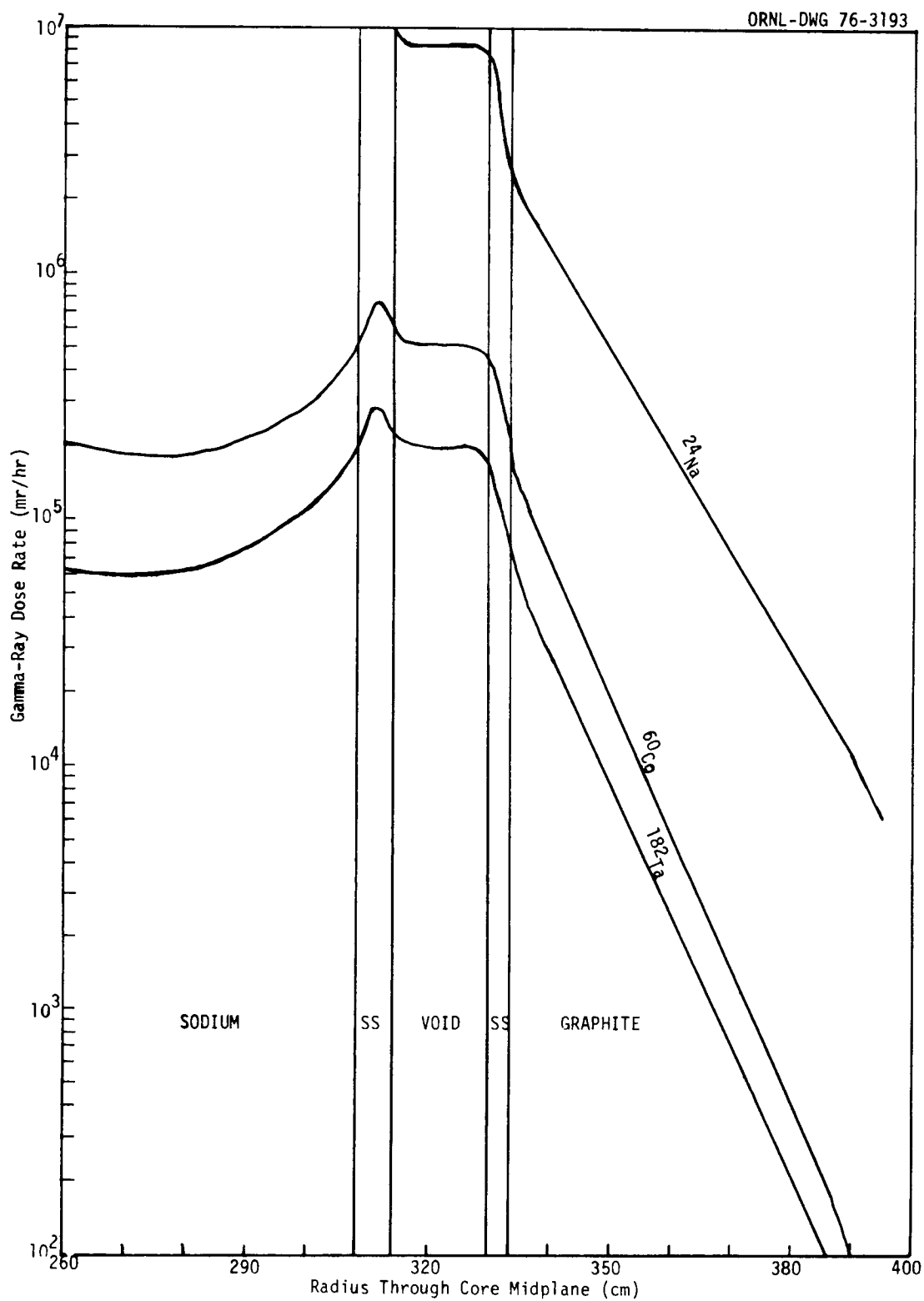


Fig. 15. Gamma-Ray Dose Rates in CRBR Horizontal Midplane Due to Activation of ^{24}Na , ^{60}Co , and ^{182}Ta .

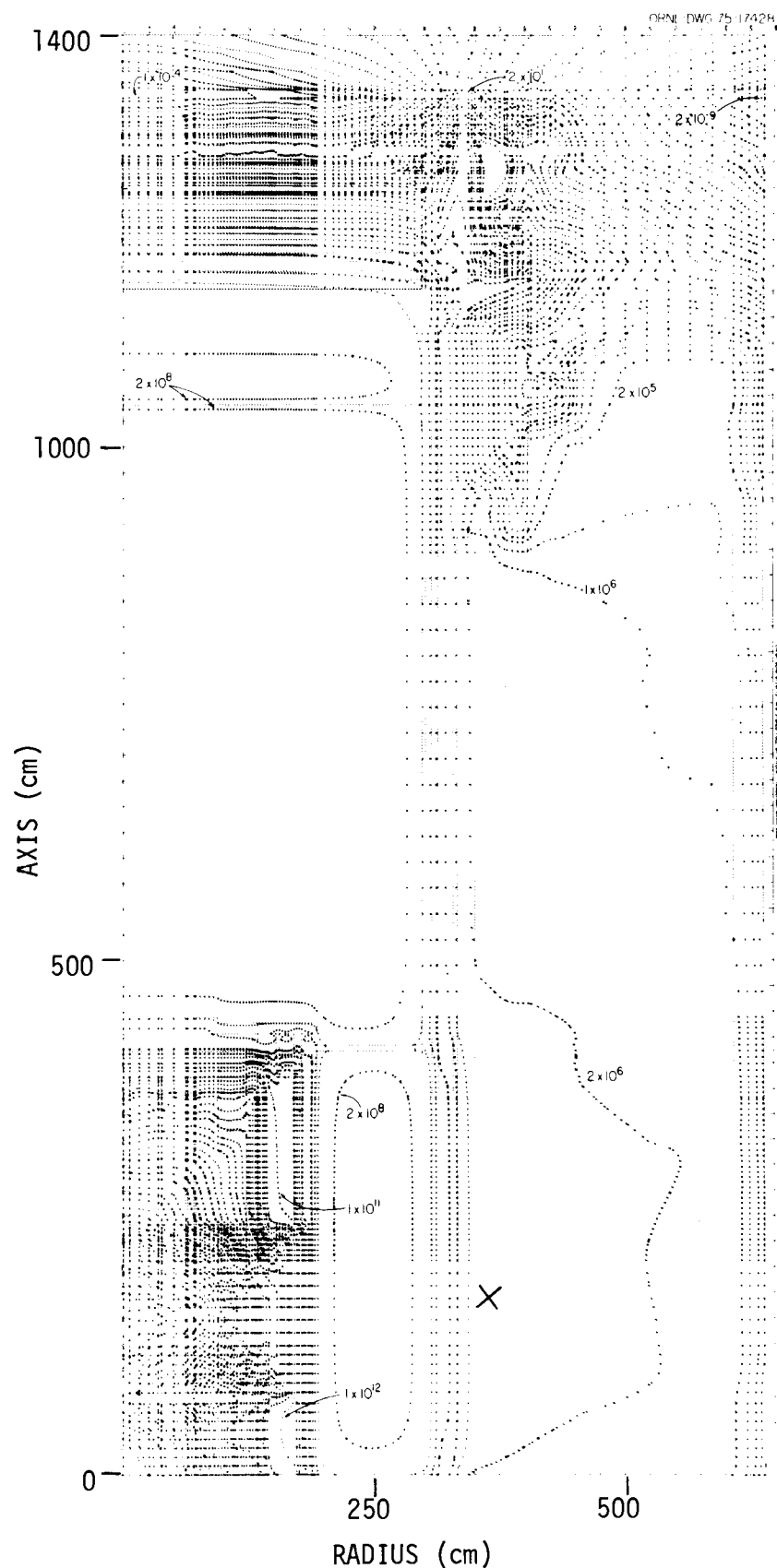


Fig. 16. Sodium-Activation Gamma-Ray Dose Rates Calculated for Early CRBR Model. Location of the ex-vessel detector is indicated by X. Units are mrem/hr.

necessary. Also, by this time (mid-1974) the new CRBR coupled cross-section library containing 51 neutron groups and 25 gamma-ray groups had been developed with the energy structure shown in Table 10. In addition, we had available the definition of the end-of-cycle "equilibrium core," which for shielding analyses presents the worst case.

Table 10. Energy Structure of Coupled Cross-Section Set Containing 51 Neutron Groups and 25 Gamma-Ray Groups

Group No.	Neutron Upper Energy (eV)	Group No.	Neutron Upper Energy (eV)	Group No.	Gamma-Ray Upper Energy (MeV)
1	1.4918(7) ^a	27	5.2475(4)	52	13.0000
2	1.2214(7)	28	4.0868(4)	53	10.1970
3	1.0000(7)	29	3.1828(4)	54	7.9983
4	8.1873(6)	30	2.4788(4)	55	6.2737
5	6.7032(6)	31	1.9305(4)	56	4.9210
6	5.4881(6)	32	1.5034(4)	57	3.8599
7	4.4933(6)	33	7.1017(4)	58	3.0277
8	3.6788(6)	34	4.3074(3)	59	2.3748
9	3.0119(6)	35	3.3546(3)	60	1.8628
10	2.4660(6)	36	2.6126(3)	61	1.4611
11	2.0190(6)	37	2.0347(3)	62	1.14610
12	1.6530(6)	38	1.5846(3)	63	0.89896
13	1.3534(6)	39	1.2341(3)	64	0.70513
14	1.1080(6)	40	9.6112(2)	65	0.55309
15	9.0718(5)	41	4.5400(2)	66	0.43383
16	7.4274(5)	42	2.1445(2)	67	0.34029
17	6.0810(5)	43	1.1030(2)	68	0.26692
18	4.9787(5)	44	4.7851(1)	69	0.20937
19	4.0762(5)	45	2.2603(1)	70	0.16422
20	3.3373(5)	46	1.0677(1)	71	0.12881
21	2.7324(5)	47	5.0435(0)	72	0.101040
22	2.2371(5)	48	2.3824(0)	73	0.079252
23	1.8316(5)	49	1.1254(0)	74	0.062164
24	1.4996(5)	50	4.1399(-1)	75	0.048760
25	1.2277(5)	51 ^b	1.0000(-1)	76 ^c	0.038247
26	8.6517(4)				

^aRead: 1.4918×10^7 eV.

^bLower limit is thermal energy.

^cLower limit is 0.030000 MeV.

4.1. Power Density of Equilibrium Core

The revised core composition and the new cross-section set prompted a new S₄P₁ DOT calculation of the core power density for use as the source in subsequent calculations. The geometry of the calculational model, shown in Figs. 17 and 18, extended axially from approximately 35 cm below the lower blanket to about 56 cm above the upper blanket and radially through two rows of the removable radial shield. The specific regions in the model are identified in Table 11, the many core and blanket zones accounting for variations of fuel and blanket burnup. The atomic densities of the materials in the various regions are given in Tables 12-15, and the volume percentages of steel (or inconel) and sodium are presented in Table 16. The k_{eff} value from this calculation is 0.996.

4.2. Neutron Fluxes and Dose Rates in Lower Axial Region

With the power density determined above, a DOT S₆P₁ calculation was performed for the region below the core, using the geometry shown in Figs. 19 and 20. Axially the geometry extended from the top of the upper axial blanket to the bottom of the lower support structure region 1, and radially it extended through the guard vessel. The various regions included in the calculation are identified in Table 11, and their compositions are given in Table 16. The critical area defined by WARD is the top of the modular inlet assembly (region 67), for which the damage criteria are a lifetime of 30 years with a 5% residual ductility.

The neutron flux and dose-rate distributions calculated for this region are presented in Figs. 21 and 22 respectively, and the spectrum of the neutrons incident on the modular inlet assembly is shown in Fig. 23. On the basis of these results, WARD determined that the modular inlet assembly would meet the lifetime requirement.

ORNL-DWG 75-18106RI

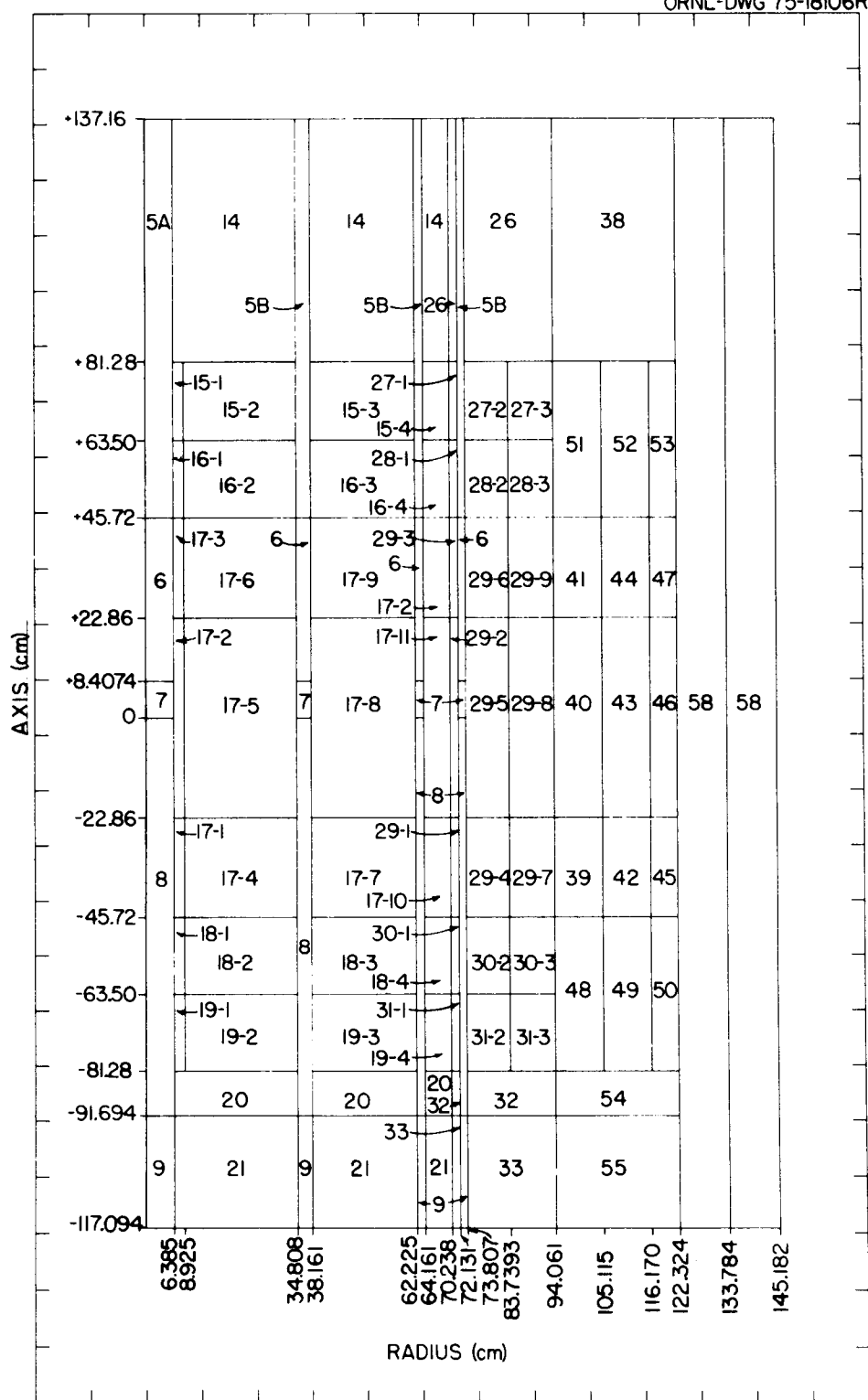


Fig. 17. Model Used for Calculations of Power Density of Equilibrium Core. See region descriptions in Table 11; see also Fig. 18.

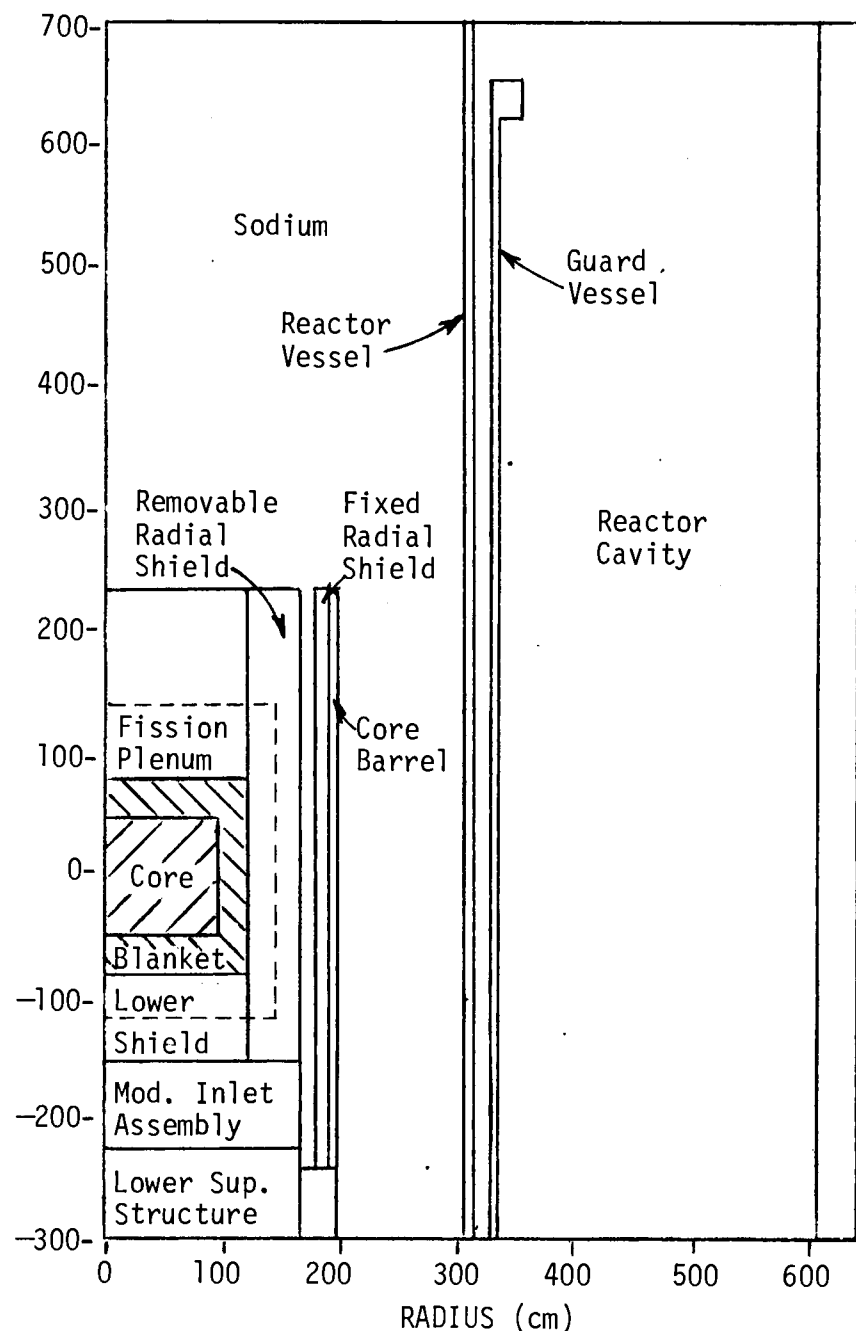


Fig. 18. Sketch Showing Dashed Outline of Region Included in Power Density Calculation for Equilibrium Core. See also Fig. 17.

Table 11. Description of Regions Used in CRBR Calculations
for Equilibrium Core^a

Region No.	Component Description
	Control rods
1	Outlet nozzle
2	Travel region
3	Upper transition
4	Upper helium plenum
5a	Natural B ₄ C
5b	50% enriched B ₄ C
6	Lower helium plenum
7	Lower transition
8	Sodium filled
9	Lower axial shield
10	Orifice region
11	Inlet/orifice transition
	Inner core fuel assembly ^b
12	Outlet nozzle
13	Upper transition
14	Fission plenum
15,16	Upper axial blanket
17	Inner core
18,19	Lower axial blanket
20	Lower transition
21	Lower axial shield
22	Orifice region
23	Inlet/orifice transition
	Outer core fuel assembly ^b
24	Outlet nozzle
25	Upper transition
26	Fission plenum
27,28	Upper axial blanket
29	Outer core
30,31	Lower axial blanket
32	Lower transition
33	Lower axial shield
34	Orifice region
35	Inlet/orifice transition
	Radial blanket assembly
36	Outlet nozzle
37	Upper transition
38	Fission plenum
39-47	Blanket zones 1 - 9
48-53	Extension zones 1 - 6
54	Lower transition
55	Lower axial shield
56	Orifice region
57	Inlet/orifice transition

Table 11. (Cont'd.)

Region No.	Component Description
58	Removable radial shield assembly
59	Sodium regions
60	Fixed radial shield
61	Core barrel
62	Reactor vessel
63	Void regions
64	Guard vessel
65	Primary concrete shield
66	Core-former ring
67	Modular inlet assembly
68	Lower support structure
69	Region 1
70	Liner inlet
71,72	Sodium
	Regions 2, 3
73	Horizontal baffle plate
74	Sodium ($0.02186 \text{ atoms} \cdot \text{barn}^{-1} \cdot \text{cm}^{-1}$)
75	Suppressor plate
76	Void
77	Thermal reflector plates
78	Reactor vessel head shield ^b
79	Inconel 750
80	Type 304 stainless steel
	Carbon steel
81	Reactor vessel closure head
82	Thermal liner

^aSee also Fig 14 and Tables 12-16.

^bIn later designs, Regions 78 and 79 were taken to be carbon steel SA508.

Table 12. Atomic Densities of Plutonium and Uranium Isotopes and Fission Products
in CRBR Equilibrium Core and Blanket^a

Region	Region No.	Atomic Densities ^b						Fission Products
		²³⁹ Pu	²⁴⁰ Pu	²⁴¹ Pu	²⁴² Pu	²³⁸ U	²³⁵ U	
Inner Core	17-1	0.8705(-3) ^c	0.3712(-3)	0.9223(-4)	0.4488(-4)	0.5029(-2)	0.6027(-5)	0.6008(-3)
	17-2	0.8465(-3)	0.3627(-3)	0.8576(-4)	0.4459(-4)	0.4964(-2)	0.5521(-5)	0.6968(-3)
	17-3	0.9084(-3)	0.3469(-3)	0.1005(-3)	0.4313(-4)	0.5154(-2)	0.7288(-5)	0.4742(-3)
	17-4	0.8781(-3)	0.3604(-3)	0.9360(-4)	0.4417(-4)	0.5061(-2)	0.6361(-5)	0.5770(-3)
	17-5	0.8416(-3)	0.3637(-3)	0.8543(-4)	0.4460(-4)	0.4957(-2)	0.5458(-5)	0.7071(-3)
	17-6	0.9043(-3)	0.3484(-3)	0.1002(-3)	0.4318(-4)	0.5148(-2)	0.7225(-5)	0.4817(-3)
	17-7	0.8984(-3)	0.3513(-3)	0.9895(-4)	0.4338(-4)	0.5132(-2)	0.7052(-5)	0.5000(-3)
	17-8	0.8719(-3)	0.3494(-3)	0.9264(-4)	0.4350(-4)	0.5070(-2)	0.6459(-5)	0.5894(-3)
	17-9	0.9290(-3)	0.3359(-3)	0.1074(-3)	0.4204(-4)	0.5231(-2)	0.8135(-5)	0.3893(-3)
	17-10	0.9156(-3)	0.3424(-3)	0.1042(-3)	0.4254(-4)	0.5194(-2)	0.7715(-5)	0.4321(-3)
	17-11	0.9020(-3)	0.3303(-3)	0.1014(-3)	0.4191(-4)	0.5184(-2)	0.7651(-5)	0.4697(-3)
	17-12	0.9522(-3)	0.3205(-3)	0.1154(-3)	0.4062(-4)	0.5312(-2)	0.9140(-5)	0.2993(-3)
Outer Core	29-1	0.1215(-2)	0.4868(-3)	0.1539(-3)	0.6134(-4)	0.4581(-2)	0.6985(-5)	0.5548(-3)
	29-2	0.1196(-2)	0.4707(-3)	0.1501(-3)	0.6047(-4)	0.4573(-2)	0.6925(-5)	0.6029(-3)
	29-3	0.1308(-2)	0.4609(-3)	0.1701(-3)	0.5874(-4)	0.4679(-2)	0.8178(-5)	0.3886(-3)
	29-4	0.1246(-2)	0.4759(-3)	0.1593(-3)	0.6024(-4)	0.4616(-2)	0.7411(-5)	0.5011(-3)
	29-5	0.1211(-2)	0.4683(-3)	0.1533(-3)	0.6001(-4)	0.4590(-2)	0.7135(-5)	0.5719(-3)
	29-6	0.1317(-2)	0.4603(-3)	0.1722(-3)	0.5848(-4)	0.4688(-2)	0.8298(-5)	0.3707(-3)
	29-7	0.1301(-2)	0.4709(-3)	0.1690(-3)	0.5942(-4)	0.4666(-2)	0.8019(-5)	0.3970(-3)
	29-8	0.1259(-2)	0.4715(-3)	0.1615(-3)	0.5986(-4)	0.4630(-2)	0.7580(-5)	0.4788(-3)
	29-9	0.1347(-2)	0.4623(-3)	0.1776(-3)	0.5831(-4)	0.4710(-2)	0.8590(-5)	0.3114(-3)
Radial Blanket	39	0.2280(-3)	0.4824(-5)	0.8484(-7)	0.6970(-9)	0.1291(-1)	0.2444(-4)	0.3737(-4)
	40	0.2845(-3)	0.7429(-5)	0.1533(-6)	0.1593(-8)	0.1284(-1)	0.2332(-4)	0.5419(-4)
	41	0.1962(-3)	0.3519(-5)	0.5298(-7)	0.3678(-9)	0.1295(-1)	0.2509(-4)	0.3013(-4)
	42	0.4124(-3)	0.1954(-4)	0.8382(-6)	0.1430(-7)	0.1267(-1)	0.2058(-4)	0.8336(-4)
	43	0.5006(-3)	0.2927(-4)	0.1477(-5)	0.3214(-7)	0.1253(-1)	0.1878(-4)	0.1217(-3)
	44	0.3559(-3)	0.1420(-4)	0.5221(-6)	0.7398(-8)	0.1275(-1)	0.2175(-4)	0.6433(-4)
	45	0.4700(-3)	0.2879(-4)	0.1788(-5)	0.3971(-7)	0.1258(-1)	0.1918(-4)	0.1045(-3)
	46	0.5646(-3)	0.4277(-4)	0.3172(-5)	0.7577(-7)	0.1242(-1)	0.1719(-4)	0.1524(-3)
	47	0.4077(-3)	0.2112(-4)	0.1127(-5)	0.1765(-7)	0.1268(-1)	0.2050(-4)	0.8020(-4)
Radial Blanket Extension	48	0.1010(-3)	0.1188(-5)	0.1596(-7)	0.6297(-10)	0.1308(-1)	0.2693(-4)	0.7563(-5)
	49	0.1902(-3)	0.4669(-5)	0.1329(-6)	0.1072(-8)	0.1298(-1)	0.2496(-4)	0.1768(-4)
	50	0.2221(-3)	0.6928(-5)	0.2633(-6)	0.2429(-8)	0.1294(-1)	0.2418(-4)	0.2256(-4)
	51	0.7853(-4)	0.6950(-6)	0.6883(-8)	0.2053(-10)	0.1310(-1)	0.2739(-4)	0.5425(-5)
	52	0.1487(-3)	0.2774(-5)	0.5987(-7)	0.3594(-9)	0.1302(-1)	0.2586(-4)	0.1204(-4)
	53	0.1749(-3)	0.4198(-5)	0.1236(-6)	0.8504(-9)	0.1299(-1)	0.2523(-4)	0.1527(-4)
Upper Axial Blanket	16-1	0.2154(-3)	0.8061(-5)	0.2560(-6)	0.3493(-8)	0.7273(-2)	0.1245(-4)	0.3894(-4)
	16-2	0.1992(-3)	0.6721(-5)	0.1955(-6)	0.2486(-8)	0.7294(-2)	0.1273(-4)	0.3489(-4)
	16-3	0.1610(-3)	0.4173(-5)	0.9188(-7)	0.8881(-9)	0.7344(-2)	0.1350(-4)	0.2523(-4)
	16-4	0.1240(-3)	0.2251(-5)	0.3167(-7)	0.2148(-9)	0.7390(-2)	0.1425(-4)	0.1842(-4)
	15-1	0.1046(-3)	0.2252(-5)	0.1016(-6)	0.7201(-9)	0.7419(-2)	0.1448(-4)	0.8405(-5)
	15-2	0.8585(-4)	0.1445(-5)	0.4911(-7)	0.2794(-9)	0.7440(-2)	0.1488(-4)	0.6182(-5)
	15-3	0.7169(-4)	0.1009(-5)	0.2917(-7)	0.1349(-9)	0.7457(-2)	0.1516(-4)	0.4723(-5)
	15-4	0.6111(-4)	0.7212(-6)	0.1711(-7)	0.6566(-10)	0.7468(-2)	0.1539(-4)	0.3849(-5)
	28-1	0.1167(-3)	0.1975(-5)	0.2572(-7)	0.1629(-9)	0.7398(-2)	0.1439(-4)	0.1737(-4)
	28-2	0.1158(-3)	0.2112(-5)	0.3381(-7)	0.2260(-9)	0.7400(-2)	0.1436(-4)	0.1652(-4)
	28-3	0.1029(-3)	0.1780(-5)	0.2966(-7)	0.1830(-9)	0.7417(-2)	0.1459(-4)	0.1264(-4)
	27-1	0.5793(-4)	0.6486(-6)	0.1463(-7)	0.5319(-10)	0.7472(-2)	0.1546(-4)	0.3582(-5)
	27-2	0.5721(-4)	0.6824(-6)	0.1818(-7)	0.6924(-10)	0.7473(-2)	0.1544(-4)	0.3381(-5)
	27-3	0.4950(-4)	0.5398(-6)	0.1408(-7)	0.4812(-10)	0.7481(-2)	0.1557(-4)	0.2616(-5)
Lower Axial Blanket	19-1	0.2054(-3)	0.1070(-4)	0.1504(-5)	0.2754(-7)	0.7302(-2)	0.1206(-4)	0.2838(-4)
	19-2	0.1924(-3)	0.9133(-5)	0.1142(-5)	0.1898(-7)	0.7320(-2)	0.1240(-4)	0.2490(-4)
	19-3	0.1647(-3)	0.6637(-5)	0.7045(-6)	0.9675(-8)	0.7357(-2)	0.1302(-4)	0.1860(-4)
	19-4	0.1391(-3)	0.4742(-5)	0.4287(-6)	0.4852(-8)	0.7390(-2)	0.1357(-4)	0.1379(-4)
	18-1	0.3221(-3)	0.2326(-4)	0.1716(-5)	0.4551(-7)	0.7121(-2)	0.1005(-4)	0.7878(-4)
	18-2	0.3051(-3)	0.1961(-4)	0.1217(-5)	0.2917(-7)	0.7150(-2)	0.1049(-4)	0.7152(-4)
	18-3	0.2670(-3)	0.1454(-4)	0.7808(-6)	0.1564(-7)	0.7210(-2)	0.1126(-4)	0.5571(-4)
	18-4	0.2302(-3)	0.1063(-4)	0.5029(-6)	0.8385(-8)	0.7263(-2)	0.1197(-4)	0.4332(-4)
	31-1	0.1305(-3)	0.4169(-5)	0.3525(-6)	0.3706(-8)	0.7401(-2)	0.1376(-4)	0.1235(-4)
	31-2	0.1117(-3)	0.3015(-5)	0.2134(-6)	0.1871(-8)	0.7424(-2)	0.1419(-4)	0.9383(-5)
	31-3	0.8271(-4)	0.1614(-5)	0.8104(-7)	0.5050(-9)	0.7458(-2)	0.1485(-4)	0.5613(-5)
	30-1	0.2179(-3)	0.9435(-5)	0.4201(-6)	0.6543(-8)	0.7281(-2)	0.1222(-4)	0.3996(-4)
	30-2	0.1901(-3)	0.6873(-5)	0.2522(-6)	0.3289(-8)	0.7319(-2)	0.1281(-4)	0.3236(-4)
	30-3	0.1485(-3)	0.4005(-5)	0.1087(-6)	0.1052(-8)	0.7374(-2)	0.1368(-4)	0.2105(-4)

^aSee also Fig. 14 and Tables 13 and 14.

^bAtomic densities in atoms·barn⁻¹·cm⁻¹.

^cRead: 0.8705 × 10⁻³.

Table 13. Atomic Densities of Other Constituents in CRBR Equilibrium Core and Blanket^a

Region	Region Nos.	Atomic Densities ^b						
		Na	O	Fe	Cr	Ni	Mo	Mn
Inner Core	17	0.9188(-2) ^c	0.1388(-1)	0.1285(-1)	0.3730(-2)	0.2548(-2)	0.2888(-3)	0.3530(-3)
Outer Core	29	0.9200(-2)	0.1395(-1)	0.1285(-1)	0.3730(-2)	0.2548(-2)	0.2888(-3)	0.3530(-3)
Radial Blanket and Extension	39 - 53	0.5667(-2)	0.2642(-1)	0.8704(-2)	0.2527(-2)	0.1726(-2)	0.1956(-3)	0.2391(-3)
Upper Axial Blanket	16, 15, 28, 27	0.8506(-2)	0.1510(-1)	0.1393(-1)	0.4044(-2)	0.2763(-2)	0.3131(-3)	0.3827(-3)
Lower Axial Blanket	19, 18, 31, 30	0.9440(-2)	0.1513(-1)	0.1287(-1)	0.3736(-2)	0.2553(-2)	0.2893(-3)	0.3536(-3)

^aSee also Fig. 14 and Tables 12 and 14.^bAtomic Densities in atoms·barn⁻¹·cm⁻¹.^cRead: 0.9188 x 10⁻².Table 14. Compositions of Control Rods in
CRBR Equilibrium Core^a

Nuclide	Atomic Density ^b		
	Region 5A (Nat. Boron Rod)	Region 5B (50% Enriched Rods)	Region 8 (Rod Channel)
Na	0.7297(-2)	0.7419(-2)	0.2041(-1)
C	0.8223(-2)	0.8226(-2)	
¹⁰ B	0.6224(-2)	0.1574(-1)	
¹¹ B	0.2524(-1)	0.1574(-1)	
Fe	0.1801(-1)	0.1803(-1)	0.5201(-2)
Cr	0.5229(-2)	0.5233(-2)	0.1510(-2)
Ni	0.3572(-2)	0.3575(-2)	0.1032(-2)
Mo	0.4048(-3)	0.4052(-3)	0.1169(-3)
Mn	0.4949(-3)	0.4953(-3)	0.1429(-3)

^aSee also Fig. 14 and Tables 12 and 13.^bAtomic densities in atoms·barn⁻¹·cm⁻¹.

Table 15. Composition of Various Materials in and near CRBR Equilibrium Core

Material	Atomic Density ^a					
	C	Fe	Cr	Ni	Mo	Mn
Stainless Steel 304		0.5960(-1) ^b	0.1740(-1)	0.7700(-2)		0.1300(-2)
Stainless Steel 316		0.5548(-1)	0.1617(-1)	0.1104(-1)	0.1255(-2)	0.1753(-2)
Carbon Steel SA508	0.1040(-2)	0.8380(-1)				0.7760(-3)
Inconel 750		0.8450(-2)	0.1481(-1)	0.6261(-1)		0.9042(-3)

^aAtomic densities in atoms·barn⁻¹·cm⁻¹.^bRead: 0.5960 × 10⁻¹.Table 16. Volume Percentages of Sodium, Stainless Steel, Carbon Steel, and Inconel Assumed for Various Regions in CRBR Calculations for Equilibrium Core^a

Region No.	Volume Percent Steel/Inconel	Region No.	Volume Percent Steel/Inconel
1	44(316) ^b	56	55
2	16	84	56
3	67	33	57
4	37	27	58
6	37	27	59
7	58	42	
9	73	27	60
10	36	64	73(316) ^b
11	38	62	36
12	44	56	38
13	19	81	62
14	23	41	64
20	28	72	58
21	73	27	64
22	36	64	66
23	38	62	80
24	44	56	100
25	19	81	100
26	23	41	100
32	28	72	74
33	73	27	75
34	36	64	100
35	38	62	77
36	44	56	100
37	10	90	80
38	34	28	81
54	37	63	100
		78	100(Inconel)

^aSee Table 11 for region descriptions.^bType 316 stainless steel for those regions identified here with numbers between 1 and 59.^cType 304 stainless steel for those regions identified here with numbers between 60 and 77 or with 79 and 82.^dCarbon steel for regions 80 and 81.

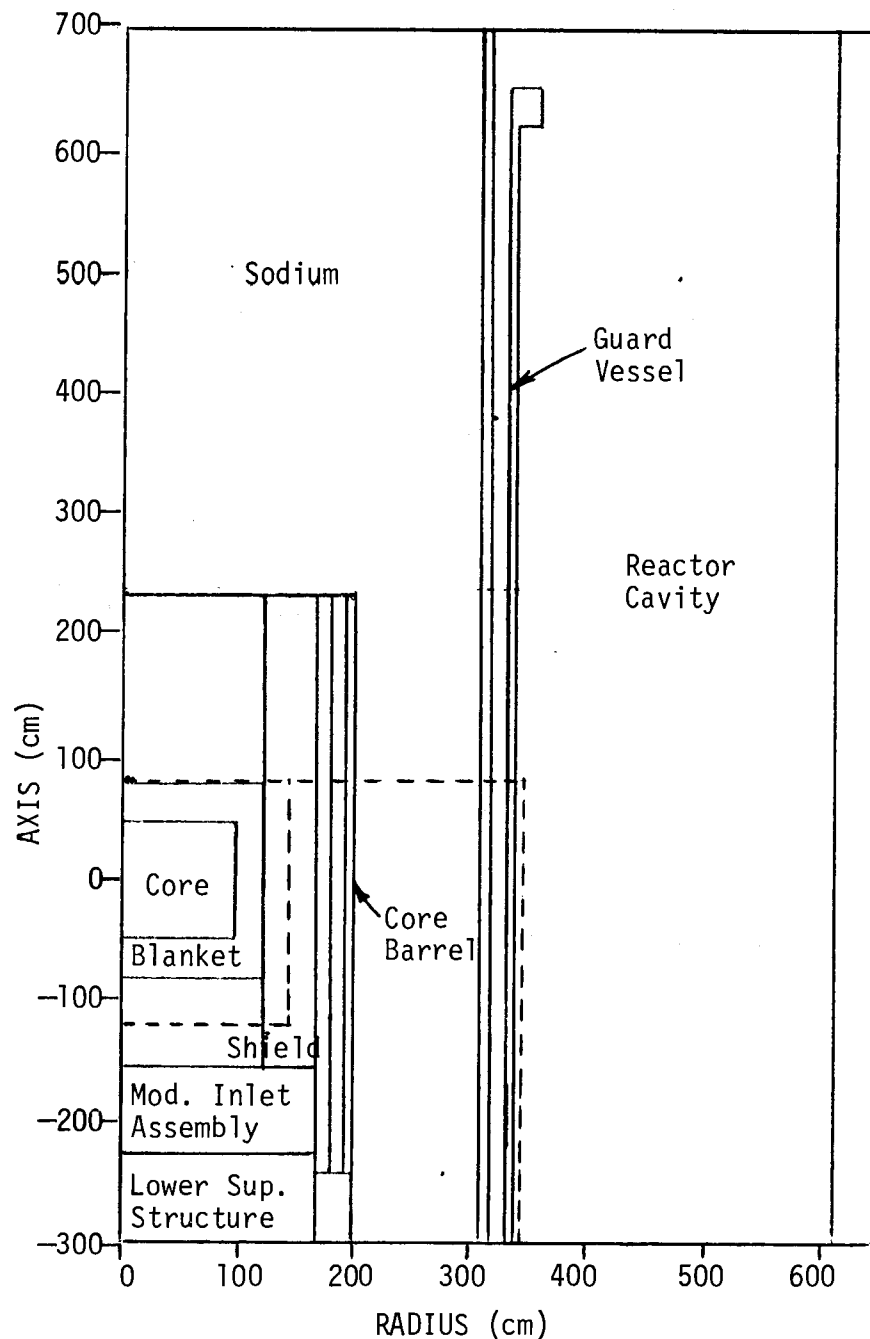


Fig. 19. Sketch Showing Dashed Outline of Region Included in Calculations for Lower Axial Region (Equilibrium Core). Inner outline defines region included in previous core density calculation; see also Figs. 18 and 20.

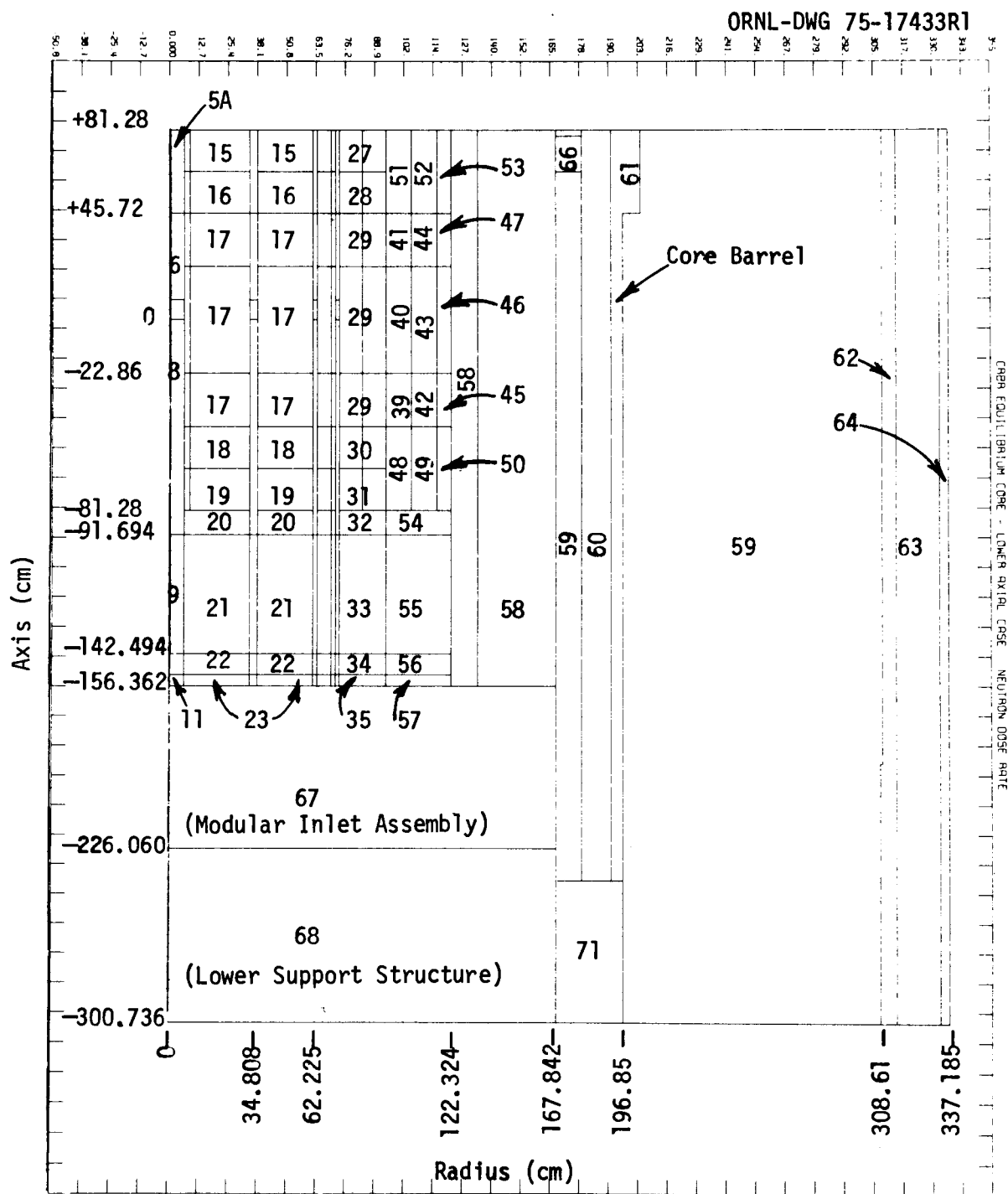


Fig. 20. Geometry Used for Calculations of CRBR Lower Axial Region (Equilibrium Core). See region descriptions in Table 11; see also Fig. 19.

ORNL-DWG 75-17434RI

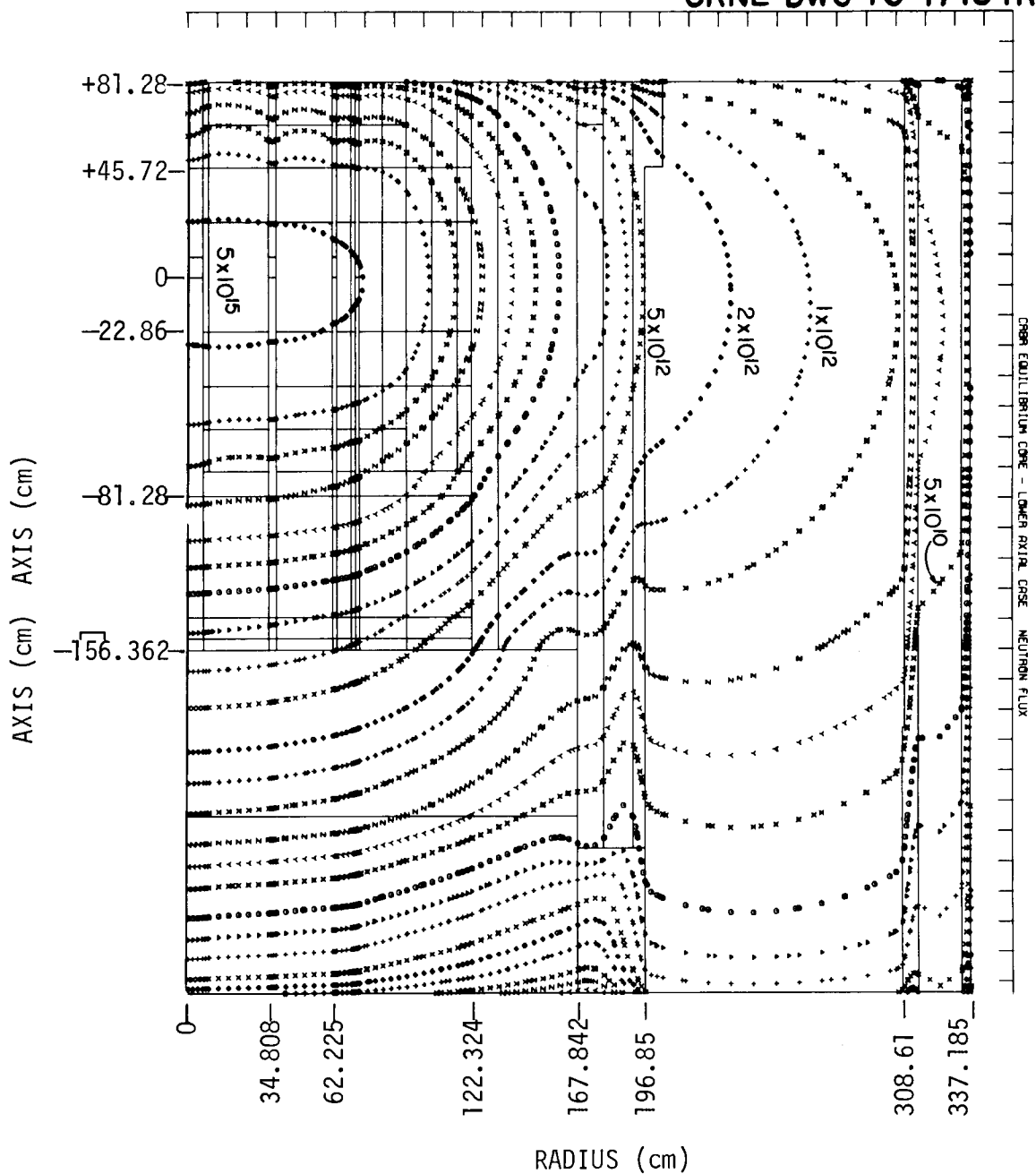


Fig. 21. Total Neutron Flux Distribution in CRBR Lower Axial Region (Equilibrium Core). Units are $\text{neutrons} \cdot \text{cm}^{-2} \cdot \text{sec}^{-1}$; see also Figs. 19 and 20.

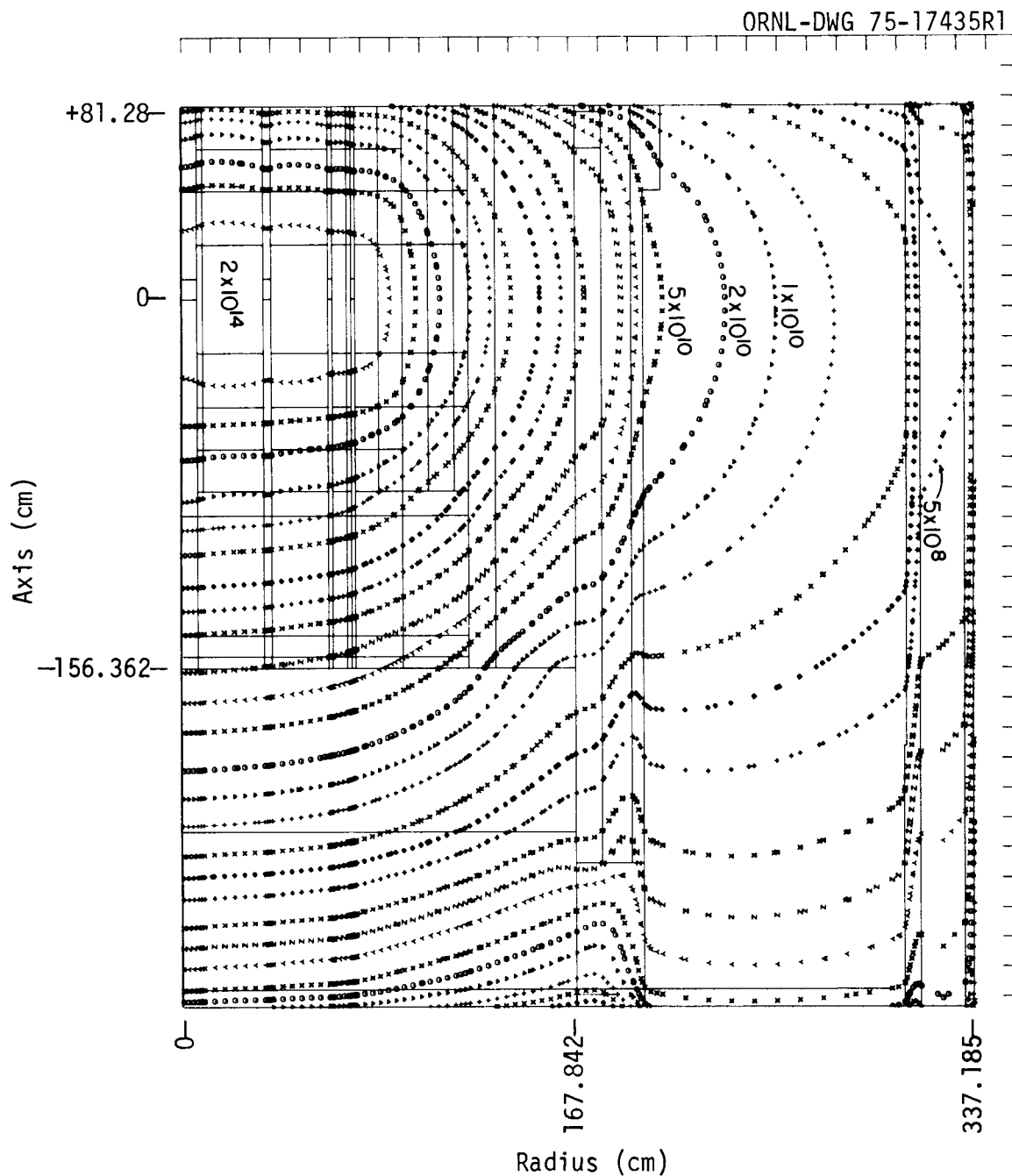


Fig. 22. Neutron Dose-Rate Distribution in CRBR Lower Axial Region (Equilibrium Core). Units are mrem/hr; see also Figs. 19 and 20.

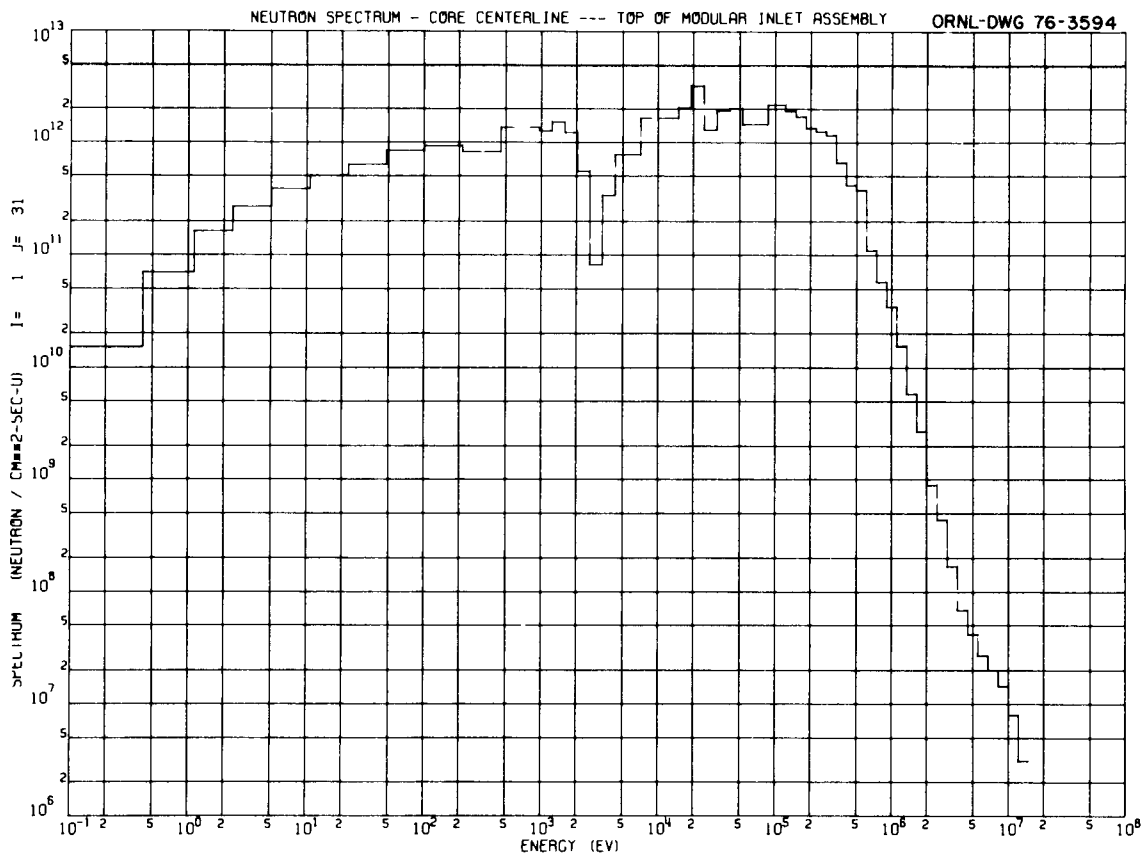


Fig. 23. Spectrum of Neutrons Incident on Modular Inlet Assembly.

4.3. Two-Boundary Source for Above-Core Calculations

All subsequent calculations in this series were aimed at determining the radiation dose rates above the vessel support system and reactor head and identifying the paths whereby radiation reached these locations. Since the region extending from the core to the cover and out through the reactor cavity was so large and the number of cross-section groups had increased considerably from those used in the calculations for the early CRBR model, it was not practical to handle the full problem in the detail required in one pass on the computer and it became necessary to perform it in steps. In studies of this type performed earlier for the FFTF, the first step always consisted of a calculation for a region that extended the full

width of the system and covered the axial distance from the core horizontal midplane to the maximum height allowable within the problem size limitations. The effect of the lower half of the core was accounted for by assuming a neutron reflection boundary at the core midplane. Angular fluxes along a horizontal boundary near the top of the region covered by this calculation were then saved and converted to the appropriate quadrature and energy grouping for use as the source for the next step. The surface chosen for the angular flux boundary was always sufficiently below the geometric boundary of the problem for reflections from above the flux boundary to be accounted for.

For these CRBR calculations it was found that including the full width of the system in the first step and extending the geometry to a reasonable distance above the core and blanket would itself comprise a problem that exceeded the computer space limitations. This was due to the fact that the full asymmetric core was described in the core power density calculation discussed above, and the same detailed mesh would be required to input the results of that calculation as the source in this calculation. And since the DOT-III code has no provisions for varying the mesh on a zone basis within a problem, it would have been necessary to use this same detailed spatial description across the full system. The alternative was to confine the geometry of the calculation to the core and the immediately surrounding regions. The angular flux data sets saved for use as the source in the next step would then be generated on both a horizontal surface and a vertical surface.

The region chosen for the first step extended axially from the core horizontal midplane to a short distance above the outlet nozzle and radially out through the first two rows of the removable radial shield, as shown by the outer dashed line in Fig. 24. Boundary fluxes were saved along a vertical surface between the blanket and the removable radial shield and along a horizontal surface just below the outlet nozzle (see inner dashed line in Fig. 24). Since both these surfaces were outside the core and blanket in regions where a coarser mesh was adequate, a larger geometric region could be covered in the second step. The

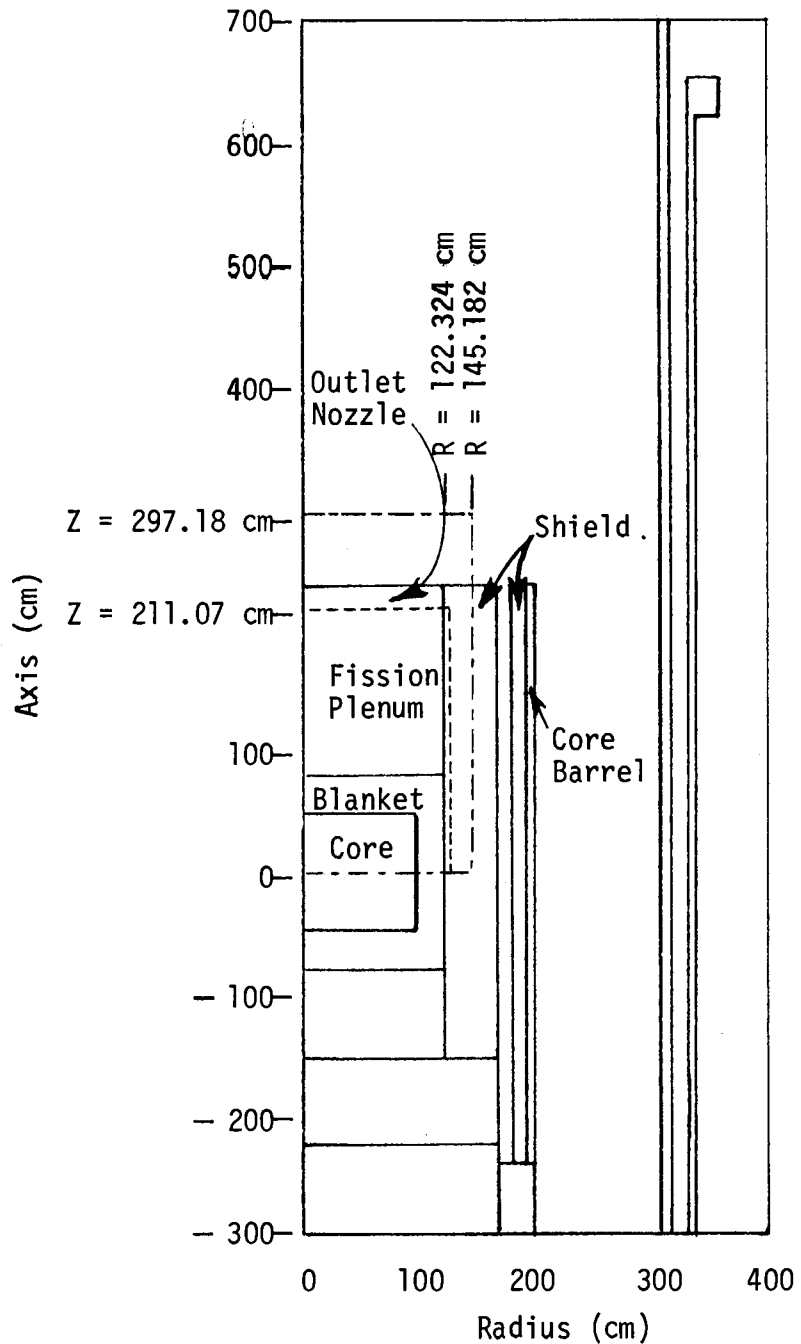


Fig. 24. Sketch Showing Dashed Outline of Region Included in Boundary Source Calculation (Equilibrium Core). Inner dashed line locates final boundary source.

boundary fluxes were converted to the new mesh by the FACT code⁸ and combined on one data set in the proper DOT format. A special code was written to "zero out" the boundary sources above $z = 211.07$ cm and beyond $r = 122.324$ cm.

4.4. Neutron and Secondary Gamma-Ray Fluxes and Dose Rates Below Reactor Head and Vessel Support System

The next calculation in this series was an S_6P_1 calculation that extended axially from the core midplane to the top of the sodium pool and radially through 1 ft of the concrete cavity wall. The geometry for the calculation is shown in Fig. 25. The regions enclosed by the boundary source (that is, the core, blanket, and fission gas plenum) were treated as pure absorbers since the DOT code does not allow internal vacuum boundary conditions. This problem prompted extensive work on the space-dependent rebalance convergence acceleration technique in DOT.

The neutron fluxes and dose rates obtained from this calculation are plotted in Figs. 26 and 27, and corresponding secondary gamma-ray dose rates are presented in Figs. 28 and 29. The fluxes in the core midplane at the position of the core barrel, together with the energy spectrum shown in Fig. 30, were used by WARD to calculate the radiation damage to the core barrel. The results indicated that the core barrel could meet the 30-year design lifetime.

From this calculation a boundary angular flux tape was prepared for use as a source for calculations of the penetration of neutrons and gamma rays through the reactor head and vessel support region. The boundary source was located approximately 3 ft below the concrete ledge and is indicated by the dashed line at $z = 733.12$ cm in Fig. 25.

4.5. Penetration of Radiation Through Reactor Head and Vessel Support System

The boundary angular fluxes generated from the preceding calculation were used as the source in calculations of the penetration of radiation

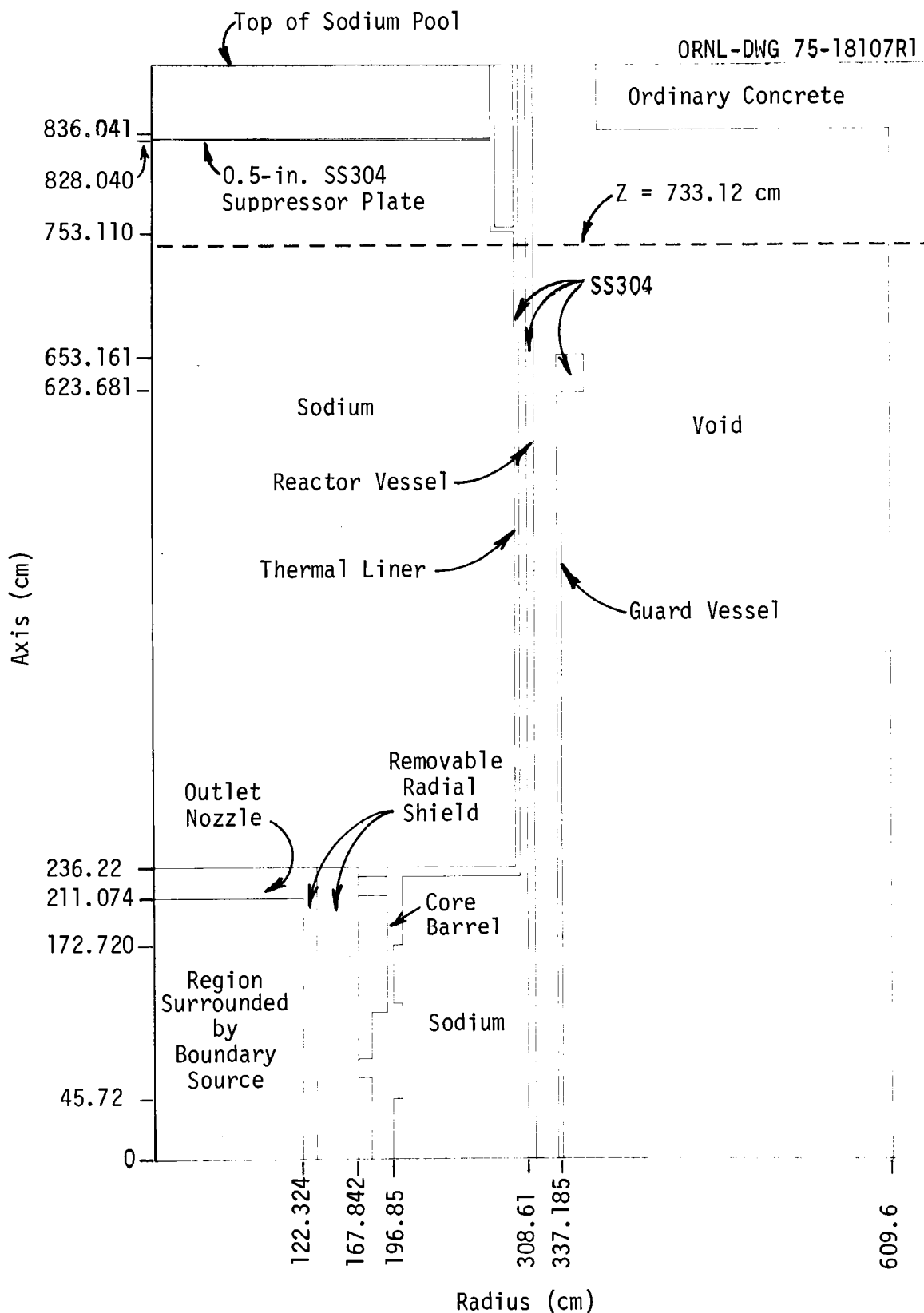


Fig. 25. Geometry Used for Calculation of Region Between CRBR Equilibrium Core Midplane and Top of Sodium Pool. Dashed line indicates location of boundary source for next calculation.

ORNL-DWG 75-17438

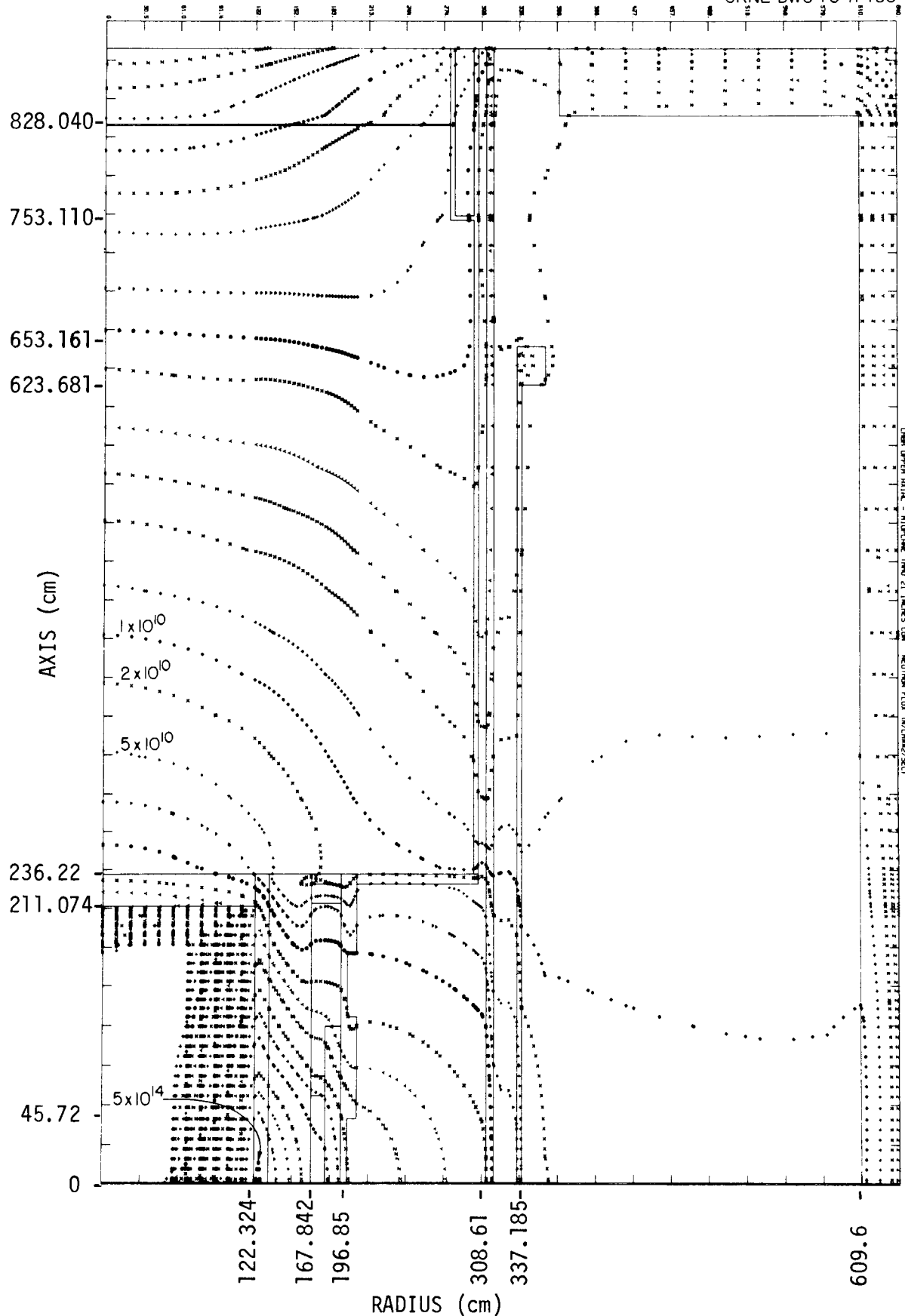


Fig. 26. Neutron Flux Distribution Below CRBR Reactor Head and Vessel Support System (Equilibrium Core). See Fig. 25 for geometry. Units are neutrons.cm⁻².sec⁻¹.

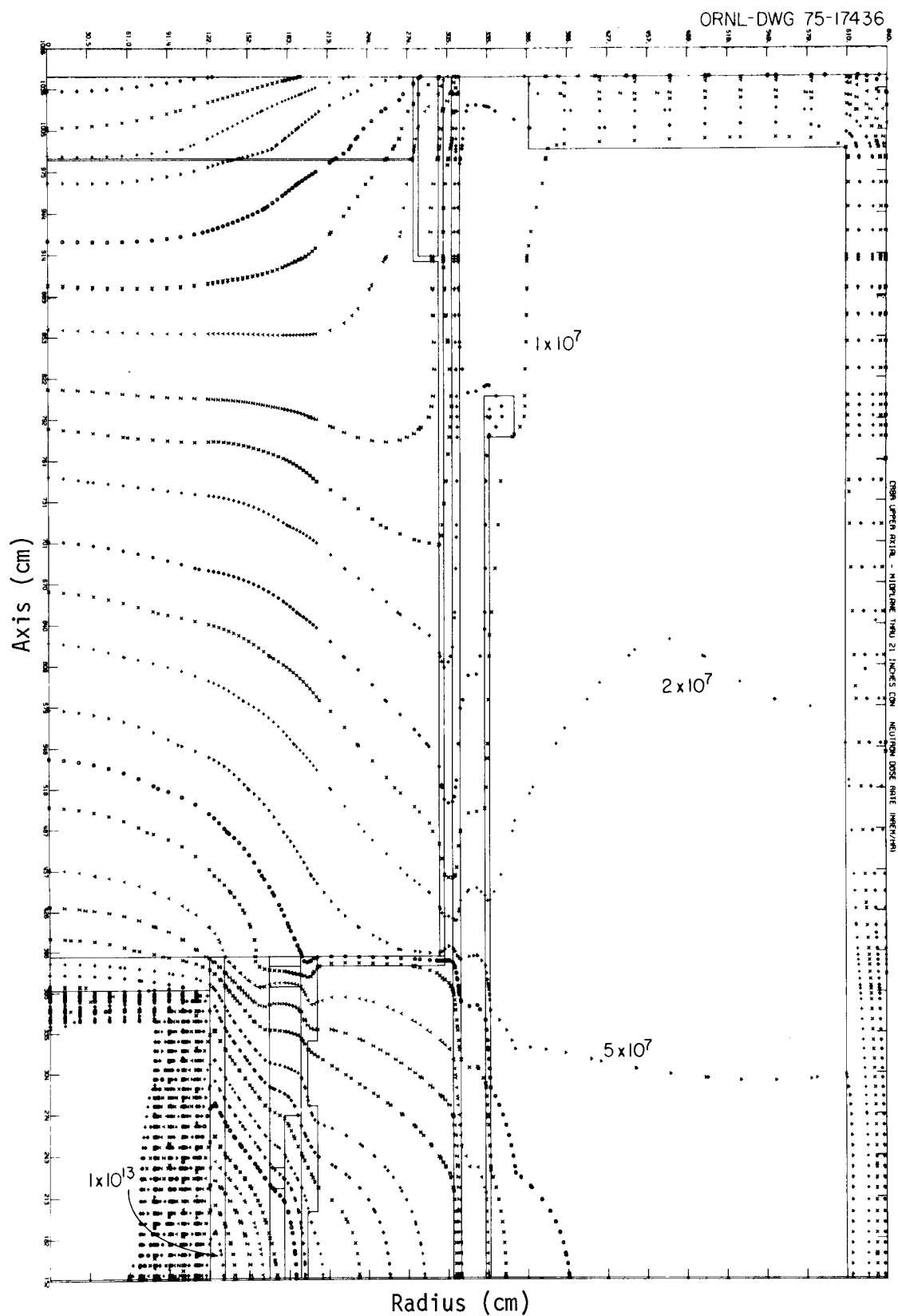


Fig. 27. Neutron Dose-Rate Distribution Below CRBR Reactor Head and Vessel Support Structure (Equilibrium Core). See Fig. 25 for geometry. Units are mrem/hr.

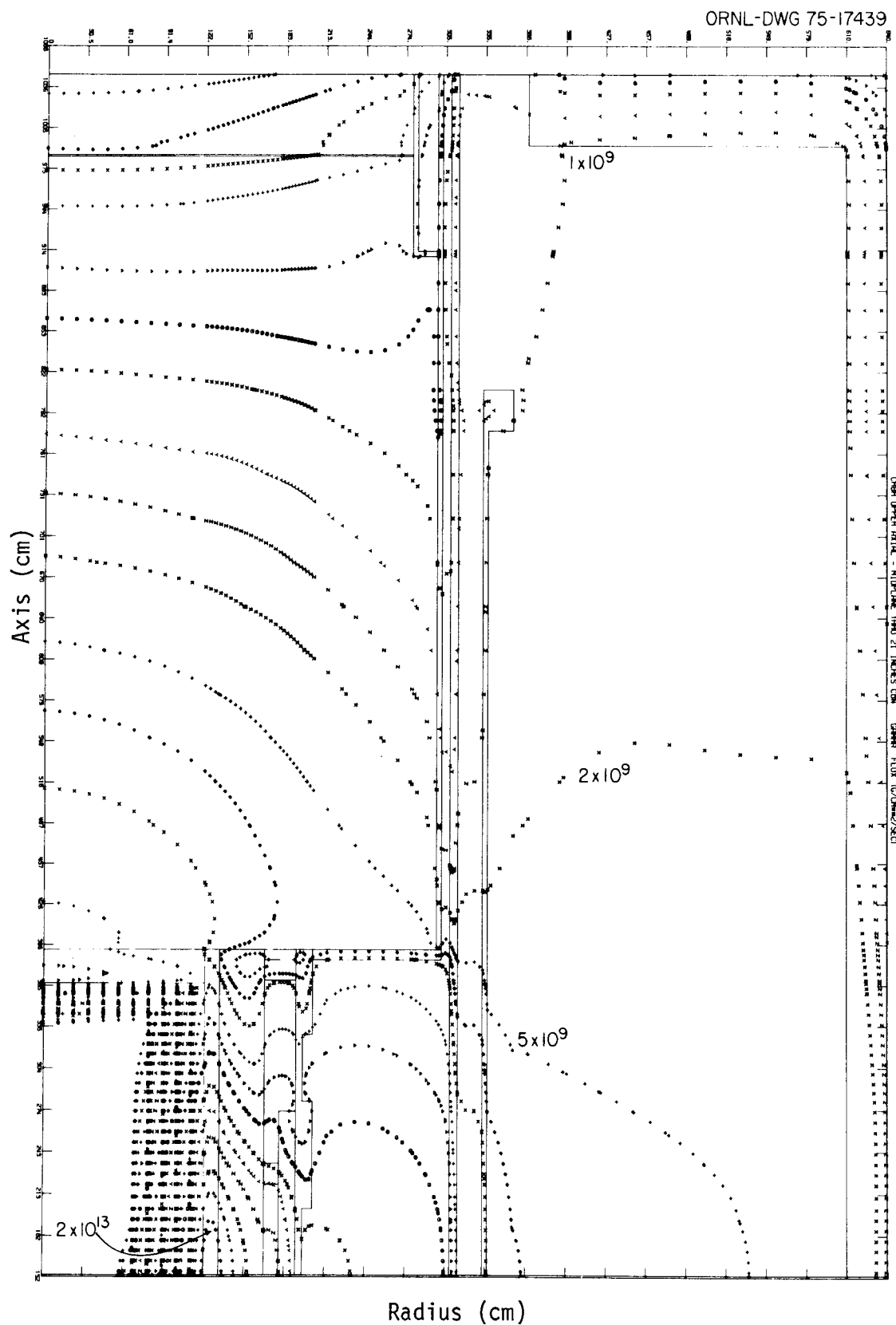


Fig. 28. Secondary Gamma-Ray Flux Distribution Below CRBR Reactor Head and Vessel Support Structure (Equilibrium Core). See Fig. 25 for geometry. Units are $\text{photons} \cdot \text{cm}^{-2} \cdot \text{sec}^{-1}$.

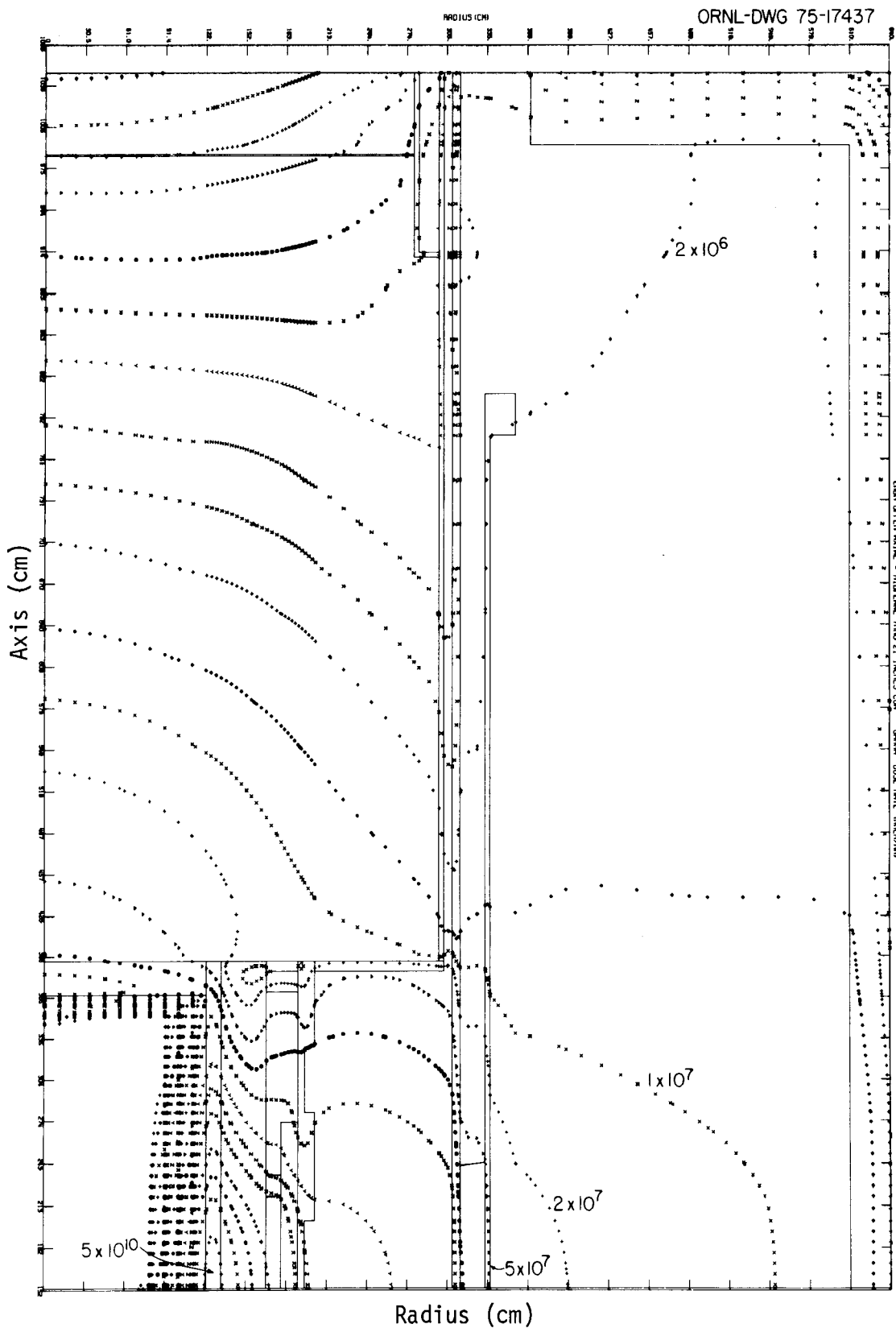


Fig. 29. Secondary Gamma-Ray Dose-Rate Distribution Below CRBR Reactor Head and Vessel Support Structure (Equilibrium Core). See Fig. 25 for geometry. Units are mrem/hr.

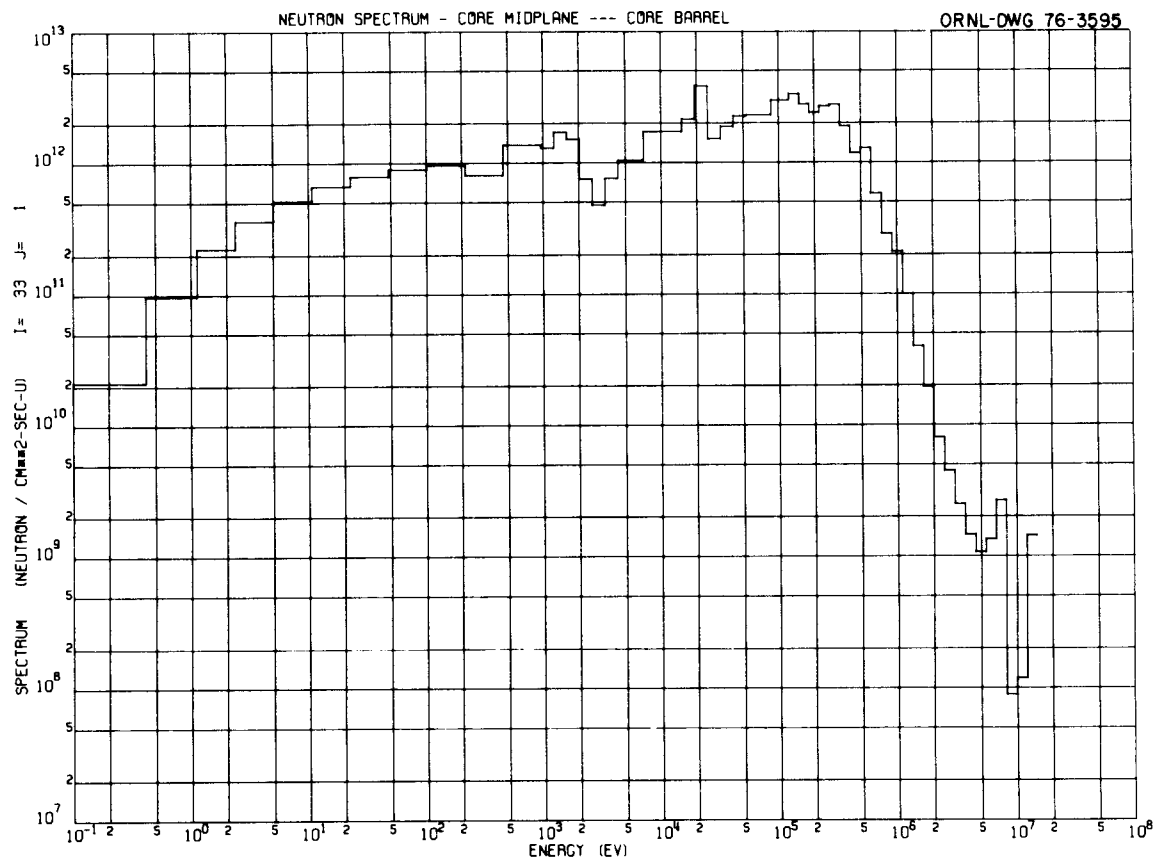


Fig. 30. Spectrum of Neutrons Incident on Core Barrel.

through three successive designs of the reactor head and vessel support region. As pointed out previously, design revisions following the calculations for the early CRBR conceptual model had resulted in the elimination of the concrete reactor cavity shield and the B₄C collar atop the guard vessel and had also resulted in a vessel support system that did not utilize support straps. In addition, the thermal shield beneath the carbon steel reactor vessel head had undergone considerable redesign.

The first calculations in this series were performed for the design that was produced by these various modifications. The geometry is shown in Fig. 31, with the compositions of the various materials given in Tables 9 and 15. (The inconel 750 "transition" sleeve inserted between the carbon steel vessel head and the stainless steel reactor vessel was a design change required to facilitate the welding together of these

components.) These calculations used a biased 166-angle quadrature which is listed in Table 17.

The neutron and gamma-ray fluxes and dose rates calculated for this first design are presented in Figs. 32-35. The peak neutron dose rate on top of the head was 220 mrem/hr, which was higher than the criterion by a factor of ~ 100 and appeared to necessitate the reintroduction of shielding in the reactor cavity. The secondary gamma-ray dose rate on the reactor head was also excessive, peaking at 306 mrem/hr.

In the meantime WARD had redesigned the vessel support ring, elevating a portion of it to set above the concrete support ledge. They had also redesigned the thermal shield, replacing some of the stainless steel 304 and the Inconel 750 with carbon steel 508. In addition, they requested that the gap surrounding the largest rotating top plug be considered in the next calculation. A more circuitous path to the neutrons streaming up the gap was presented by the introduction of SA508 and SS304 linings at the inner top surface of the reactor vessel. Finally, they surrounded the reactor vessel with a B_4C ring ($\rho = 2.51 \text{ g/cc}$) just below the corner of the support ledge and adjacent to the reactor vessel. The resulting design is shown in Fig. 36. (The atomic densities of the B_4C constituents were 0.02720, 0.0250, and $0.08730 \text{ atoms} \cdot \text{barn}^{-1} \cdot \text{cm}^{-1}$ for C, ^{10}B , and ^{11}B respectively.)

The neutron fluxes and dose rates calculated for this second design are shown in Figs. 37 and 38, and the corresponding gamma-ray dose rates are presented in Fig. 39. With this configuration the peak neutron dose rate was lowered to 25 mrem/hr and the peak secondary gamma-ray dose rate to 92 mrem/hr, both of which were still too high and prompted another calculation for a subsequent design in which more shielding was added.

The third design of the reactor head and vessel support region is shown in Fig. 40. It differs from the previous design in that SA508 shielding was added in the reactor cavity immediately below the vessel support ring and concrete shielding was added outside the support ring on

Table 17. Description of 166-Angle Quadrature

ANGLE	WEIGHT	MU	ETA	ANGLE	WEIGHT	MU	ETA
1	0	-2.26980E-01	-9.73900E-01	43	1.53650E-05	4.61060E-03	9.99680E-01
2	1.66720E-02	-1.48890E-01	-9.73900E-01	44	1.66820E-04	1.99370E-02	9.99680E-01
3	1.66720E-02	1.48890E-01	-9.73900E-01	45	0	-5.72480E-02	9.98360E-01
4	0	-5.01670E-01	-8.65060E-01	46	3.90650E-04	-4.51130E-02	9.98360E-01
5	2.44470E-02	-4.33400E-01	-8.65060E-01	47	3.59810E-05	-1.04330E-02	9.98360E-01
6	1.29240E-02	-1.48880E-01	-8.65060E-01	48	2.05600E-05	-4.98969E-03	9.98360E-01
7	1.29240E-02	1.48880E-01	-8.65060E-01	49	1.54210E-05	-1.49870E-03	9.98360E-01
8	2.44470E-02	4.33400E-01	-8.65060E-01	50	1.54210E-05	1.49870E-03	9.98360E-01
9	0	-7.33770E-01	-6.79400E-01	51	2.05600E-05	4.98969E-03	9.98360E-01
10	2.70170E-02	-6.79420E-01	-6.79400E-01	52	3.59810E-05	1.04330E-02	9.98360E-01
11	8.55190E-03	-4.33400E-01	-6.79400E-01	53	3.90650E-04	4.51130E-02	9.98360E-01
12	1.92140E-02	-1.48880E-01	-6.79400E-01	54	0	-8.95759E-02	9.95980E-01
13	1.92140E-02	1.48880E-01	-6.79400E-01	55	6.14480E-04	-7.05869E-02	9.95980E-01
14	8.55190E-03	4.33400E-01	-6.79400E-01	56	5.65970E-05	-1.63240E-02	9.95980E-01
15	2.70170E-02	6.79420E-01	-6.79400E-01	57	3.23410E-05	-7.80720E-03	9.95980E-01
16	0	-9.01210E-01	-4.33390E-01	58	2.42560E-05	-2.34500E-03	9.95980E-01
17	2.44470E-02	-8.65070E-01	-4.33390E-01	59	2.42560E-05	2.34500E-03	9.95980E-01
18	8.55190E-03	-6.79410E-01	-4.33390E-01	60	3.23410E-05	7.80720E-03	9.95980E-01
19	2.74740E-02	-4.33400E-01	-4.33390E-01	61	5.65970E-05	1.63240E-02	9.95980E-01
20	6.85849E-03	-1.48870E-01	-4.33390E-01	62	6.14480E-04	7.05869E-02	9.95980E-01
21	6.85849E-03	1.48870E-01	-4.33390E-01	63	0	-1.21920E-01	9.92540E-01
22	2.74740E-02	4.33400E-01	-4.33390E-01	64	8.36200E-04	-9.60739E-02	9.92540E-01
23	8.55190E-03	6.79410E-01	-4.33390E-01	65	7.70180E-05	-2.22180E-02	9.92540E-01
24	2.44470E-02	8.65070E-01	-4.33390E-01	66	4.40100E-05	-1.06260E-02	9.92540E-01
25	0	-9.88860E-01	-1.48870E-01	67	3.30080E-05	-3.19170E-03	9.92540E-01
26	1.66720E-02	-9.73910E-01	-1.48870E-01	68	3.30080E-05	3.19170E-03	9.92540E-01
27	1.29240E-02	-8.65060E-01	-1.48870E-01	69	4.40100E-05	1.06260E-02	9.92540E-01
28	1.92150E-02	-6.79410E-01	-1.48870E-01	70	7.70180E-05	2.22180E-02	9.92540E-01
29	6.85859E-03	-4.33400E-01	-1.48870E-01	71	8.36200E-04	9.60739E-02	9.92540E-01
30	1.82290E-02	-1.48870E-01	-1.48870E-01	72	0	-1.54130E-01	9.88050E-01
31	1.82290E-02	1.48870E-01	-1.48870E-01	73	1.05790E-03	-1.21460E-01	9.88050E-01
32	6.85859E-03	4.33400E-01	-1.48870E-01	74	9.74390E-05	-2.80890E-02	9.88050E-01
33	1.92150E-02	6.79410E-01	-1.48870E-01	75	5.56800E-05	-1.34340E-02	9.88050E-01
34	1.29240E-02	8.65060E-01	-1.48870E-01	76	4.17610E-05	-4.03500E-03	9.88050E-01
35	1.66720E-02	9.73910E-01	-1.48870E-01	77	4.17610E-05	4.03500E-03	9.88050E-01
36	0	-2.52980E-02	9.99680E-01	78	5.56800E-05	1.34340E-02	9.88050E-01
37	1.66820E-04	-1.99370E-02	9.99680E-01	79	9.74390E-05	2.80890E-02	9.88050E-01
38	1.53650E-05	-4.61060E-03	9.99680E-01	80	1.05790E-03	1.21460E-01	9.88050E-01
39	8.77990E-06	-2.20510E-03	9.99680E-01	81	0	-1.86210E-01	9.82510E-01
40	6.58510E-06	-6.62320E-04	9.99680E-01	82	1.27760E-03	-1.46740E-01	9.82510E-01
41	6.58510E-06	6.62320E-04	9.99680E-01	83	1.17670E-04	-3.39340E-02	9.82510E-01
42	8.77990E-06	2.20510E-03	9.99680E-01	84	6.72400E-05	-1.62300E-02	9.82510E-01

Table 17 (cont.)

ANGLE	WEIGHT	MU	ETA	ANGLE	WEIGHT	MU	ETA
85	5.04310E-05	-4.87470E-03	9.82510E-01	126	0	-3.42910E-01	9.39370E-01
86	5.04310E-05	4.87470E-03	9.82510E-01	127	2.35660E-03	-2.70210E-01	9.39370E-01
87	6.72400E-05	1.62300E-02	9.82510E-01	128	2.17050E-04	-6.24900E-02	9.39370E-01
88	1.17670E-04	3.39340E-02	9.82510E-01	129	1.24030E-04	-2.98870E-02	9.39370E-01
89	1.27760E-03	1.46740E-01	9.82510E-01	130	9.30240E-05	-8.97679E-03	9.39370E-01
90	0	-2.18080E-01	9.75930E-01	131	9.30240E-05	8.97679E-03	9.39370E-01
91	1.49710E-03	-1.71850E-01	9.75930E-01	132	1.24030E-04	2.98870E-02	9.39370E-01
92	1.37890E-04	-3.97430E-02	9.75930E-01	133	2.17050E-04	6.24900E-02	9.39370E-01
93	7.87950E-05	-1.90080E-02	9.75930E-01	134	2.35660E-03	2.70210E-01	9.39370E-01
94	5.90970E-05	-5.70910E-03	9.75930E-01	135	0	-5.01670E-01	8.65060E-01
95	5.90970E-05	5.70910E-03	9.75930E-01	136	2.44470E-02	-4.33400E-01	8.65060E-01
96	7.87950E-05	1.90080E-02	9.75930E-01	137	1.29240E-02	-1.48880E-01	8.65060E-01
97	1.37890E-04	3.97430E-02	9.75930E-01	138	1.29240E-02	1.48880E-01	8.65060E-01
98	1.49710E-03	1.71850E-01	9.75930E-01	139	2.44470E-02	4.33400E-01	8.65060E-01
99	0	-2.49710E-01	9.68320E-01	140	0	-7.33770E-01	6.79400E-01
100	1.71460E-03	-1.96780E-01	9.68320E-01	141	2.70170E-02	-6.79420E-01	6.79400E-01
101	1.57930E-04	-4.55070E-02	9.68320E-01	142	8.55190E-03	-4.33400E-01	6.79400E-01
102	9.02440E-05	-2.17640E-02	9.68320E-01	143	1.92140E-02	-1.48880E-01	6.79400E-01
103	6.76840E-05	-6.53709E-03	9.68320E-01	144	1.92140E-02	1.48880E-01	6.79400E-01
104	6.76840E-05	6.53709E-03	9.68320E-01	145	8.55190E-03	4.33400E-01	6.79400E-01
105	9.02440E-05	2.17640E-02	9.68320E-01	146	2.70170E-02	6.79420E-01	6.79400E-01
106	1.57930E-04	4.55070E-02	9.68320E-01	147	0	-9.01210E-01	4.33390E-01
107	1.71460E-03	1.96780E-01	9.68320E-01	148	2.44470E-02	-8.65070E-01	4.33390E-01
108	0	-2.81100E-01	9.59680E-01	149	8.55190E-03	-6.79410E-01	4.33390E-01
109	1.93010E-03	-2.21510E-01	9.59680E-01	150	2.74740E-02	-4.33400E-01	4.33390E-01
110	1.77770E-04	-5.12260E-02	9.59680E-01	151	6.85849E-03	-1.48870E-01	4.33390E-01
111	1.01580E-04	-2.45000E-02	9.59680E-01	152	6.85849E-03	1.48870E-01	4.33390E-01
112	7.61870E-05	-7.35870E-03	9.59680E-01	153	2.74740E-02	4.33400E-01	4.33390E-01
113	7.61870E-05	7.35870E-03	9.59680E-01	154	8.55190E-03	6.79410E-01	4.33390E-01
114	1.01580E-04	2.45000E-02	9.59680E-01	155	2.44470E-02	8.65070E-01	4.33390E-01
115	1.77770E-04	5.12260E-02	9.59680E-01	156	0	-9.88860E-01	1.48870E-01
116	1.93010E-03	2.21510E-01	9.59680E-01	157	1.66720E-02	-9.73910E-01	1.48870E-01
117	0	-3.12160E-01	9.50030E-01	158	1.29240E-02	-8.65060E-01	1.48870E-01
118	2.14540E-03	-2.45980E-01	9.50030E-01	159	1.92150E-02	-6.79410E-01	1.48870E-01
119	1.97600E-04	-5.68870E-02	9.50030E-01	160	6.85859E-03	-4.33400E-01	1.48870E-01
120	1.12910E-04	-2.72070E-02	9.50030E-01	161	1.82290E-02	-1.48870E-01	1.48870E-01
121	8.46880E-05	-8.17189E-03	9.50030E-01	162	1.82290E-02	1.48870E-01	1.48870E-01
122	8.46880E-05	8.17189E-03	9.50030E-01	163	6.85859E-03	4.33400E-01	1.48870E-01
123	1.12910E-04	2.72070E-02	9.50030E-01	164	1.92150E-02	6.79410E-01	1.48870E-01
124	1.97600E-04	5.68870E-02	9.50030E-01	165	1.29240E-02	8.65060E-01	1.48870E-01
125	2.14540E-03	2.45980E-01	9.50030E-01	166	1.66720E-02	9.73910E-01	1.48870E-01

top of the concrete support ledge. In addition, insulation was added between the support ring and the support ledge.

The neutron and gamma-ray fluxes and dose rates for this third design are presented in Figs. 41-44. Unfortunately, even with the added shielding, the peak dose rates on top of the reactor head were still slightly too high -- 2.04 mrem/hr for neutrons and 2.66 mrem/hr for secondary gamma rays. In order to gain some insight into the spectrum of neutrons contributing to the dose rates, two additional plotting runs of the neutron fluxes were made with lower cutoff energies of 0.1 and 1.0 MeV. The results are plotted in Figs. 45 and 46 respectively.

In an attempt to determine the pathways whereby the neutrons contributing to the peak neutron dose rate penetrated the reactor head, an adjoint calculation of the flux was performed. The source for the adjoint calculation was the neutron flux-to-dose conversion factors distributed uniformly between $r = 264.16$ cm and $r = 426.72$ cm in the top row of the mesh. Figure 47 is a contour plot of the adjoint flux which displays qualitatively the relative importance of neutrons anywhere in the system to the neutron dose rate in the area covered by the adjoint source.

The forward and adjoint fluxes and flux moments for the region were folded with the VIP code⁹ and used to generate isometric graphical representations of the contribution as a function of both the radius r and the elevation z . The results are shown in Figs. 48 and 49, along with three-dimensional computer drawings of the zones included in the calculation. These figures show that essentially all of the neutrons contributing to the peak neutron dose rate pass through the gap between the B_4C ring and the reactor vessel, with a lesser fraction passing between the ring and the concrete support ledge.

In the final calculation in this series, a DOT void calculation with a boundary source from the top of the preceding DOT calculation was used to calculate the distribution of the neutrons and gamma rays at the operating floor. Radial dose-rate profiles at the operating floor level are shown in Figs. 50-52.

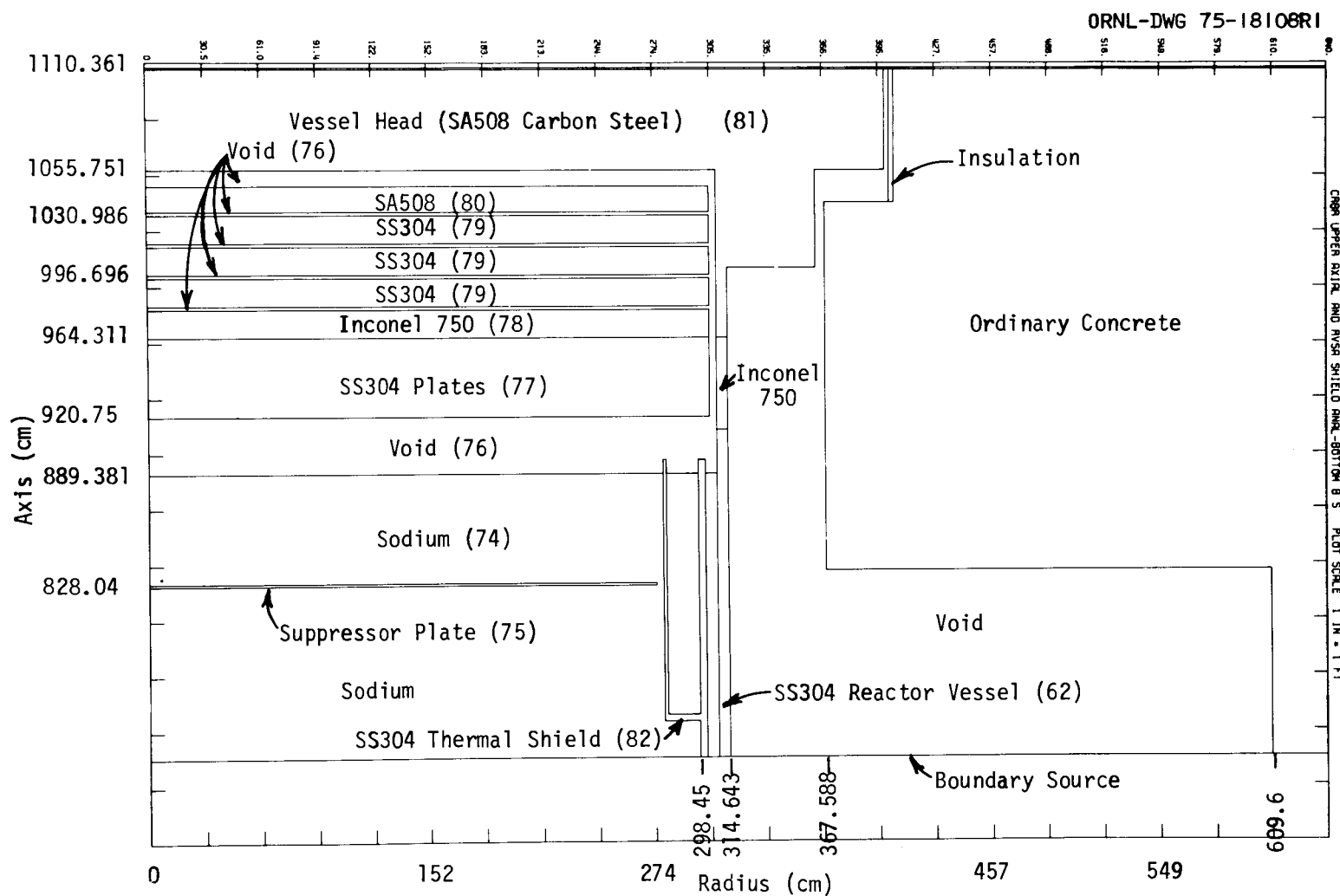


Fig. 31. Geometry Used for Calculation of Reactor Head and Vessel Support System Design No. 1 (Equilibrium Core). Boundary source located at $z = 733.12$ cm. See Figs. 20 and 25 for geometry of lower regions in CRBR assembly.

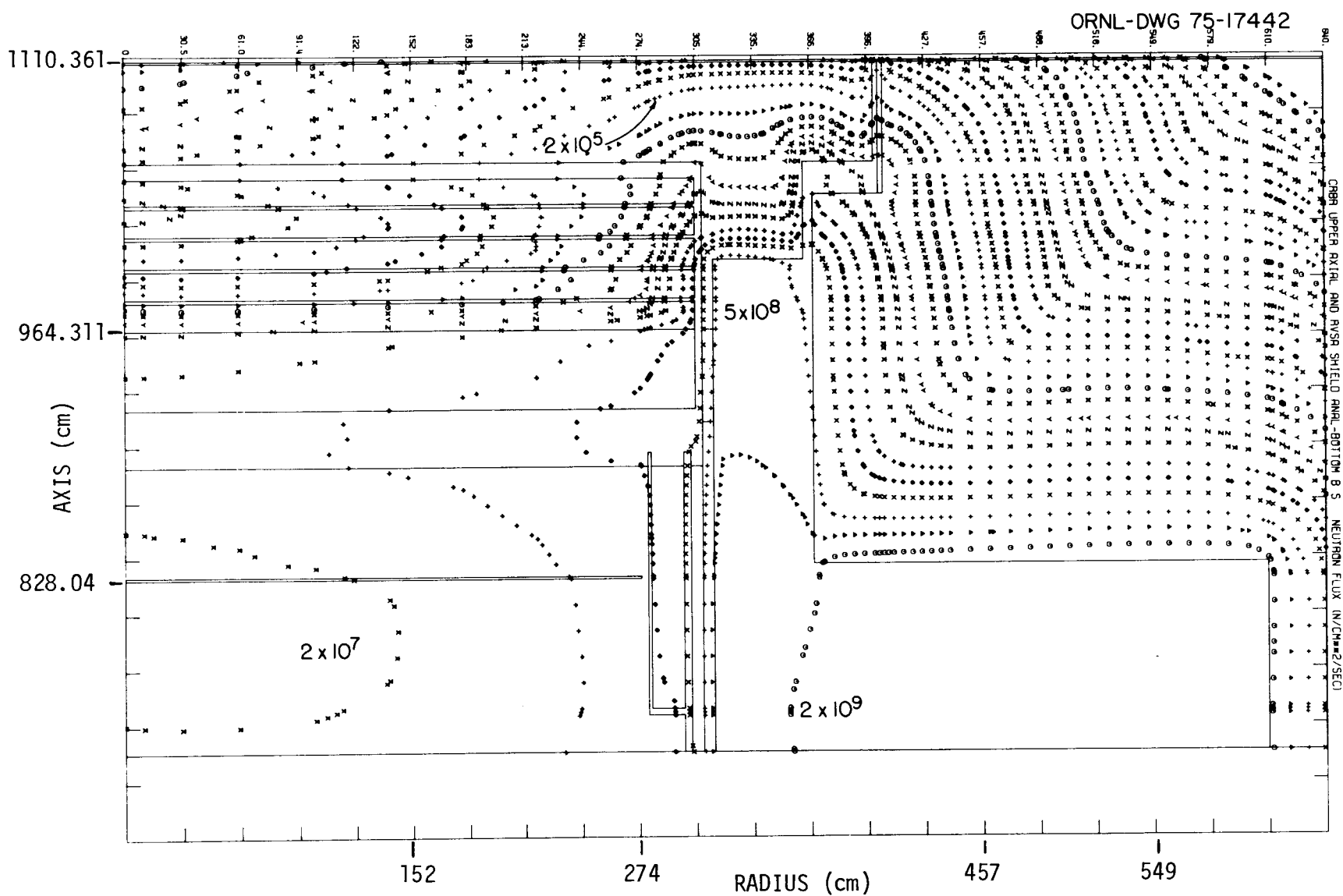


Fig. 32. Neutron Flux Distribution in Reactor Head and Vessel Support System Design No. 1 (Equilibrium Core). See Fig. 31 for description of geometry; units are $\text{neutrons} \cdot \text{cm}^{-2} \cdot \text{sec}^{-1}$.

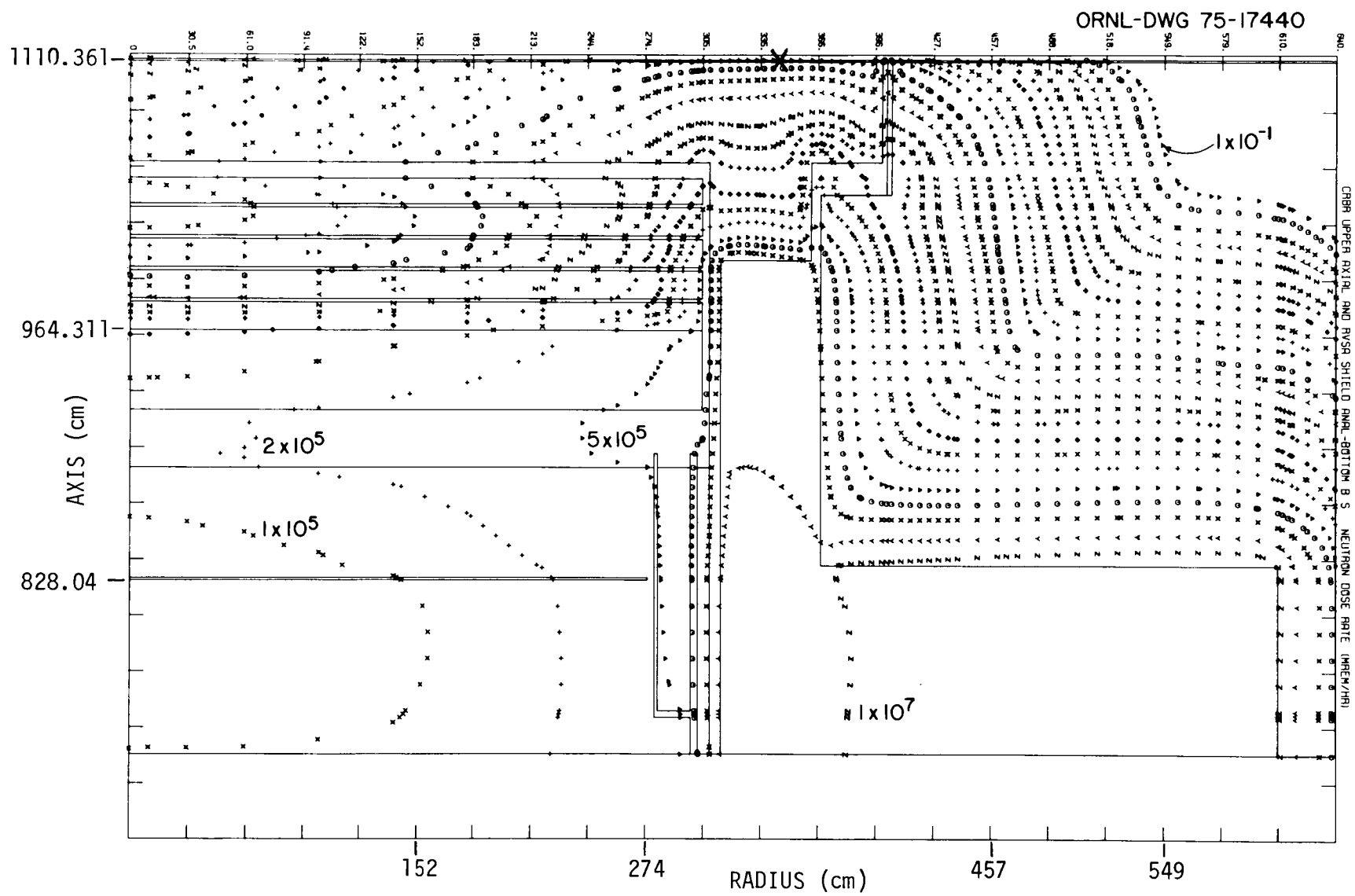


Fig. 33. Neutron Dose-Rate Distribution in Reactor Head and Vessel Support System Design No. 1 (Equilibrium Core). See Fig. 31 for description of geometry. Units are mrem/hr; peak dose rate on head is 220 mrem/hr at $R = \sim 340$ cm (see X).

ORNL-DWG 75-17443

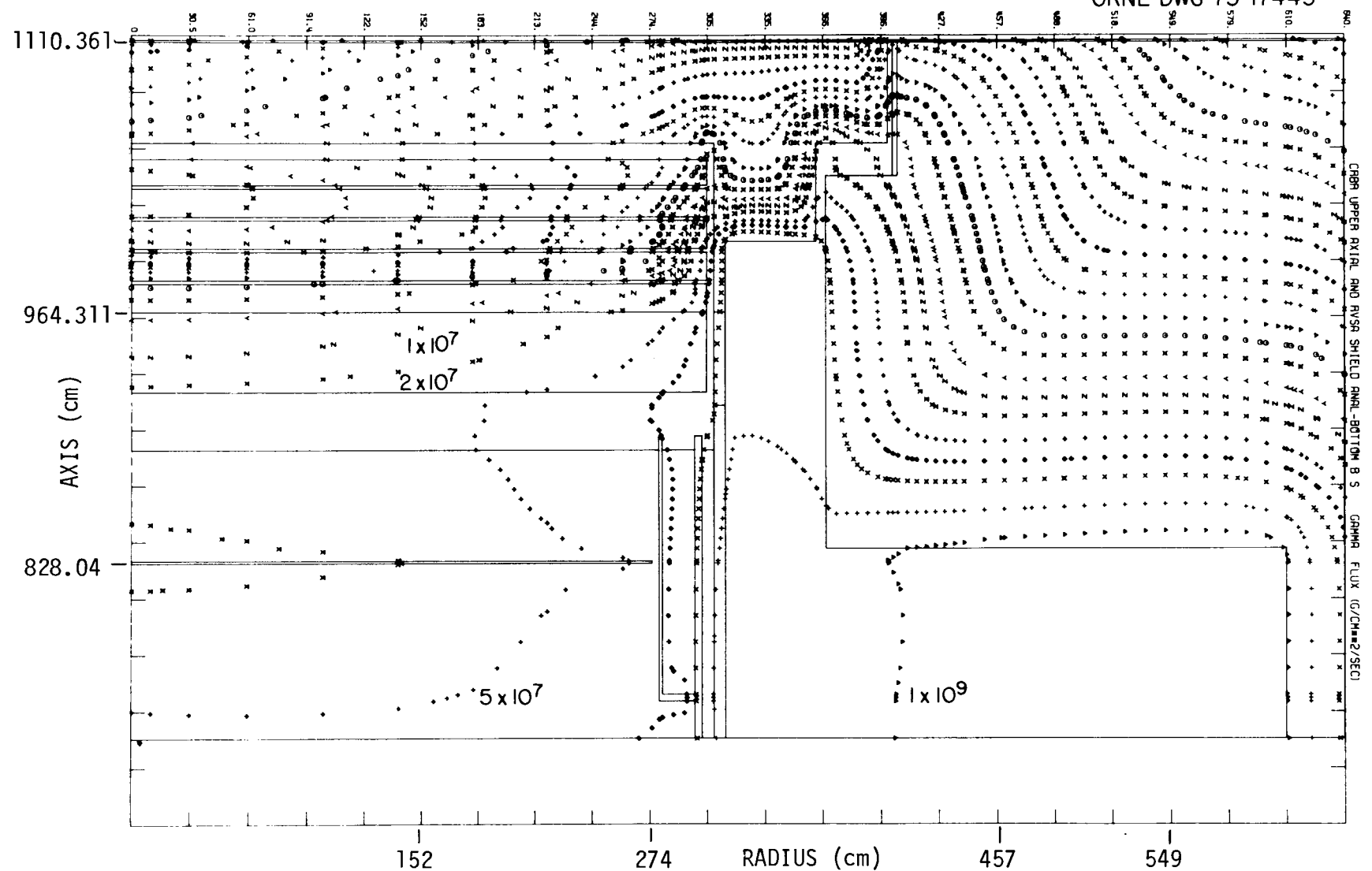


Fig. 34. Secondary Gamma-Ray Flux Distribution in Reactor Head and Vessel Support System Design No. 1 (Equilibrium Core). See Fig. 31 for description of geometry. Units are photons·cm⁻²·sec⁻¹.

ORNL-DWG 75-17441

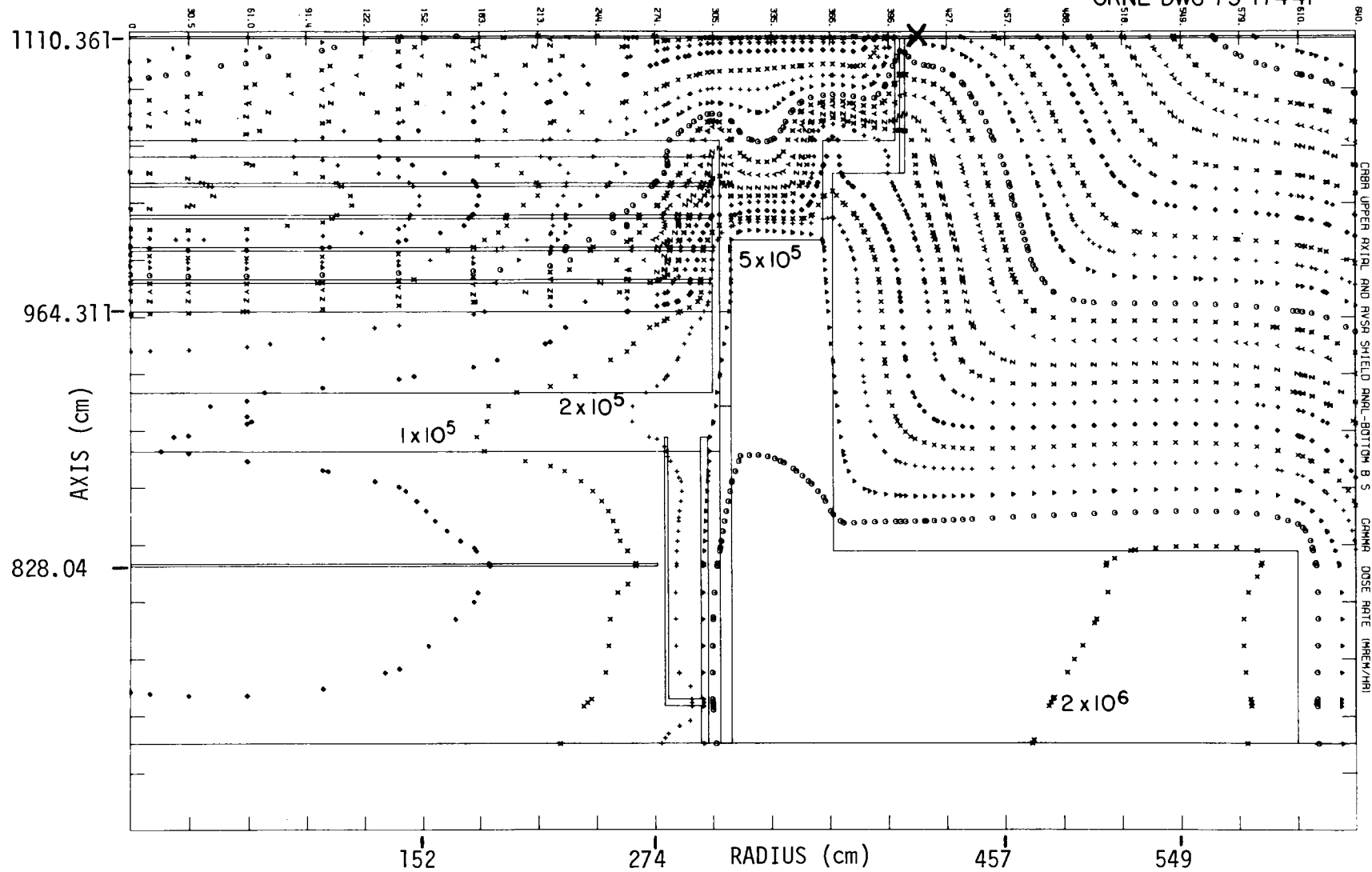
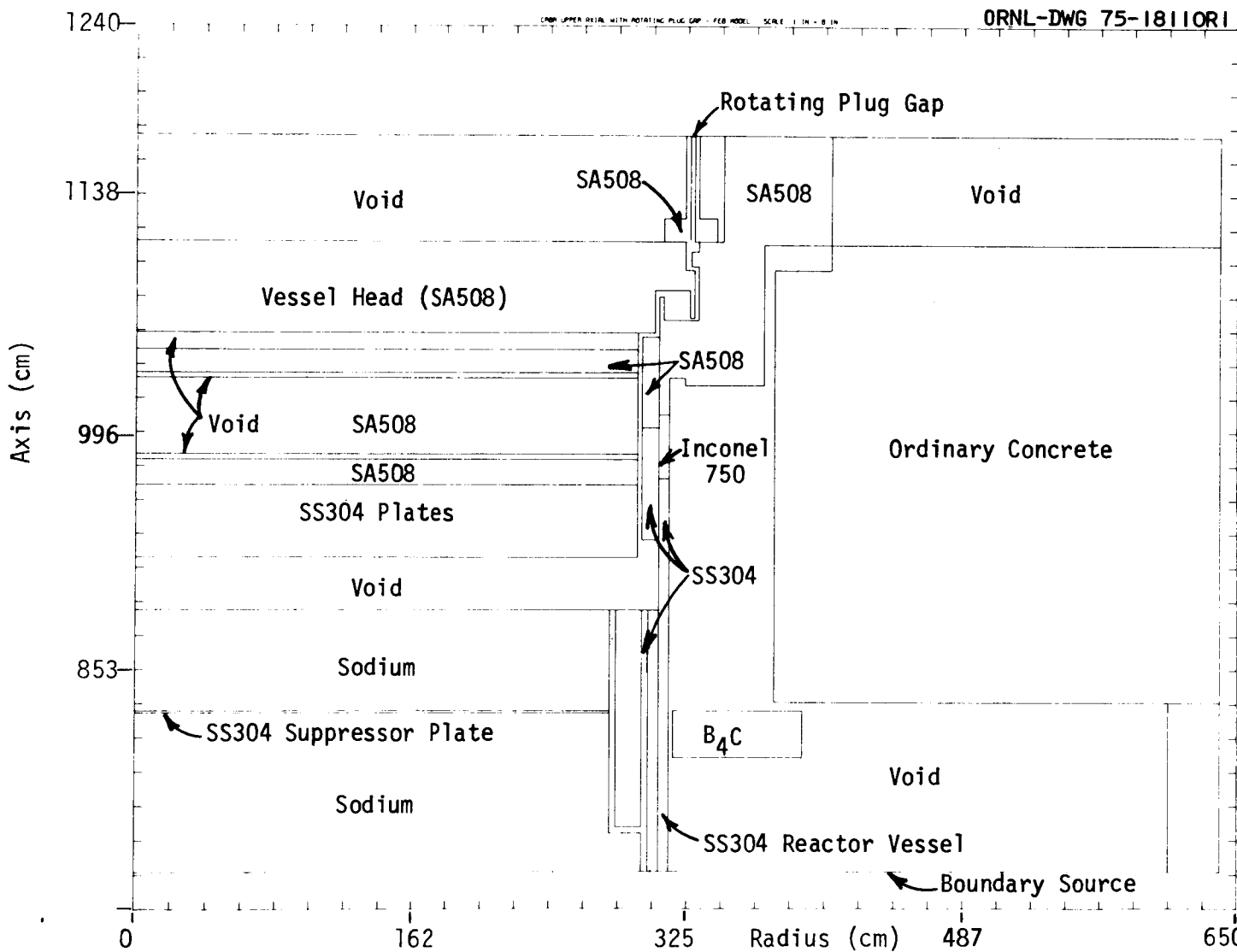


Fig. 35. Secondary Gamma-Ray Dose-Rate Distribution in Reactor Head and Vessel Support System Design No. 1 (Equilibrium Core). See Fig. 31 for description of geometry. Units are mrem/hr; peak dose rate on head is 306 mrem/hr at $R = \sim 404$ cm (see X).



62

Fig. 36. Geometry Used for Calculation of Reactor Head and Vessel Support System Design No. 2 (Equilibrium Core). Boundary source located at $z = 733.12$ cm. See Figs. 20 and 25 for geometry of lower regions in CRBR assembly.

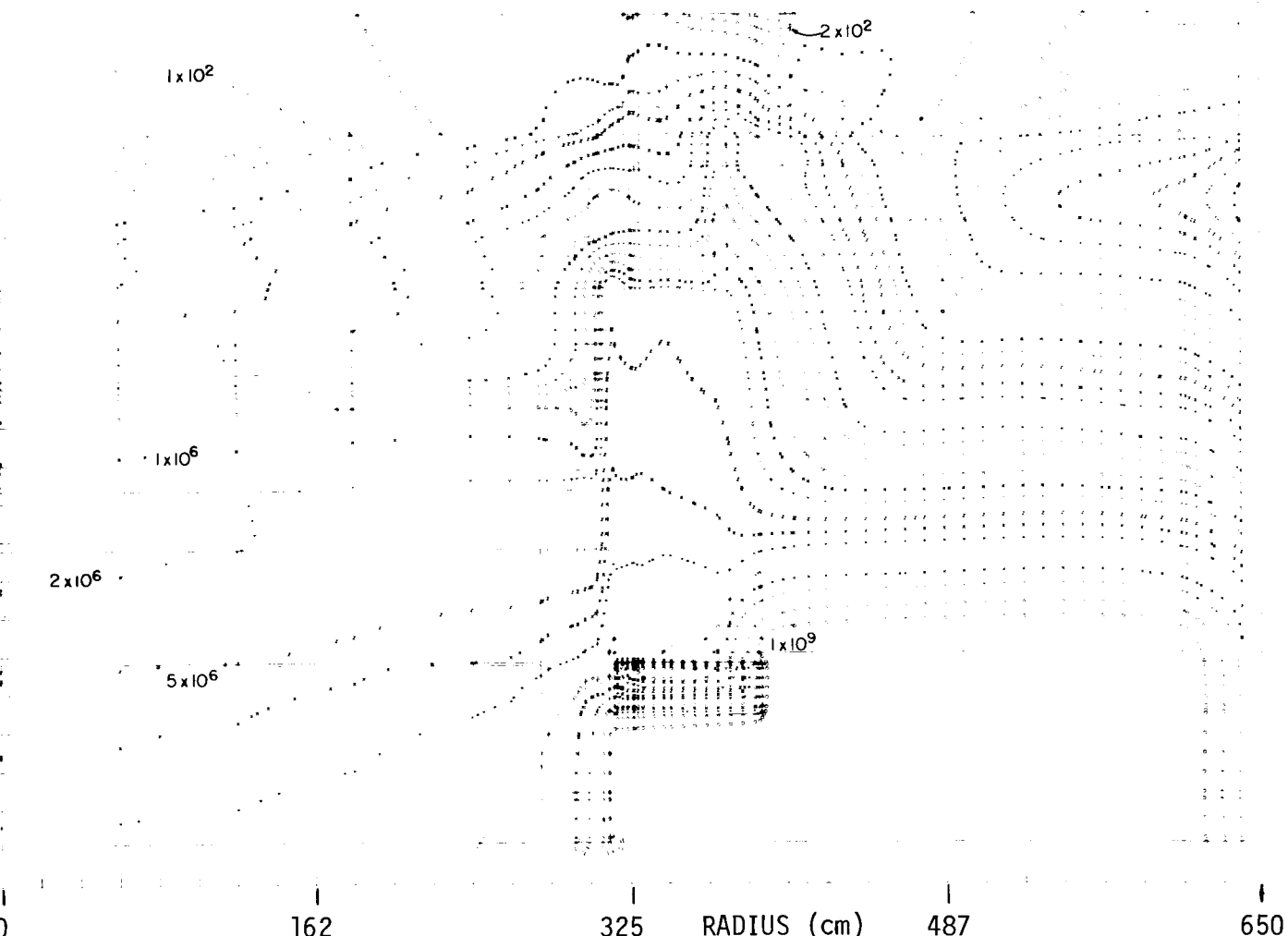
1240-

ORNL-DWG 75-17444

AXIS (cm)

1138-

853-



59

Fig. 37. Neutron Flux Distribution in Reactor Head and Vessel Support System Design No. 2 (Equilibrium Core). See Fig. 36 for description of geometry. Units are $\text{neutrons} \cdot \text{cm}^{-2} \cdot \text{sec}^{-1}$.

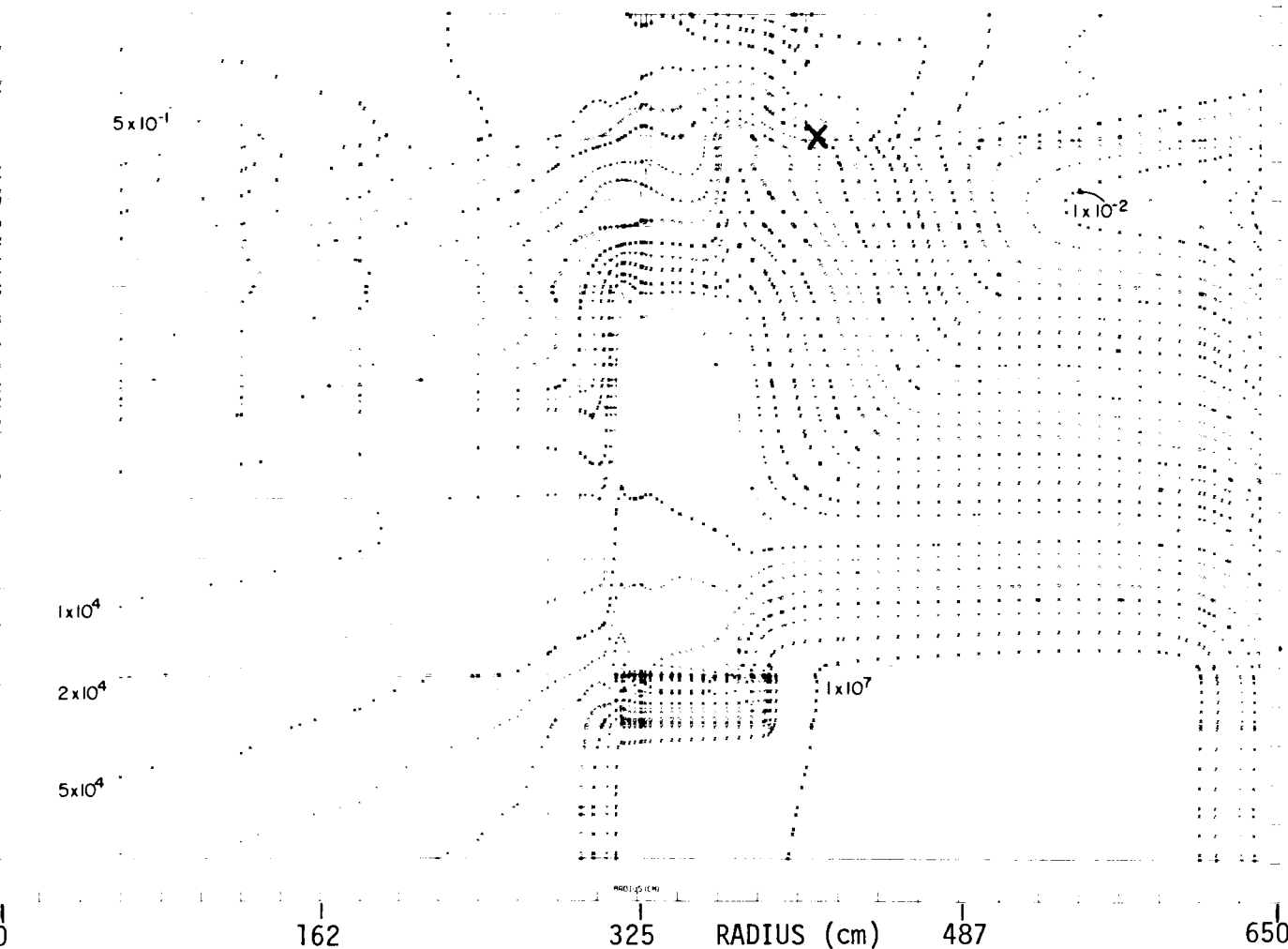
1240-

ORNL-DWG 75-3613

1138-

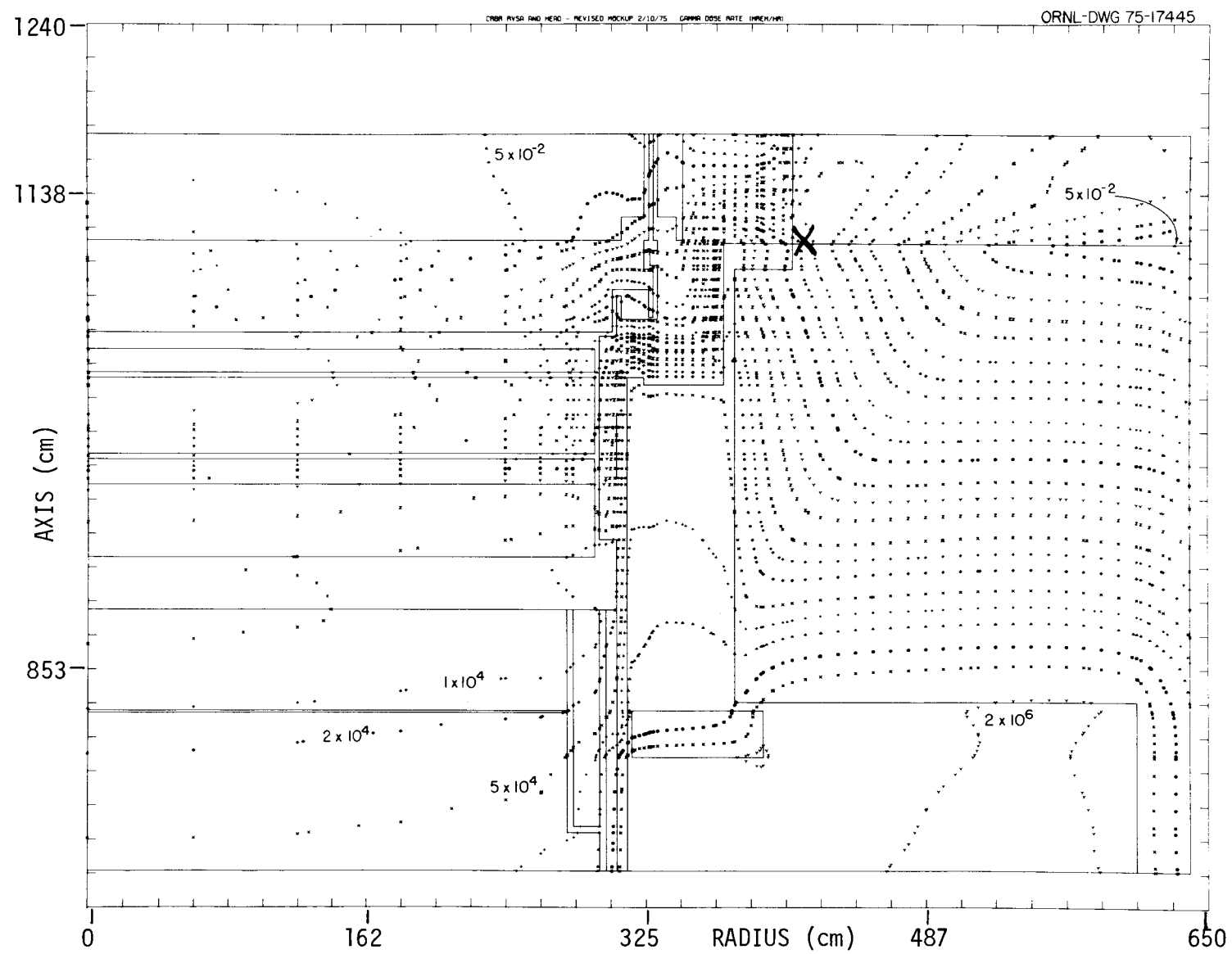
AXIS (cm)

853-



64

Fig. 38. Neutron Dose-Rate Distribution in Reactor Head and Vessel Support System Design No. 2 (Equilibrium Core). See Fig. 36 for description of geometry. Units are mrem/hr; peak dose rate on head is 25 mrem/hr at $R = 414$ cm (see X).



59

Fig. 39. Secondary Gamma-Ray Dose-Rate Distribution in Reactor Head and Vessel Support System Design No. 2 (Equilibrium Core). See Fig. 36 for description of geometry. Units are mrem/hr; peak dose rate on head is 92 mrem/hr at $R = 414$ cm (see X).

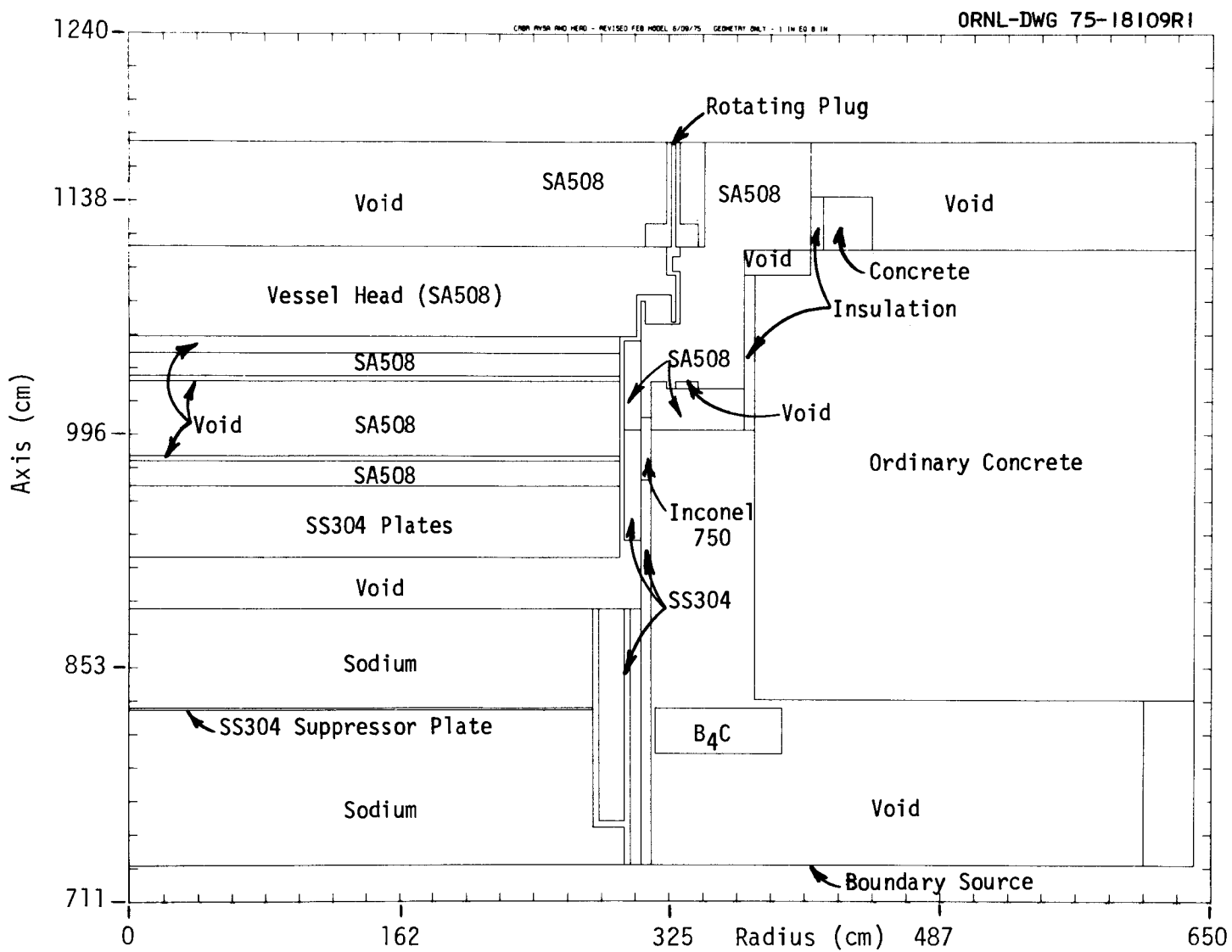


Fig. 40. Geometry Used for Calculation of Reactor Head and Vessel Support System Design No. 3 (Equilibrium Core). Boundary source located at $z = 733.12$ cm. See Figs. 20 and 25 for geometry of lower regions in CRBR assembly.

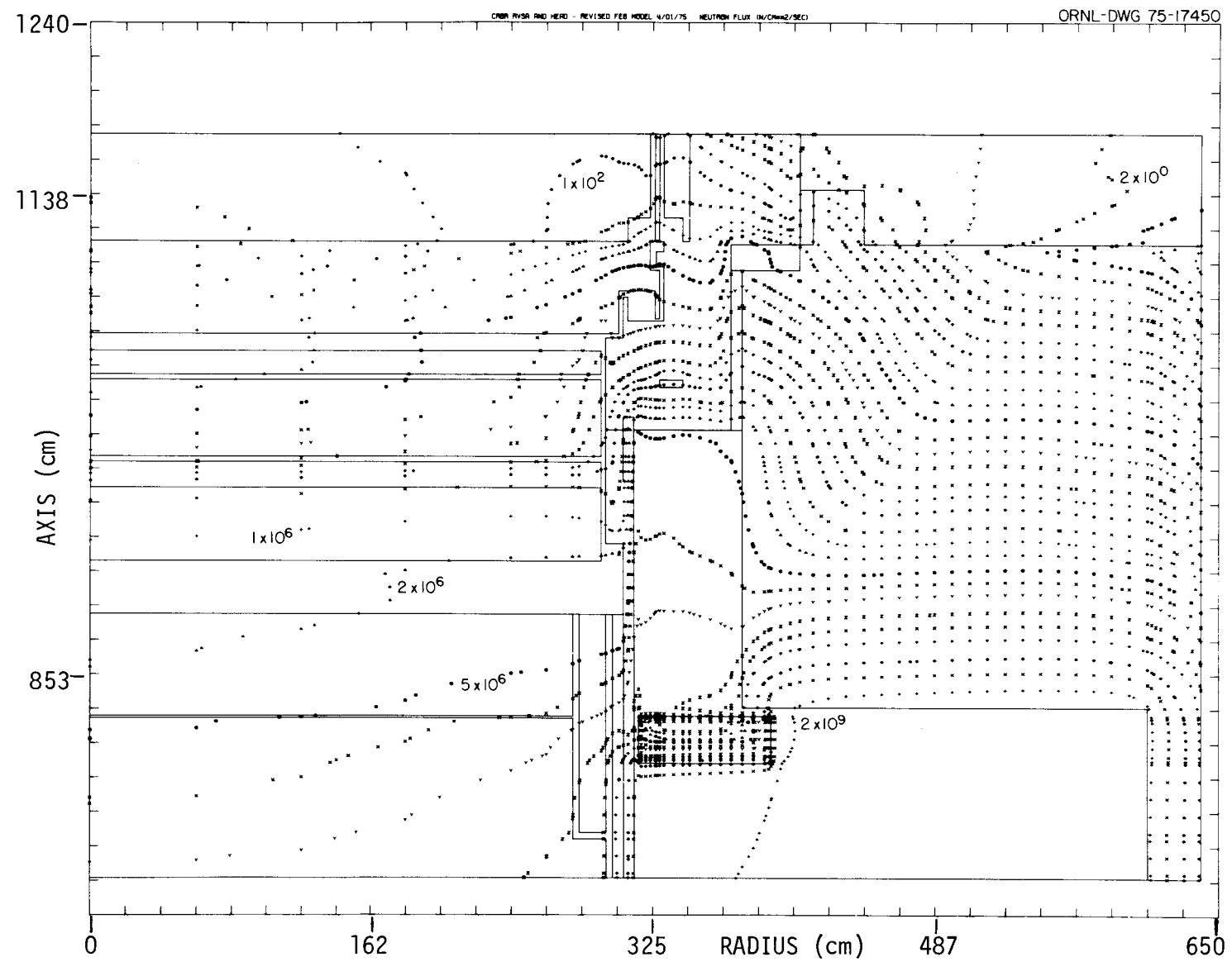


Fig. 41. Neutron Flux Distribution in Reactor Head and Vessel Support System Design No. 3 (Equilibrium Core). See Fig. 40 for description of geometry. Units are neutrons·cm⁻²·sec⁻¹.

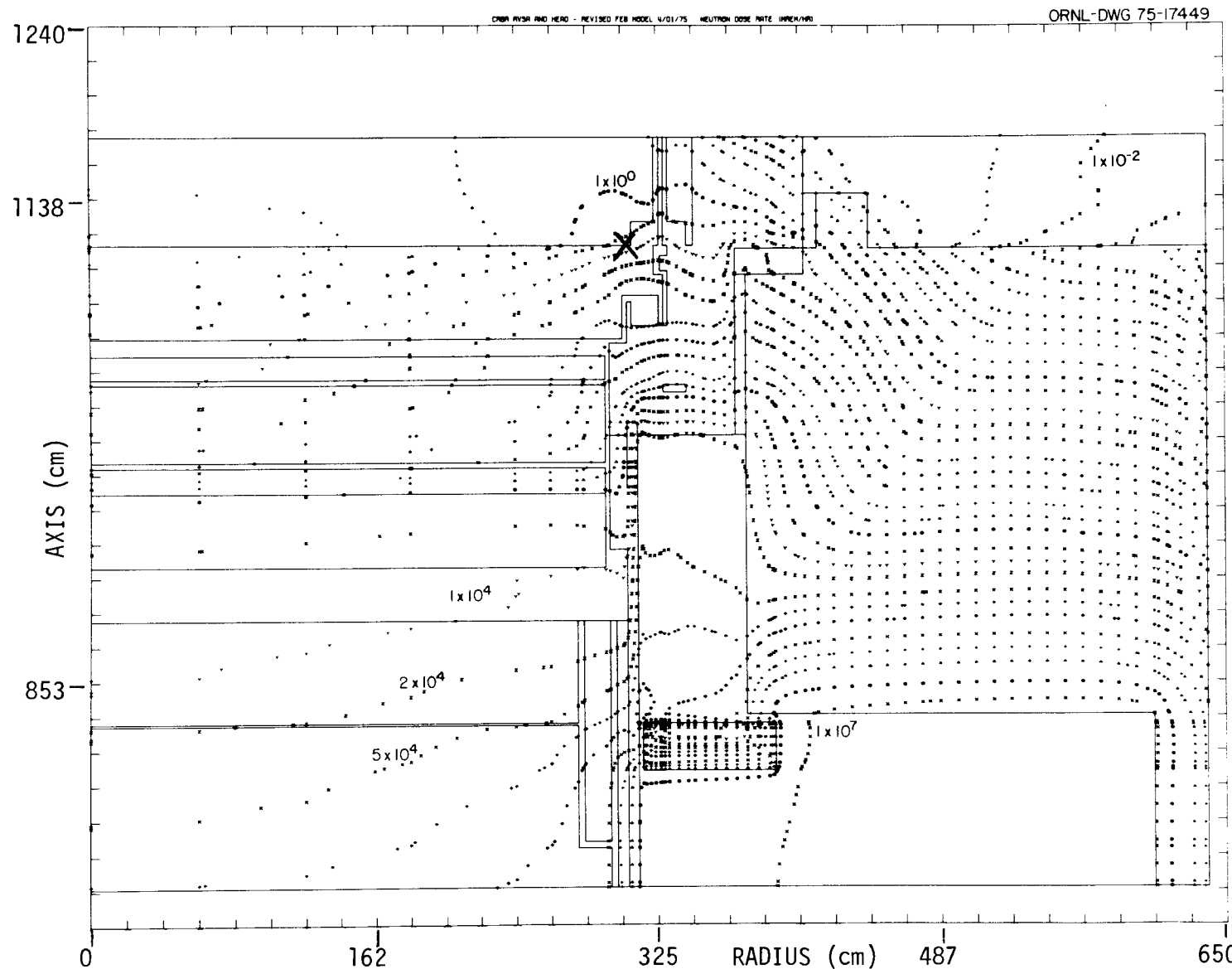


Fig. 42. Neutron Dose-Rate Distribution in Reactor Head and Vessel Support System Design No. 3 (Equilibrium Core). See Fig. 40 for description of geometry. Units are mrem/hr; peak dose rate on reactor head is 2.04 mrem/hr at $R = \sim 310$ cm (see X).

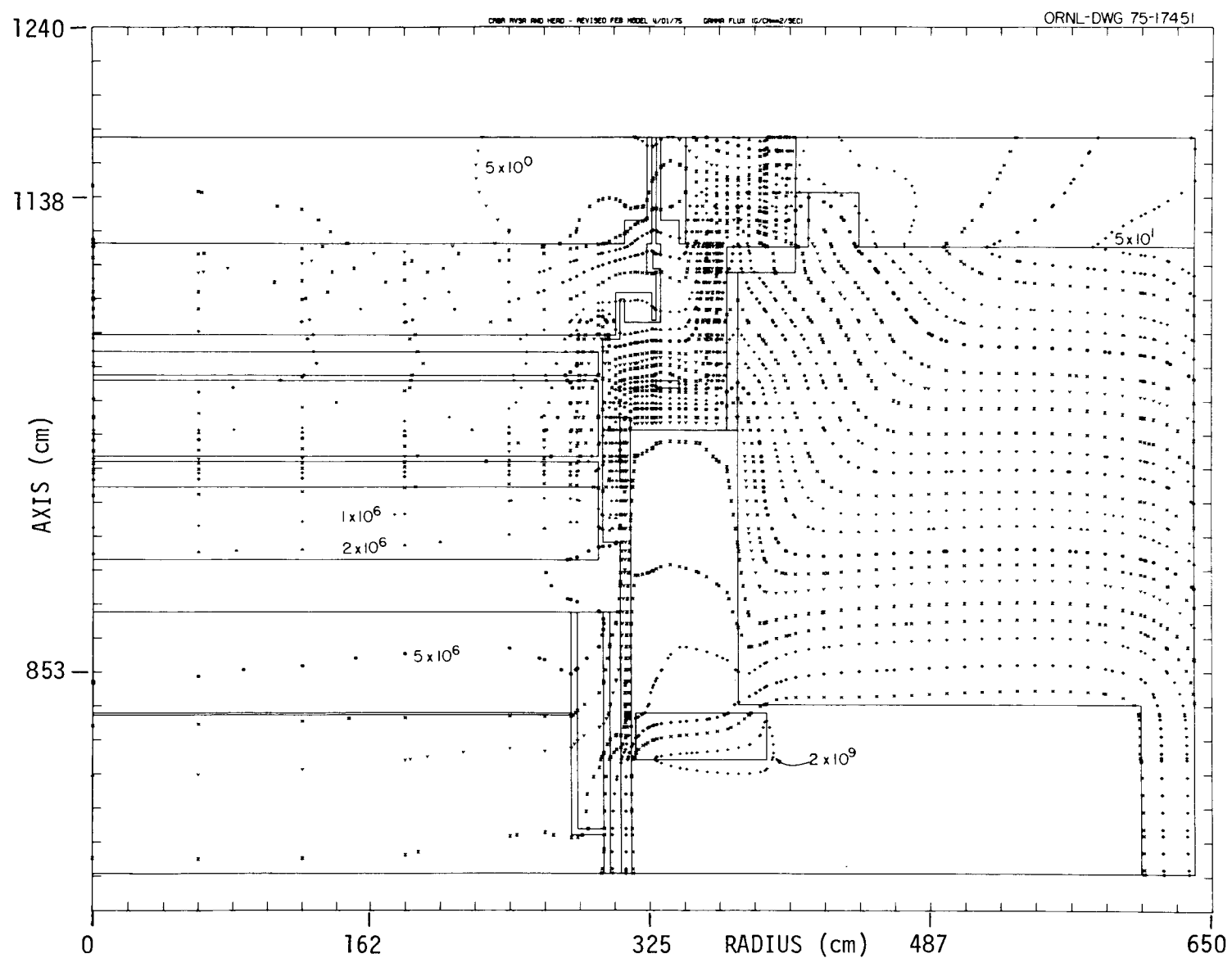


Fig. 43. Secondary Gamma-Ray Flux Distribution in Reactor Head and Vessel Support System Design No. 3 (Equilibrium Core). See Fig. 40 for description of geometry. Units are photons·cm⁻²·sec⁻¹.

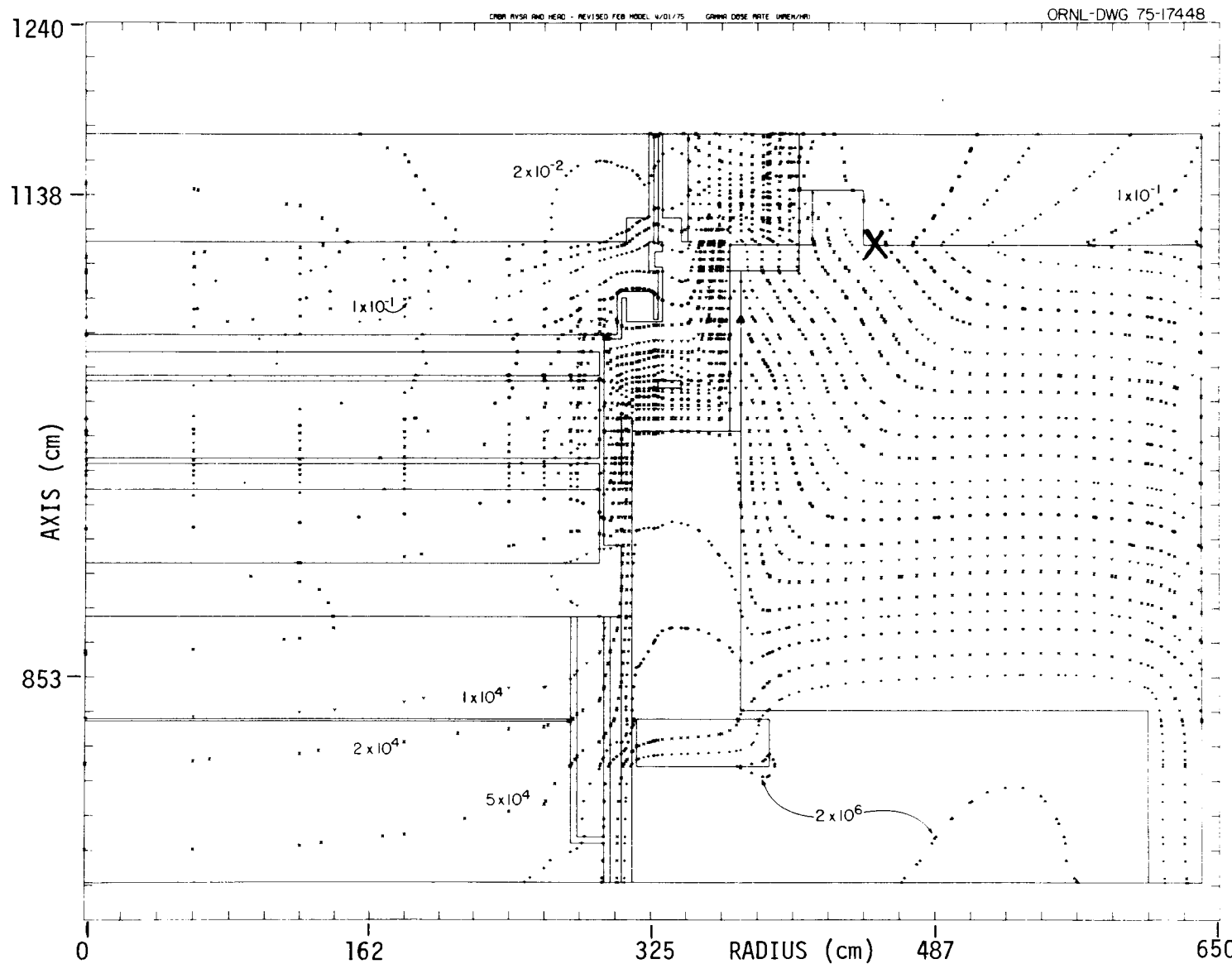


Fig. 44. Secondary Gamma-Ray Dose-Rate Distribution in Reactor Head and Vessel Support System Design No. 3 (Equilibrium Core). See Fig. 40 for description of geometry. Units are mrem/hr; peak dose rate on head is 2.66 mrem/hr at $R = 452$ cm (see X).

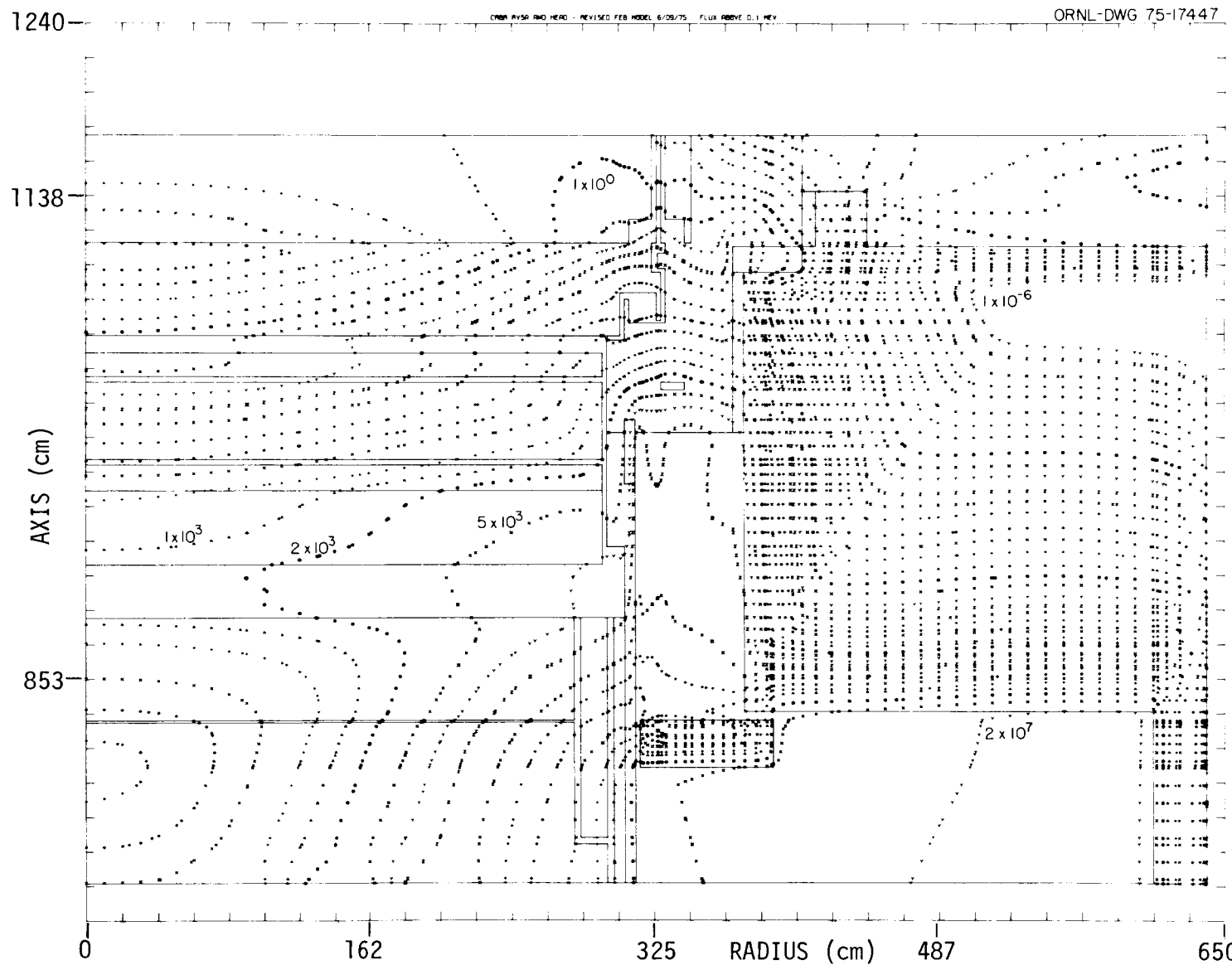


Fig. 45. Distribution of Neutron Fluxes > 0.1 MeV in Reactor Head and Vessel Support System Design No. 3 (Equilibrium Core). See Fig. 40 for description of geometry. Units are $\text{neutrons} \cdot \text{cm}^{-2} \cdot \text{sec}^{-1}$.

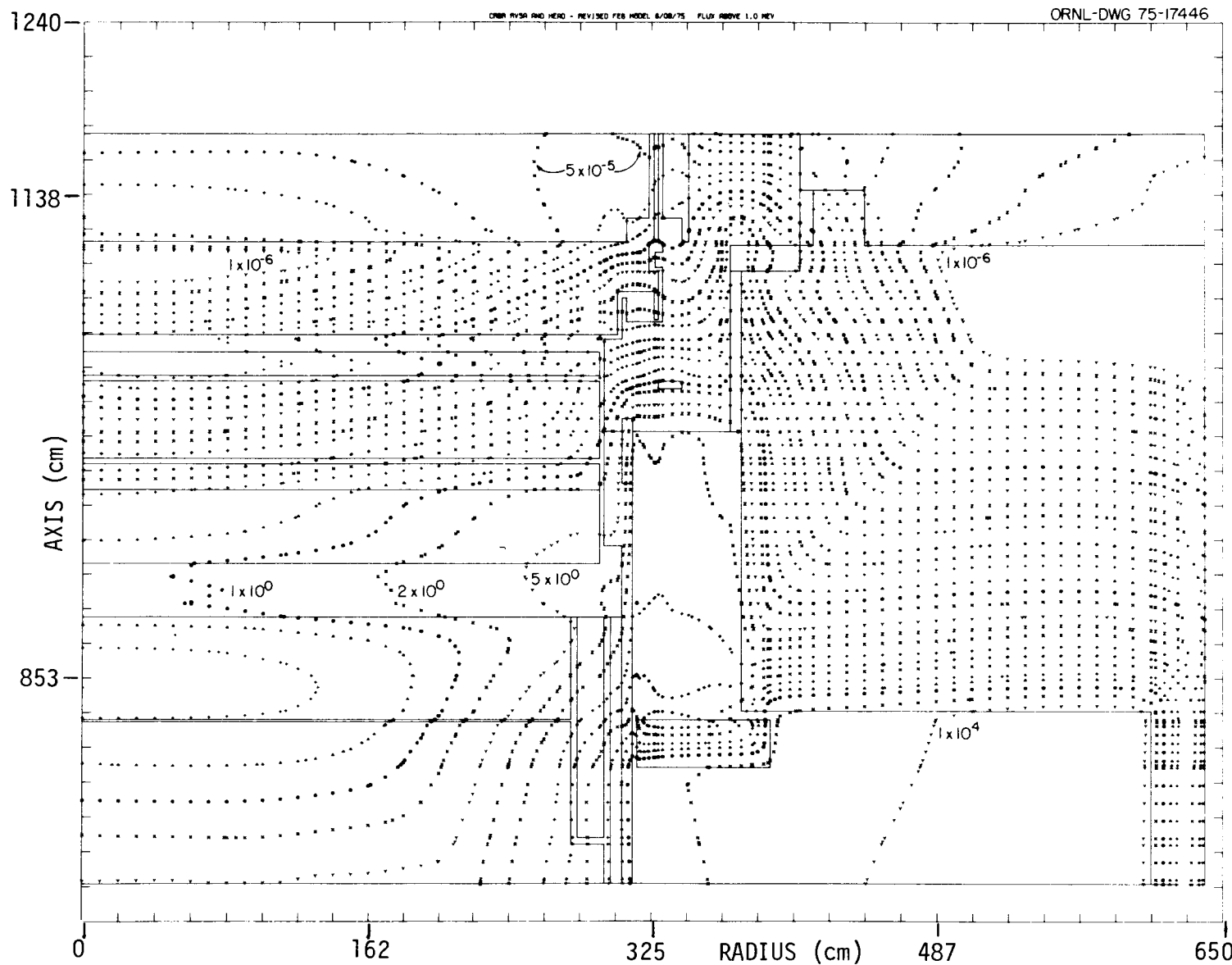


Fig. 46. Distribution of Neutron Fluxes > 1.0 MeV in Reactor Head and Vessel Support System Design No. 3 (Equilibrium Core). See Fig. 40 for description of geometry. Units are $\text{neutrons} \cdot \text{cm}^{-2} \cdot \text{sec}^{-1}$.

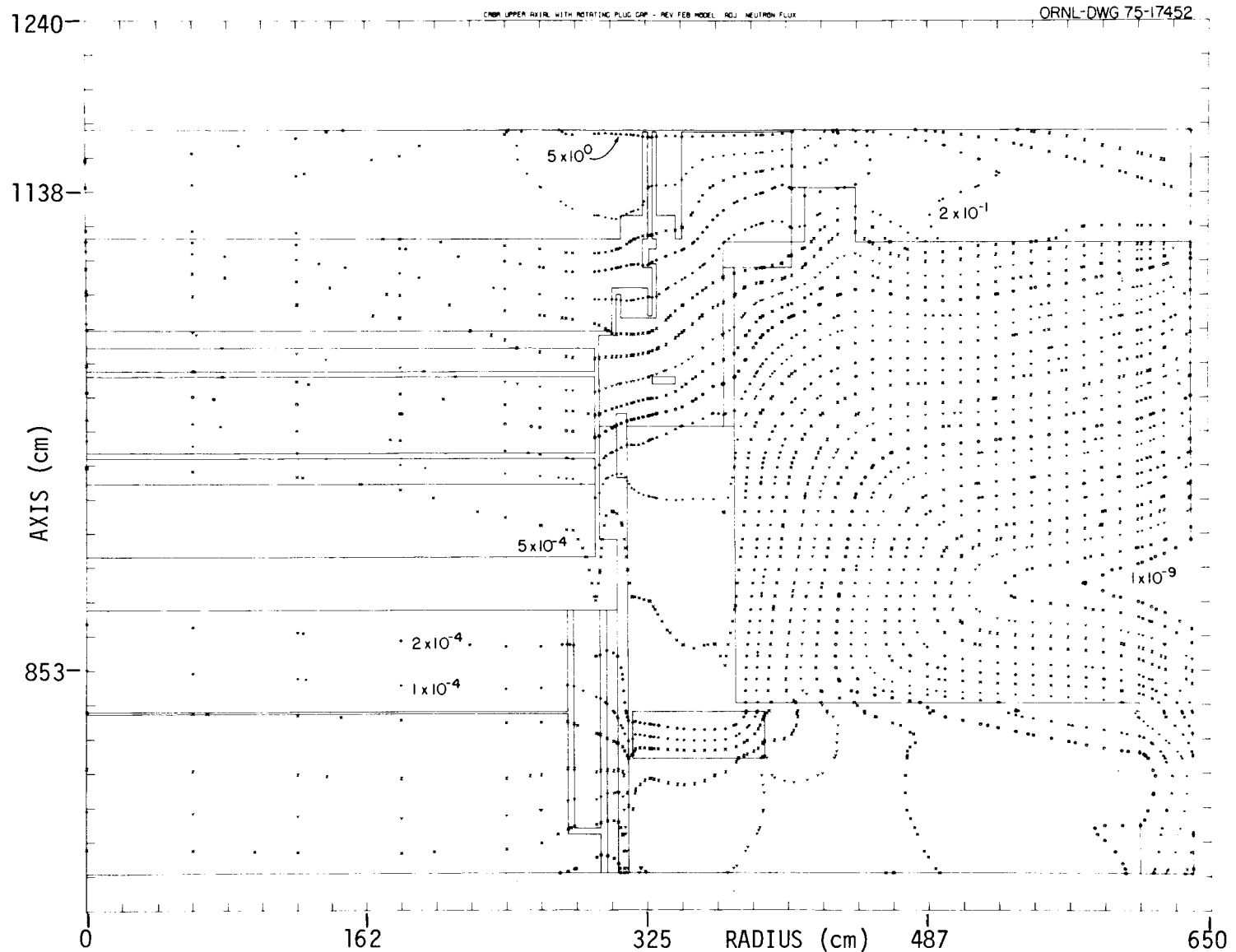


Fig. 47. Distribution of Adjoint Neutron Fluxes in Reactor Head and Vessel Support System Design No. 3 (Equilibrium Core). See Fig. 40 for description of geometry; see text for meaning of adjoint flux in this case.

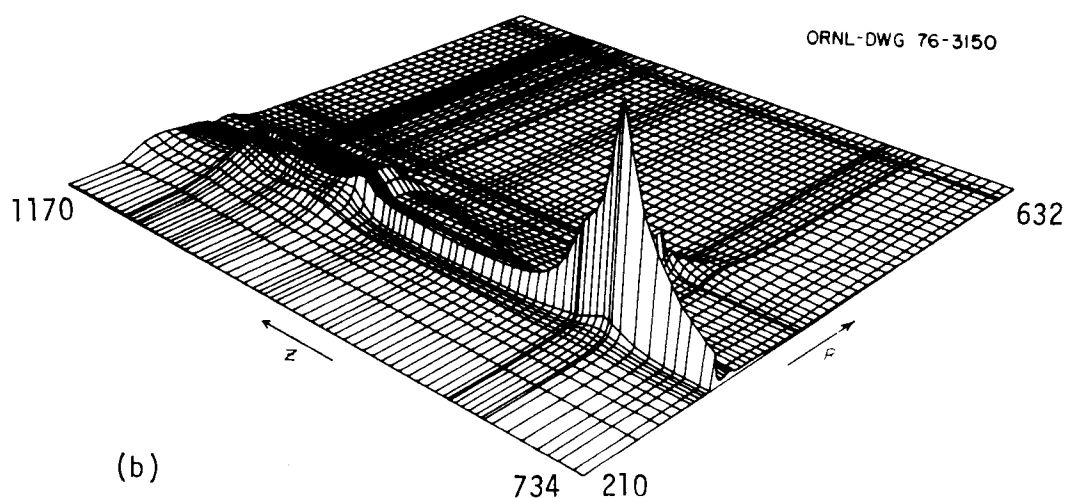
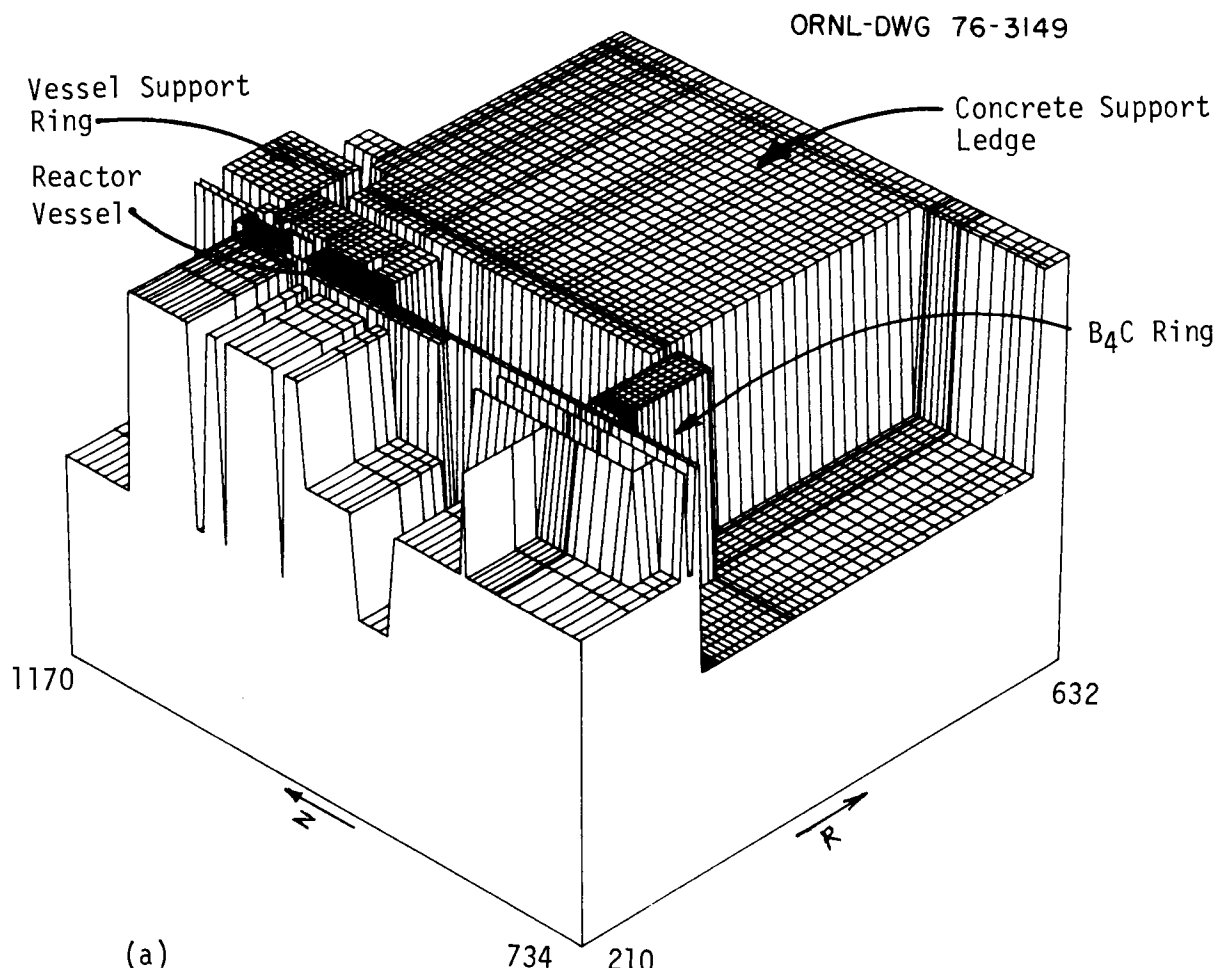


Fig. 48. Isometric Plot Showing Neutron Streaming Paths Through CRBR Vessel Support System. (a) Three-dimensional computer drawing of zones calculated; (b) plot showing dominant streaming paths.

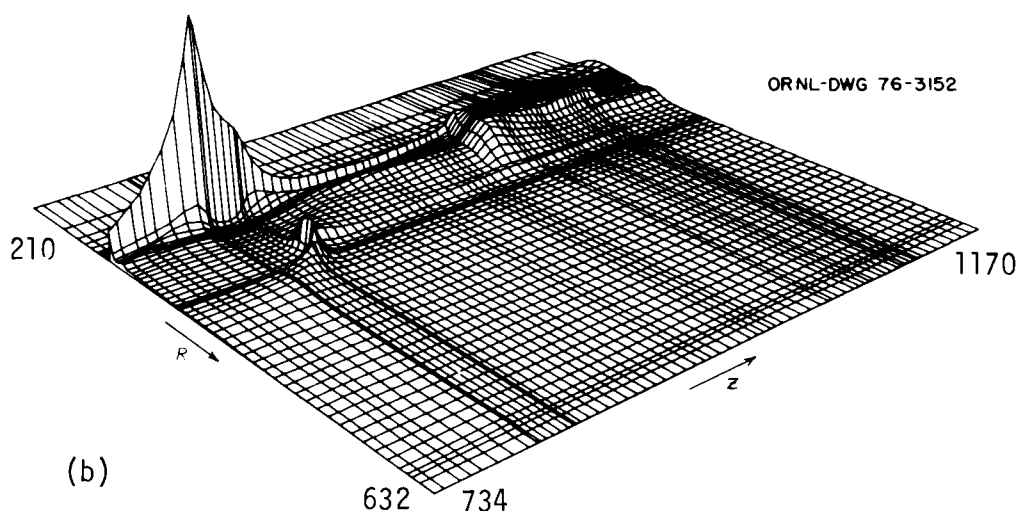
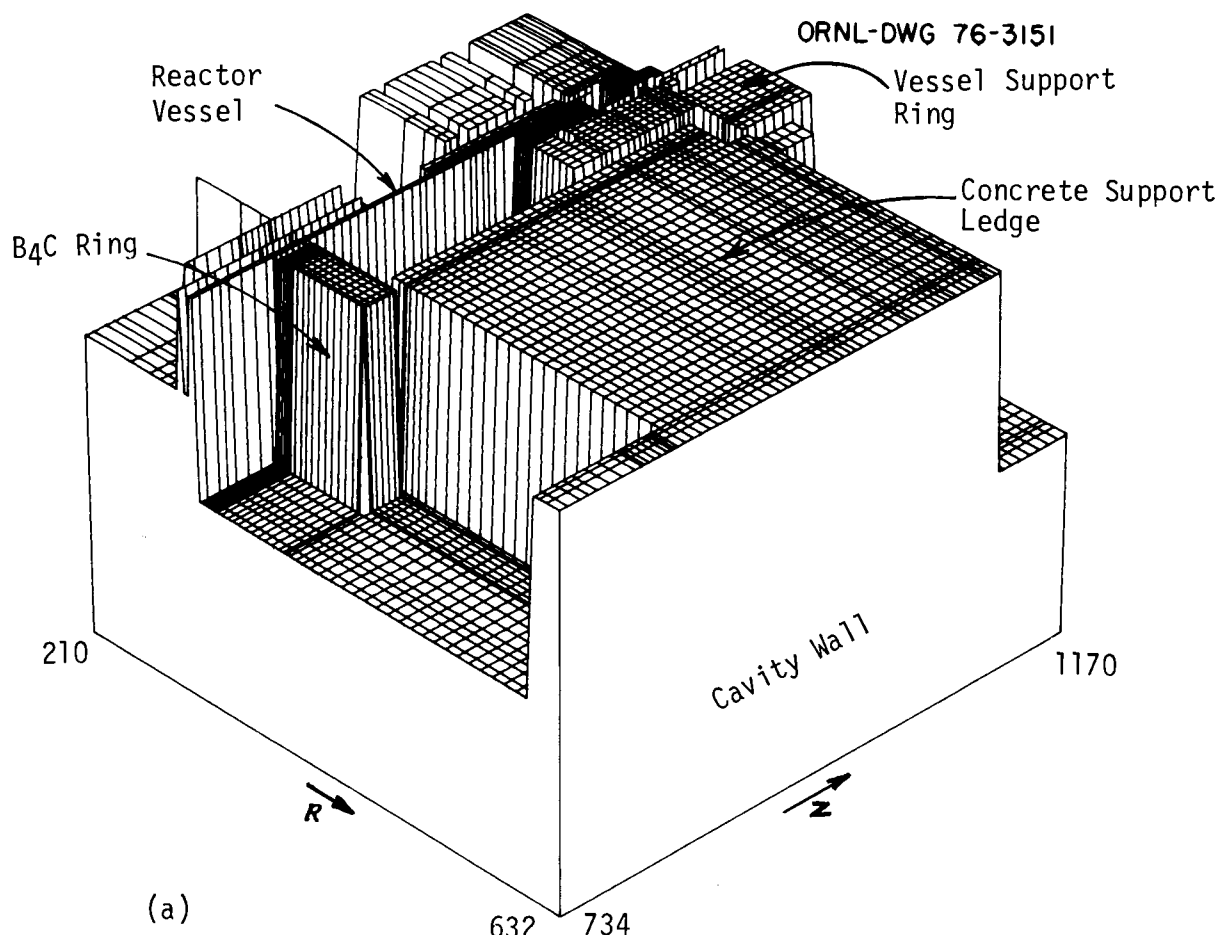


Fig. 49. Isometric Plot Showing Neutron Streaming Paths Through CRBR Vessel Support System. (a) Three-dimensional computer drawing of zones calculated; (b) plot showing dominant streaming paths.

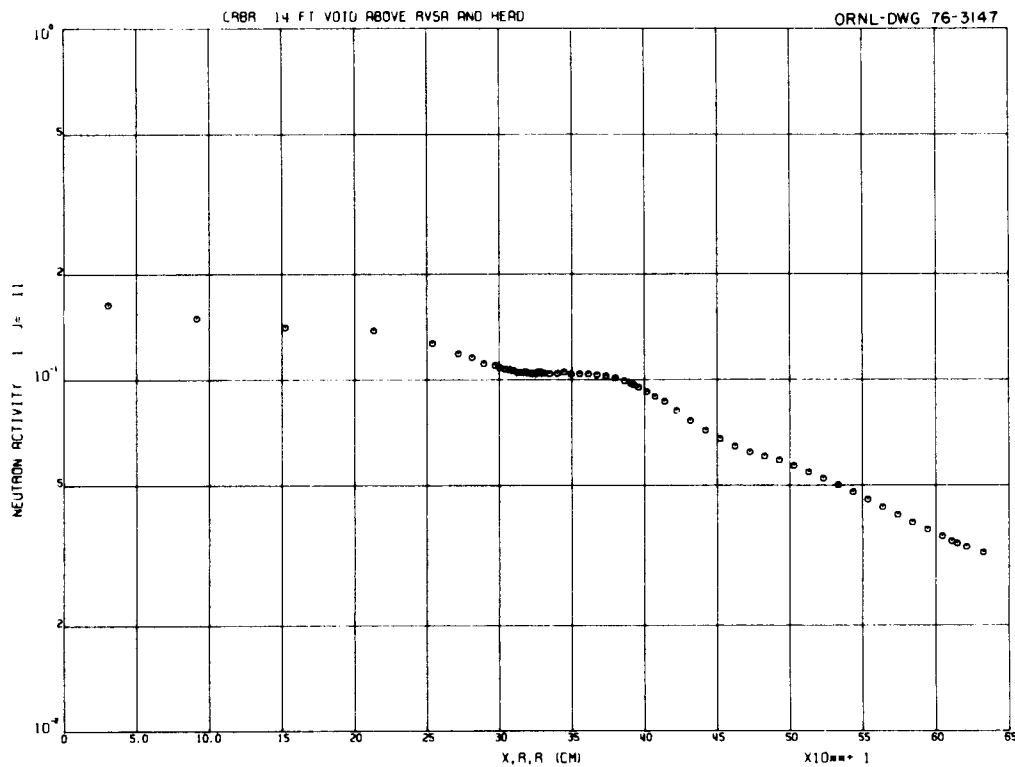


Fig. 50. Radial Distribution of Neutron Dose Rate in Horizontal Plane 14 ft Above CRBR Head.

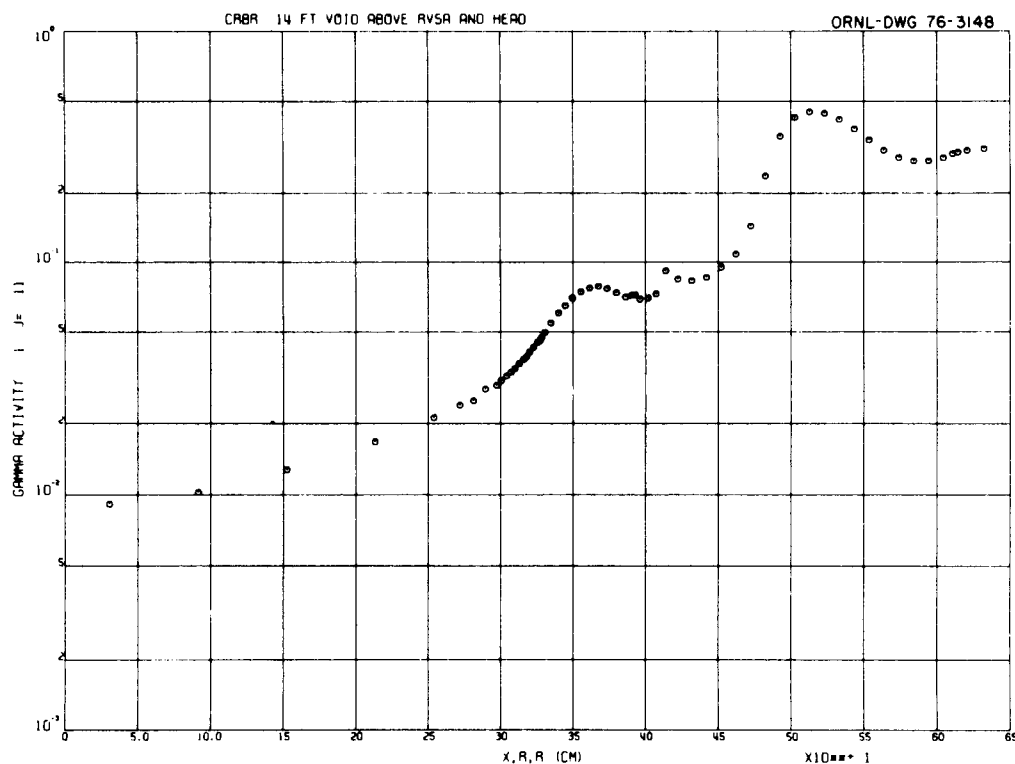


Fig. 51. Radial Distribution of Secondary Gamma-Ray Dose Rate in Horizontal Plane 14 ft Above CRBR Head.

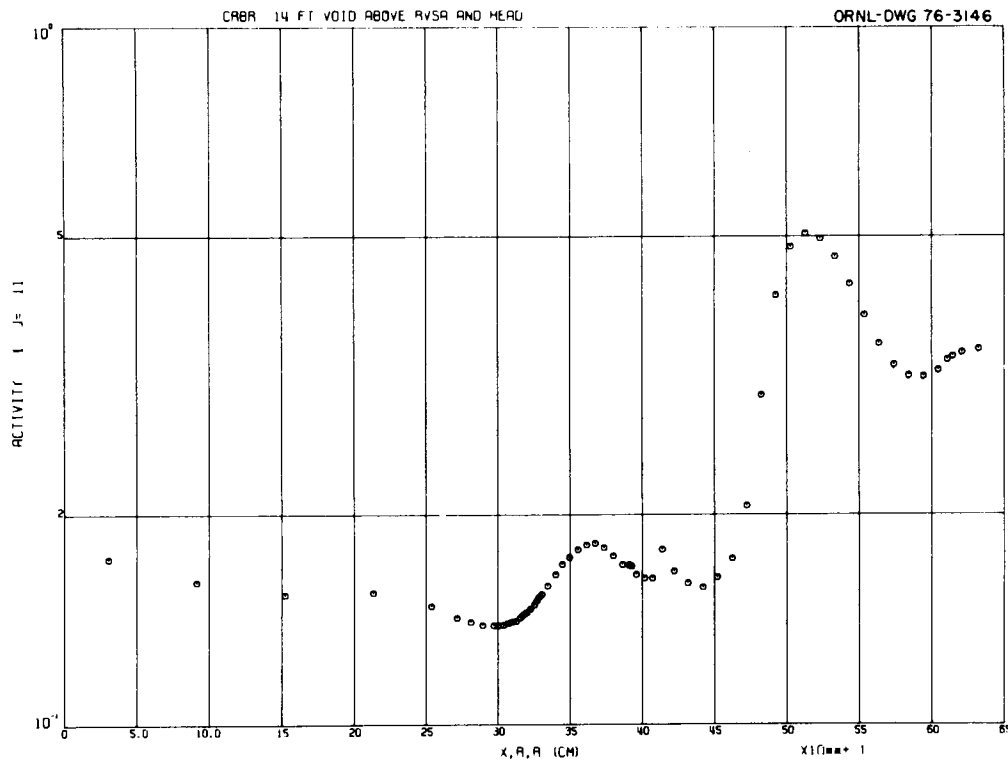


Fig. 52. Radial Distribution of Total Dose Rate in Horizontal Plane 14 ft Above CRBR Head.

5. SUMMARY AND CONCLUSIONS

The iterative series of calculations described in this report have impacted the design of the CRBR in several respects. On the basis of the earliest calculations, performed to predict the neutron fluxes in the lower axial region, WARD estimated an extremely long life time for the reactor grid plate, and on the basis of subsequent calculations for the same region they substantially reduced the thickness of the lower axial shield that protects the grid plate and the modular inlet assembly.

The first full-assembly calculations were performed for a CRBR design that closely resembled the FFTF, incorporating the same vessel support

system, stored-fuel modules, concrete reactor cavity shield, and B₄C collar around the guard vessel. These calculations covered the entire region from the lower axial shield up through the reactor head and out through the reactor cavity, which necessitated the use of spatial and angular grids that were too coarse for a detailed analysis of the calculated results to be meaningful. However, trends observed in this series in conjunction with the results of another ORNL study⁷ led to the decision by WARD not to routinely store fuel within the reactor vessel, which, in turn, resulted in the elimination of the FFTF-type reactor cavity shield and the B₄C collar. Concurrently, engineering and economic considerations dictated a change in the design of the vessel support system. All these changes, plus the availability of a new core model and an improved set of cross sections, led to a second series of full-assembly calculations that were considerably more sophisticated. In the meantime, the neutron fluxes from this first series were used in calculations of the activation of sodium, tantalum, and cobalt within the reactor vessel, the concern being that activation gamma rays might overpower the after-shutdown neutron-monitoring system. The results indicated that the shutdown gamma-ray dose rates would not create a problem for fission detectors; however, WARD later changed the design so as to use BF₃ detectors which are much more susceptible to gamma rays.

The first calculation in the new full-assembly series revealed that even with no stored fuel in the reactor vessel, neutrons leaking into the reactor cavity and streaming upward produced a peak neutron dose rate above the head that was a factor of 100 higher than the criterion. This prompted the reintroduction of a B₄C shield in the upper region of the cavity. At the same time WARD redesigned the vessel support system and thermal shield and also expressed concern that a gap surrounding the largest of three rotating plugs in the reactor head would provide a neutron streaming path. A subsequent calculation for the new support design with the B₄C shield and the top-plug gap included yielded a peak neutron dose rate on the reactor head that was a factor of 12.5 higher than that allowed by the criterion. Thus still more shielding was required.

For the final calculation in this series, a concrete ring was added around a section of the vessel support ring protruding above the vessel head, and steel was added to the bottom of the support ring. While the resulting peak neutron and secondary gamma-ray dose rates above the vessel head were considerably reduced over those calculated for the earlier designs, the dose rates still exceeded the criteria. The calculations were therefore suspended until a re-evaluation of the dose constraints could be made by WARD.

REFERENCES

1. Lorraine S. Abbott and F. R. Mynatt, "Review of ORNL Radiation Shielding Analyses of the Fast Flux Test Facility Reactor," ORNL-5027 (July 1975).
2. "Clinch River Breeder Reactor Plant Design," a brochure prepared for the Breeder Reactor Corporation by Project Management Corporation and the Advanced Reactors Division of Westinghouse Electric Corporation, October, 1975, CRBRP Project Office, P. O. Box U, Oak Ridge, TN 37830.
3. "The Clinch River Breeder Reactor Plant Project: Chief Executive Briefing. Proceedings of the Breeder Reactor Corporation October 1975 Information Session," CRBRP Project Office, P. O. Box U, Oak Ridge, TN. 37830.
4. W. A. Rhoades and F. R. Mynatt, "The DOT-III Two-Dimensional Discrete Ordinates Transport Code," ORNL/TM-4280 (September 1973); available from ORNL Radiation Shielding Information Center's computer code collection as CCC/209.
5. W. W. Engle, Jr., "User's Manual for ANISN, A One-Dimensional Discrete Ordinates Transport Code with Anisotropic Scattering," Computing Technology Center, Union Carbide Nuclear Division, K-1693 (1967); available from ORNL Radiation Shielding Information Center's computer code collection as CCC/254 (IBM-360 version) or CCC/255 (CDC version).
6. These calculations have been reported previously in "Fast Reactor Analytical Shielding Progress Report for July and August 1973," ORNL/TM-4402 (November 1973).
7. W. W. Engle, Jr., L. R. Williams, and F. R. Mynatt in "Fast Reactor Analytical Shielding Progress Report for September and October 1973," ORNL/TM-4482 (May 1974).
8. The FACT code is undocumented; the current version is maintained at ORNL by W. W. Engle, Jr.
9. The VIP code is undocumented; the current version is maintained at ORNL by R. L. Childs.

ORNL/TM-5338
UC-79d - Liquid Metal
Fast Breeder Reactor
Physics

INTERNAL DISTRIBUTION

- | | | | |
|--------|---------------------------|--------|---|
| 1-4. | L. S. Abbott | 26. | M. L. Tobias |
| 5. | D. E. Bartine | 27. | D. B. Trauger |
| 6. | R. G. Alsmiller, Jr. | 28. | C. R. Weisbin |
| 7. | R. L. Childs | 29. | G. E. Whitesides |
| 8. | C. E. Clifford | 30. | L. R. Williams |
| 9. | M. B. Emmett | 31. | A. Zucker |
| 10-14. | W. W. Engle, Jr. | 32. | RSIC |
| 15. | G. F. Flanagan | 33. | P. F. Fox (consultant) |
| 16. | H. Goldstein (consultant) | 34. | W. W. Havens, Jr. (consultant) |
| 17. | W. O. Harms | 35. | A. F. Henry (consultant) |
| 18. | R. E. Maerker | 36. | R. E. Uhrig (consultant) |
| 19. | F. C. Maienschein | 37-38. | Central Research Library |
| 20. | F. R. Mynatt | 39. | ORNL Y-12 Technical Library
Document Reference Section |
| 21. | R. W. Peelle | 40-41. | Laboratory Records Department |
| 22. | F. G. Perey | 42. | Laboratory Records ORNL RC |
| 23. | C. O. Slater | | |
| 24. | P. N. Stevens | | |
| 25. | J. H. Swanks | | |

EXTERNAL DISTRIBUTION

- | | |
|---------|--|
| 43-44. | USERDA Division of Reactor Research and Development, Washington,
D. C. 20545: Director |
| 45. | USERDA Oak Ridge Operations, Reactor Division, P. O. Box E,
Oak Ridge, Tennessee 37830: Director |
| 46. | USERDA Oak Ridge Operations, Research and Technical Support
Division, P. O. Box E, Oak Ridge, Tennessee 37038: Director |
| 47-227. | For distribution as shown in TID-4500 Distribution Category
UC-79d, Liquid Metal Fast Breeder Reactor Physics |